Project 1916 | April 2021

SJSU SAN JOSÉ STATE UNIVERSITY

MTI MINETA TRANSPORTATION INSTITUTE

Novel Method for Probabilistic Evaluation of the Post-Earthquake Functionality of a Bridge

Vesna Terzic, PhD
William Andy Pasco

CSUTC California State University Transportation Consortium

CALIFORNIA STATE UNIVERSITY LONG BEACH

MINETA TRANSPORTATION INSTITUTE

Founded in 1991, the Mineta Transportation Institute (MTI), an organized research and training unit in partnership with the Lucas College and Graduate School of Business at San José State University (SJSU), increases mobility for all by improving the safety, efficiency, accessibility, and convenience of our nation's transportation system. Through research, education, workforce development, and technology transfer, we help create a connected world. MTI leads the Mineta Consortium for Transportation Mobility (MCTM) funded by the U.S. Department of Transportation and the California State University Transportation Consortium (CSUTC) funded by the State of California through Senate Bill 1. MTI focuses on three primary responsibilities:

Research

MTI conducts multi-disciplinary research focused on surface transportation that contributes to effective decision making. Research areas include: active transportation; planning and policy; security and counterterrorism; sustainable transportation and land use; transit and passenger rail; transportation engineering; transportation finance; transportation technology; and workforce and labor. MTI research publications undergo expert peer review to ensure the quality of the research.

Education and Workforce Development

To ensure the efficient movement of people and products, we must prepare a new cohort of transportation professionals who are ready to lead a more diverse, inclusive, and equitable transportation industry. To help achieve this, MTI sponsors a suite of workforce development and education opportunities. The Institute supports educational programs offered by the Lucas Graduate School of Business: a Master of Science in Transportation Management, plus graduate certificates that include High-Speed and Intercity Rail Management and Transportation Security Management. These flexible programs offer live online classes so that working transportation professionals can pursue an advanced degree regardless of their location.

Information and Technology Transfer

MTI utilizes a diverse array of dissemination methods and media to ensure research results reach those responsible for managing change. These methods include publication, seminars, workshops, websites, social media, webinars, and other technology transfer mechanisms. Additionally, MTI promotes the availability of completed research to professional organizations and works to integrate the research findings into the graduate education program. MTI's extensive collection of transportation-related publications is integrated into San José State University's world-class Martin Luther King, Jr. Library.

Report 21-03

Novel Method for Probabilistic Evaluation of the Post-Earthquake Functionality of a Bridge

Vesna Terzic, Ph.D.
William Andy Pasco

April 2021

A publication of the
Mineta Transportation Institute
Created by Congress in 1991

College of Business
San José State University
San José, CA 95192-02

TECHNICAL REPORT DOCUMENTATION PAGE

1. Report No. 21-03	**2. Government Accession No.**	**3. Recipient's Catalog No.**
4. Title and Subtitle Novel Method for Probabilistic Evaluation of the Post-Earthquake Functionality of a Bridge		**5. Report Date** April 2021 **6. Performing Organization Code**
7. Authors Vesna Terzic, Ph.D. William Andy Pasco		**8. Performing Organization Report** CA-MTI-1916
9. Performing Organization Name and Address Mineta Transportation Institute College of Business San José State University San José, CA 95192-0219		**10. Work Unit No.** **11. Contract or Grant No.** ZSB12017-SJAUX
12. Sponsoring Agency Name and Address State of California SB1 2017/2018 Trustees of the California State University Sponsored Programs Administration 401 Golden Shore, 5th Floor Long Beach, CA 90802		**13. Type of Report and Period Covered** Final Report **14. Sponsoring Agency Code**
15. Supplemental Notes DOI: 10.31979/mti.2021.1916		

16. Abstract

While modern overpass bridges are safe against collapse, their functionality will likely be compromised in case of design-level or beyond design-level earthquake, which may generate excessive residual displacements of the bridge deck. Presently, there is no validated, quantitative approach for estimating the operational level of the bridge after an earthquake due to the difficulty of accurately simulating residual displacements. This research develops a novel method for probabilistic evaluation of the post-earthquake functionality state of the bridge; the approach is founded on an explicit evaluation of bridge residual displacements and associated traffic capacity by considering realistic traffic load scenarios.

This research proposes a high-fidelity finite-element model for bridge columns, developed and calibrated using existing experimental data from the shake table tests of a full-scale bridge column. This finite-element model of the bridge column is further expanded to enable evaluation of the axial load-carrying capacity of damaged columns, which is critical for an accurate evaluation of the traffic capacity of the bridge. Existing experimental data from the crushing tests on the columns with earthquake-induced damage support this phase of the finite-element model development.

To properly evaluate the bridge's post-earthquake functionality state, realistic traffic loadings representative of different bridge conditions (e.g., immediate access, emergency traffic only, closed) are applied in the proposed model following an earthquake simulation. The traffic loadings in the finite-element model consider the distribution of the vehicles on the bridge causing the largest forces in the bridge columns.

17. Key Words Continuous girder bridges, Loss and damage, Traffic capacity, Traffic loads, Dynamic models	**18. Distribution Statement** No restrictions. This document is available to the public through The National Technical Information Service, Springfield, VA 22161		
19. Security Classif. (of this report) Unclassified	**20. Security Classif. (of this page)** Unclassified	**21. No. of Pages** 74	**22. Price**

Form DOT F 1700.7 (8-72)

DOI: 10.31979/mti.2021.1916

Mineta Transportation Institute
College of Business
San José State University
San José, CA 95192-0219

Tel: (408) 924-7560
Email: mineta-institute@sjsu.edu

transweb.sjsu.edu/research/1916

ACKNOWLEDGMENTS

This work was supported by the California State University Transportation Consortium. Any opinions, findings, and conclusions expressed herein are the authors' and do not necessarily reflect those of the sponsors.

CONTENTS

List of Figures

List of Tables

Executive Summary

California has more than a 99% chance of having one or more earthquakes of magnitude 6.7 or larger within the next 30 years; such an event will generate significant economic losses and cause major societal disruptions. Furthermore, the likelihood of one or more mega-earthquakes of magnitude 8 or larger occurring within the next 30 years is 7%. Such an earthquake will generate an economic loss of more than $200 billion, as well as about 1,800 deaths, and it will affect the lives of close to 38 million people. Awareness of earthquakes' possible detrimental consequences is the main engine for city ordinances throughout California that have mandated seismic retrofits of potentially hazardous types of buildings to increase safety and minimize casualties. In addition, a new methodology for performance-based seismic design of buildings has been released by FEMA and is used by engineers in the design of new buildings and the retrofitting of existing ones to achieve beyond-the-code seismic performance that meets stakeholder needs. Also, in 2017, California passed Senate Bill 1 to improve the traffic safety of transportation networks through stewardship activities based on a "fix it first" approach.

In California, modern highway bridges designed using the Caltrans Seismic Design Criteria are expected to maintain bridge integrity and provide safety in case of a design-level earthquake. However, their functionality will likely be compromised in case of a design-level (or beyond-design-level) earthquake that generates excessive residual drifts. There currently exists no validated, quantitative approach for estimating the functionality level of a bridge after an earthquake due to the difficulty of accurately simulating the residual drifts of the bridge columns. Due to the lack of such guidelines for estimating bridges' post-earthquake functionality, bridge inspectors and maintenance engineers provide an estimate of the functional capacity of the bridge based on qualitative observations, with each judgment founded on personal experience. But objective evaluation of the capacity of a bridge to carry self-weight and traffic loads after an earthquake is essential for a safe and timely reopening of the bridge. Hence, this research develops a novel method for probabilistically evaluating the post-earthquake functionality state of the bridge founded on an explicit evaluation of residual drifts and associated traffic capacity considering realistic traffic load scenarios.

To accurately simulate the post-earthquake residual drifts, this research proposes a high-fidelity finite-element model for bridge columns, which is developed and calibrated using existing experimental data from the shake table tests of a full-scale bridge column. This finite-element model of the bridge column is further expanded to enable evaluation of the axial load-carrying capacity of damaged columns, which is critical for an accurate evaluation of the traffic capacity of the bridge. Existing experimental data from the crushing tests on the columns with earthquake-induced damage are utilized to support this phase of the finite-element model development.

The finite-element model of the bridge column is developed in OpenSees. The proposed model utilizes a nonlinear beam with a hinge element—an extension of the force-based element formulation where the locations and weights of integration points are based on plastic hinge integration, allowing for an explicit definition of plastic hinge lengths at the element ends. The reinforced concrete section in the plastic hinge regions is modeled as a fiber section that accounts for the axial-bending interaction. The fiber section is divided into three parts: concrete cover, concrete core, and reinforcing steel, where fibers of the concrete cover (unconfined concrete) and concrete core (confined concrete) are modeled using Concrete02 material, and reinforcing steel fibers (longitudinal bars) are modeled using ReinforcingSteel material. To accurately simulate the axial load-carrying capacity of the damaged column, the post-peak degrading slope of confined concrete is set to 5% of its initial modulus of elasticity. The interior portion of the beam with the hinges element is modeled as elastic, where the effective moment of inertia, expressed as a ratio to the total moment of inertia, is 0.35 for the design-level earthquake and 0.25 for the beyond-design-level earthquake. Damping is modeled with a mass- and stiffness-proportional Rayleigh damping model using the damping ratio of 1%, the first two modes of vibration, and tangent stiffness of the column updated at every step of the analysis.

This research next proposes a method for directly evaluating the post-earthquake traffic capacity and functionality of a reinforced concrete highway overpass bridge through finite-element simulations. The method includes a definition of the bridge's functionality limit states (FLSs): full traffic, limited traffic, emergency vehicles only, or no traffic. It also presents recommendations for modeling a bridge structure by incorporating the proposed bridge column model, a definition of realistic traffic load scenarios that correspond to different traffic load restrictions, an evaluation of the post-earthquake traffic capacity for selected FLSs, and finally an evaluation of post-earthquake functionality that compares traffic capacity with traffic demand. A distinguishing feature of the method is given by the quantitative links between the earthquake intensity, component-level engineering demand parameters, and system-level traffic capacity. The main outcome of the method is a reliable assessment of the probability that a traffic loading, given the functionality limit state of the bridge, can be safely accommodated following an earthquake event. The method is demonstrated in a case study considering a modern single-column bent bridge.

The information on the post-earthquake functionality state of the bridge generated with the proposed method can be effectively used to support bridge maintenance decision-making processes by enabling an identification of retrofit needs that will generate long-term benefits to transportation agencies through reduced business interruptions. Furthermore, an objective evaluation of the post-earthquake bridge functionality may be used in place of current practices to improve public safety and minimize economic impact caused by disruption of the transportation network from possibly unnecessary bridge closures.

I. Introduction

California has more than a 99% chance of having one or more earthquakes of magnitude 6.7 or larger within the next 30 years (Field at al. 2013) that will generate significant economic losses and cause major societal disruptions. Furthermore, the likelihood of one or more mega-earthquakes of magnitude 8 or larger occurring within the next 30 years is 7% (Field at al. 2013). Based on the 2008 study by Jones et al., such an earthquake will generate an economic loss of more than $200 billion (the number is likely even higher now), as well as about 1,800 deaths, and it will affect the lives of close to 38 million people. That study conducted by Jones and colleagues was the main engine for city ordinances throughout California that mandated seismic retrofitting of potentially hazardous types of buildings to increase safety and minimize casualties. In addition, a new methodology for performance-based seismic design of buildings has been released by FEMA (FEMA P-58 2018) and is used by engineers in the design of new buildings, as well as the retrofitting of existing buildings, to achieve beyond-the-code seismic performance that meets stakeholder needs. Also, in 2017, California passed Senate Bill 1 to improve the traffic safety of transportation networks through stewardship activities based on a "fix it first" approach (California Transportation Asset Management Plan [CTAMP] 2018).

In California, modern highway bridges designed using the Caltrans Seismic Design Criteria (SDC) (2013) are expected to dissipate earthquake forces through incurring damage mostly in bridge columns and abutments while maintaining bridge integrity and providing safety. Although the CTAMP indicates that 74.9% of California bridges are in "good condition" based on age, condition, level of service, and frequency of repair, the performance of these bridges may be altered in the event of a major earthquake. Experimental investigations conducted on full-scale typical modern bridge columns designed for a hypothetical location in San Francisco (Schoettler et al. 2015) highlighted the potential for significant residual (permanent) drift in case of an earthquake with a magnitude of 6.9 due to significant damage accumulation. Furthermore, Terzic and Stojadinovic (2010a,b) have demonstrated through a set of analytical and experimental studies that excessive residual drifts compromise the functionality of typical overpass bridges in California, as they generate a significant reduction of bridge traffic capacity. While researchers have proposed new design methods that utilize different technologies to eliminate residual drifts (e.g., Sakai and Mahin 2004; Jeong et al. 2008; Guerrini et al. 2014), these methods have not been used in modern bridge construction.

While modern bridges are safe against collapse and will maintain traffic capacity in the absence of residual drifts (Terzic and Stojadinovic 2010a, 2014, 2015a), their functionality will likely be compromised in case of design-level or beyond-design-level earthquake that may generate excessive residual drifts. Presently, there is no validated, quantitative approach for estimating a bridge's capacity to function after an earthquake in the presence of residual drifts due to the difficulty of accurately predicting the residual drifts. A recent blind prediction contest of a full-scale modern reinforced concrete bridge column, where professionals and researchers were invited to predict column response for a set of ground motions, revealed the tremendous scatter in predictions of basic response quantities, where residual drifts, compared to the other response quantities, were predicted with the largest average error, 74% (Terzic et al. 2015). Even the contest winner predicted the residual drifts poorly, with an average error of about 60% (Qu 2012). Following the contest, several other research investigations were conducted to propose an analytical model for bridge columns, and while the proposed models were successful in predicting basic response quantities (e.g., displacements, accelerations, forces), they were unable to accurately predict the residual drifts (e.g., Tazarv and Saiidi 2013; Moshref et al. 2015; Moharrami and Koutromanos 2017).

To evaluate the post-earthquake functionality of the bridge, which is the level of traffic that can safely pass over the bridge, it is necessary to define distinct functionality limit states representative of different possible traffic load scenarios on the bridge. Mackie and Stojadinovic (2006) were the first to establish five traffic limit states: immediate access (100% of traffic volume), weight restriction (75% of traffic volume), only one lane open (50% of traffic volume), emergency access only (25% of traffic volume), and closed. The functionality state of a damaged bridge was then established from the levels of the remaining vertical and lateral load-carrying capacity of the bridge that were simply derived from pushunder and pushover analysis of the damaged bridge, without explicit consideration of the realistic residual drifts and traffic loading on the bridge. In 2012, DecRoches et al. proposed a new framework to evaluate overpass bridges' system-level post-earthquake functionality. Their framework considers four levels of traffic limit states including open to normal traffic, open to limited traffic, emergency vehicles only, and closed. The post-earthquake functionality (traffic) state of the bridge was simply established by directly mapping the damage state of the most severely damaged bridge component to the state of the entire bridge. While the mapping of the component damage onto the operational level of the bridge was aligned with the inspection/maintenance closure decisions and the guides for post-earthquake inspections employed by Caltrans, it was not founded on quantified links between component damage and bridge traffic capacity but instead on prescriptive links.

This study proposes a novel method for probabilistically evaluating the post-earthquake functionality state of the bridge by providing quantifiable links between earthquake intensity, component-level engineering demand parameters (EDPs), system-level traffic capacity, and the bridge's associated functionality state. To support the method, this research proposes an analytical model of bridge columns that accurately simulates the post-earthquake residual drifts and axial load-carrying capacity. The unique features of the proposed framework are its consideration of the post-earthquake residual drift of a bridge when evaluating the functionality state of the bridge and its direct evaluation of the post-earthquake traffic capacity of the bridge by considering realistic traffic load scenarios. The information on the post-earthquake functionality state of the bridge generated with the proposed method can be effectively used to support bridge maintenance decision-making processes by enabling an identification of retrofit needs that will generate long-term benefits to transportation agencies through reduced business interruptions.

II. Framework for Evaluating the Post-Earthquake Functionality of Modern Bridges

The overarching goal of this study is the development of a framework for evaluating the post-earthquake functionality of modern overpass bridges, which includes the development of two primary moduli schematically presented in Figure 1: (1) a bridge column model for evaluating post-earthquake residual drifts and axial load-carrying capacity, and (2) a method for evaluating post-earthquake bridge functionality.

Figure 1. Framework for Evaluating Overpass Bridges' Retrofit Needs

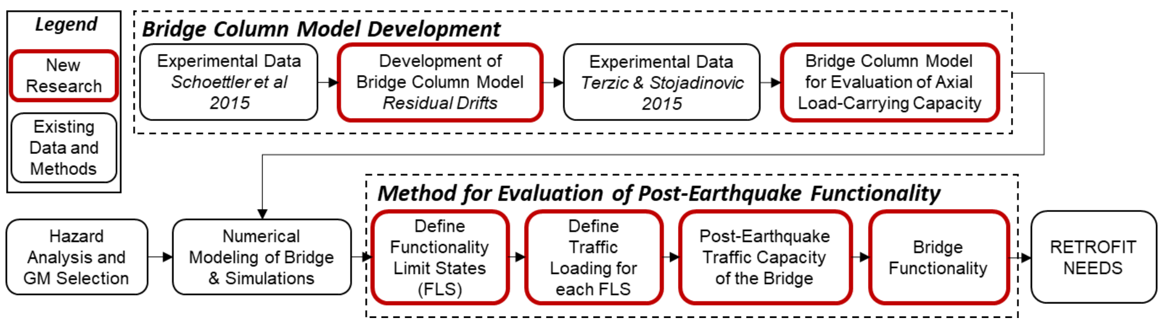

The development of a bridge column model for evaluating post-earthquake residual drifts and load-carrying capacity includes two phases. The first phase focuses on the development of a robust, high-fidelity analytical model of bridge columns to evaluate earthquake damage and the associated structural response with a particular emphasis on the accurate prediction of residual drifts. Experimental data provided by Schoetler et al. (2015) are used for the bridge column model development and calibration: these data originate from the most comprehensive experimental investigation to date of the seismic response of the full-scale modern bridge column. Importantly, the tested column experienced significant residual drifts during the earthquake shaking. The second phase expanded the bridge column model to simulate seismic responses to enable an evaluation of the axial load-carrying capacity of damaged columns. Experimental data provided by Terzic and Stojadinovic (2015a,b) from crushing tests on the columns with earthquake-induced damage are utilized to support this phase of the project.

The method for evaluating the post-earthquake functionality of a reinforced concrete highway overpass bridge includes several steps: (1) definition of the bridge's functionality limit states (FLSs), (2) establishment of traffic load scenarios that correspond to different FLSs, (3) method for directly evaluating post-earthquake traffic capacity, and (4) method for evaluating post-earthquake functionality through comparing traffic capacity with traffic demand. The main outcome of the method is a reliable assessment of the probability that a traffic loading associated with each functionality limit state of the bridge can be safely accommodated following an earthquake event.

The information on the post-earthquake functionality state of the bridge generated with the proposed framework can be used to facilitate decision-making processes by enabling identification of retrofit needs that will generate long-term benefits to transportation investments through reduced business interruptions.

III. Developing a High-Fidelity Model of a Bridge Column

To develop a bridge column model for evaluating a bridge's post-earthquake load-carrying capacity in the presence of residual drifts, the researchers used the publicly available computer software program OpenSees (McKenna 1997) and proceeded with two phases. The first phase focused on the development of a robust, high-fidelity analytical model for bridge columns to evaluate earthquake damage and the associated structural response with a particular emphasis on accurately predicting residual drifts. The second phase used the developed model of the bridge column to simulate seismic response so that the axial load-carrying capacity of damaged columns can be evaluated.

3.1 Column Model for Evaluating Residual Drifts

Experimental data provided by Schoetler et al. (2015) are used for the bridge column model development and calibration. These data are selected as they originate from the most comprehensive experimental investigation of the seismic response of the full-scale modern bridge column to date. Importantly, the tested column experienced significant residual drifts during the earthquake shaking. The data are acquired from the web-based database DesignSafe.

In Schoetler et al. (2015), the tested column was detailed according to Caltrans' Seismic Design Criteria (2006) and Bridge Design Specifications (2004). The 1.22-m (4-ft) diameter cantilever column spanned 7.31 m (24 ft) above the footing. To mobilize its capacity during shake table tests, a large concrete block weighing 2.32 MN (521.9 kips) was cast on the top of the column. With a height-to-diameter aspect ratio of six, the test specimen was intended to respond in the nonlinear range with predominantly flexural behavior. The test protocol included six consecutive earthquake simulations at targeted displacement ductilities of 1, 2, 4, 2, 8, and 4. Four historical earthquake recordings were selected as shake table input motions corresponding to the displacement ductilities of 1, 2, 4, and 8. Three input motions were selected from the 1989 Loma Prieta earthquake (Agnew State Hospital, Corralitos, and LGPC stations). The fourth record was from the Takatori station from the 1995 Kobe earthquake.

Schoetler et al. (2015) reported that in the first earthquake (EQ1), the column exhibited a fully elastic response. While the second earthquake (EQ2) initiated a nonlinear response, the plastic deformations were very small. The third earthquake (EQ3) was a representation of a design-level earthquake. In EQ3, the spalling of concrete was initiated and significant cracks developed, resulting in a residual drift ratio of -0.87%. The fourth earthquake (EQ4, a repeat of EQ2), which simulated an aftershock to EQ3, enlarged the regions of the spalled concrete caused by EQ3 while almost maintaining the residual drift ratio (-0.81%). The fifth earthquake (EQ5) was the strongest (beyond-design-level) earthquake and caused the spalled concrete to extend to 1.07 m (3.5 ft) above the column base. EQ5 generated a residual drift ratio of 1.43%, causing a total change in the residual drift ratio (relative to its initial position at the end of EQ4) of 2.24%. Finally, the last earthquake (EQ6) was a repeat of EQ3 (a design-level earthquake). It generated a residual drift ratio of 0.68%, causing a total change in the residual drift ratio (relative to its initial position at the end of EQ5) of -0.75%. Notice that this change in the residual drift ratio is comparable to the residual drift ratio of EQ3 (-0.87%).

To evaluate the uncertainty in predicting the seismic response of the full-scale bridge column, a blind prediction contest was organized by Terzic et al. (2015), where professionals and researchers were invited to predict column response for a set of ground motions. The contest results revealed the tremendous scatter in people's predictions of basic seismic response quantities, where the residual drifts compared to the other response quantities were predicted with the largest average error, 74%, across six consecutive earthquakes (Terzic et al. 2015). Even the contest winner predicted the residual drifts poorly, with an average error of about 60% (Qu 2012). Following the contest, several other research investigations were conducted to propose an analytical model for bridge columns, and while the proposed models were successful in predicting basic response quantities (e.g., displacements, accelerations, forces), they were unable to accurately predict the residual drifts (e.g., Tazarv and Saiidi 2013; Moshref et al. 2015; Moharrami and Koutromanos 2017).

The aim of the present study is to evaluate the capabilities of different element formulations and material models of OpenSees in predicting the seismic response of the full-scale bridge column. Furthermore, given that numerous past studies of bridge columns' seismic response have demonstrated the importance of the damping model for the accuracy of predictions (e.g., Qu 2012, Moshref et al. 2015, Jeong et al. 2008), this study also explores the effect of different damping model implementations. In sum, the authors conducted the parametric investigation considering different existing modeling approaches for bridge columns: (1) different numerical formulations of frame elements, (2) different material models for concrete and reinforcing steel, and (3) different damping model implementations. These parametric investigations highlight the capabilities and limitations of existing modeling approaches and yield recommendations for the nonlinear modeling of bridge columns.

Three different types of beam-column elements were considered in the parametric study: force-based element (FBE), displacement-based element (DBE), and beam-column element with distributed plastic hinges, designated in OpenSees as a beam with hinges element (BWHE). Two uniaxial material models were considered for modeling concrete: a Kent-Scott-Park model with no tensile strength and the same unloading and reloading paths, and a Kent-Scott-Park model with linear softening in tension and different unloading and reloading paths. Reinforcing steel was modeled with a Giuffre-Manegotto-Pinto model that has the same backbone curve in tension and compression and with a Mohle-Kunnath model with different backbone curves in tension and compression. To model viscous damping of the system, three implementations of the Rayleigh damping model were considered: damping matrix based on the initial stiffness (DM1), damping matrix based on the tangent stiffness with Rayleigh proportionality constants updated before each earthquake (DM2), and damping matrix based on the tangent stiffness with Rayleigh proportionality constants updated after each analytical step (DM3).

3.2 Numerical Formulations of Frame Elements Considered

The three elements considered in this study—FBE, DBE, and BWHE—all consider the spread of plasticity along the element or one of its parts. Although they are objective in predicting the hardening response, FBE and DBE are not objective in predicting the softening response. This is due to stress concentration either at the integration point (FBE) or the element (DBE). However, BWHE is capable of predicting the softening response. A comparison of these element formulations is provided by Terzic (2011).

The force-based beam-column element (FBE) is a line element based on the force or flexibility method (Taucer et al. 1991). It is discretized using the Gauss-Lobatto integration scheme with the integration points at the ends of the element and along the element length. Additional integration points along the length are used to improve the accuracy and computational stability of the element. Fiber cross-sections are assigned to the integration points. The cross-sections of the element are represented as assemblages of longitudinally oriented, unidirectional steel and concrete fibers. Each material in the cross-section has a uniaxial stress-strain relation assigned to it. The deformation compatibility of the cross-section fibers is enforced assuming that plane sections remain planar after deformation. In a flexibility-based formulation of this element, nodal loads imposed on the element ends are used to calculate axial force and moment distribution along the length of the element. Given the moment and axial load values at each integration point, the curvature and the axial deformation of a section are subsequently computed. Since the response of the cross-section fiber materials may be nonlinear, the deformation state determination of the cross-section may be iterative. The deformation of the element is finally obtained through weighted integration of the section deformations along the length of the element.

The displacement-based beam-column element (DBE) is a line element based on the displacement or stiffness method. It follows standard finite-element procedures where section deformations are interpolated from an approximate displacement field. Interpolation functions of conventional frame elements are based on a cubic Hermitian polynomial for the transverse displacement field and linear Lagrangian shape functions for the axial displacement field. This formulation results in constant axial strain and linear curvature along the element, which provides an exact solution only for a linear elastic prismatic beam element.

The beam with hinges element (BWHE) is an extension of the force-based element formulation where the locations and weights of integration points are based on the "plastic hinge integration," which allows for an explicit definition of plastic hinge lengths at the element ends (Scott and Fenves 2006). The element formulation includes six integration points: two for each plastic hinge and two for the interior portion of the element. To calculate element deformations from the sectional deformation, the element ends (i.e., plastic hinges) utilize two-point Gauss-Radau integration, and the interior of the element utilizes two-point Gauss integration. It is to be noted that the element implementation in OpenSees provides an opportunity to define the interior portion of the element as elastic or nonlinear.

3.3 Modeling the Fiber Section of the RC Column

To model the reinforced concrete section, the fiber section that accounts for the axial-bending interaction was divided into three parts: concrete cover, concrete core, and reinforcing steel. Fibers of the concrete cover (unconfined concrete) and concrete core (confined concrete) were modeled using two OpenSees uniaxial concrete material models, Concrete01 and Concrete02. Reinforcing steel fibers (longitudinal bars) were modeled using two OpenSees uniaxial material models, Steel02 and ReinforcingSteel. Transverse reinforcement was not modeled directly, but its effect was accounted for through the uniaxial stress-strain relationship of the confined concrete core assigned to core fibers (Mander et al. 1988).

The Concrete01 material model uses the Kent-Scott-Park model (Kent and Park 1971) to represent the stress-strain relationship of concrete under compression. The material model has degraded linear unloading-reloading stiffness (Karsan and Jirsa 1969) and no tensile strength. The Concrete02 material model is an extension of the Concrete01 material model and uses the Kent-Scott-Park model (Kent and Park 1971) to represent the stress-strain relationship of concrete under compression as well as a bilinear relationship to represent the stress-strain relationship in tension. Figure 2 compares the stress-strain response under the cycling loading of the two concrete materials.

Figure 2. Stress-Strain Response under Cyclic Loading (Computed using OpenSees Concrete01 and Concrete02 material models for concrete)

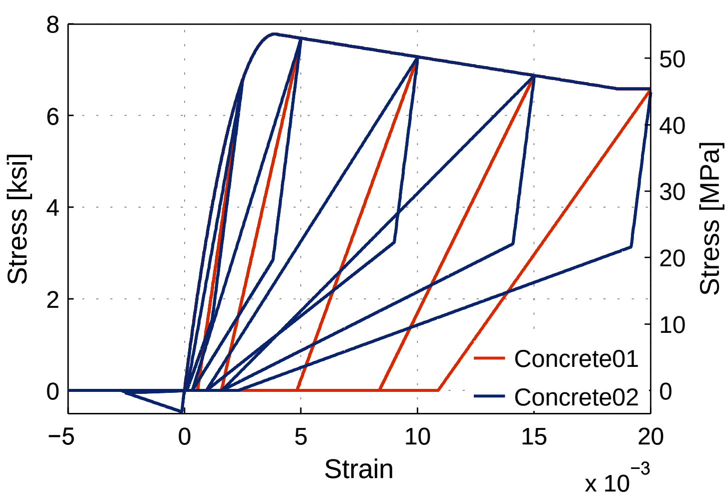

The Steel02 material model is defined using the Giuffre-Manegotto-Pinto uniaxial strain-hardening material model (Menegotto and Pinto 1973). The model has the same backbone curve in tension and compression. The backbone curve is a bilinear curve with a post-yield stiffness expressed as a fraction of the initial stiffness. The model accounts for the Bauschinger effect and is characterized by continuity in the tangent stiffness during loading and unloading.

The ReinforcingSteel material model uses a nonlinear backbone curve developed by Kunnath et al. (2009). To account for the change in area as the bar is stressed, the backbone curve is transformed from engineering stress space to natural space and is thus different in tension and compression. Figure 3 depicts the difference in the stress-strain response of the two steel materials for one cycle of loading.

Figure 3. Stress-Strain Response under Cyclic Loading (Computed using OpenSees Steel02 and ReinforcingSteel material models for reinforcing bars)

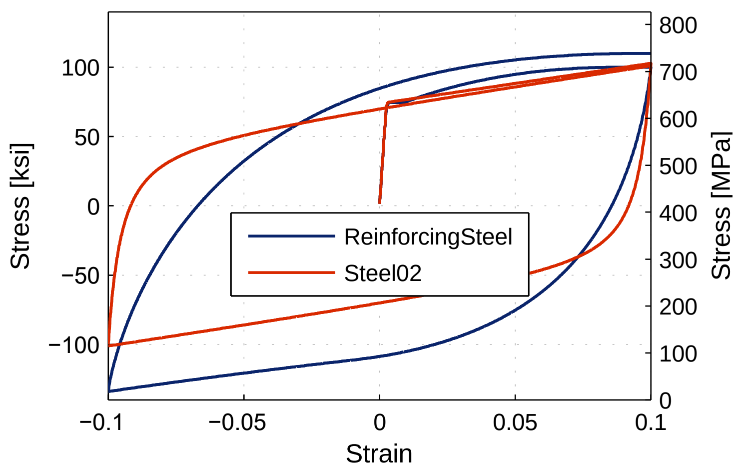

3.4 A Finite-Element Model of the Full-Scale RC Bridge Column and the Main Model Parameters Varied in the Study

To evaluate different modeling approaches, the full-scale bridge column is modeled with each of the three previously described finite-element types (FBE, DBE, and BWHE). All of the considered elements used the same fiber section, which was divided into three parts: concrete cover, concrete core, and reinforcing steel. The section was discretized as suggested by Terzic and Stojadinovic (2015a); the fiber section included 32 fibers for unconfined cover concrete, 152 fibers for confined core concrete, and 18 fibers for steel reinforcement. Fibers of the concrete cover and core were modeled with either Concret01 or Concrete02 uniaxial material model, and the reinforcing steel fibers were modeled with either Steel02 or ReinforcingSteel material. Transverse reinforcement was not modeled directly, but its effect was accounted for through the uniaxial stress-strain relationship of the confined concrete core (Mander et al. 1988) assigned to core fibers. The modeling parameters of these uniaxial materials were calibrated using concrete cylinder compression tests (Figure 4) and steel coupons pull-out tests (Figure 5), and details are provided in Table 1 through Table 4.

To account for the large concrete block at the top of the column, the block mass was assigned along the horizontal degree of freedom (in the direction of shaking), and the mass moment of inertia was assigned along the rotational degree of freedom. The weight of the concrete block was also assigned as a gravity load on the column. The response of the column was computed using nonlinear response analysis, Newton-Raphson integration algorithm, Newmark integrator (implying constant acceleration within a time step of the analysis), and corotational geometric transformation to account for geometric nonlinearity. Six ground motion records imposed on the column were applied consequently, one after another, preserving the damaged condition of the column for the subsequent earthquakes.

In the parametric study, the following parameters were varied: number of elements and number of integration points for FBE and DBE, and effective moment of inertia of the interior portion of the BWHE, which was modeled as elastic. Furthermore, to evaluate the effect of the damping model on the results, the three previously introduced damping models utilized damping ratios of 1%, 2%, and 3%, and they were considered to be either mass- and stiffness-proportional or only stiffness-proportional. For each case, the Rayleigh proportionality constants were calculated using the first and second period of vibration.

Figure 4. Calibration of the Unconfined Concrete Material using Data from the Compression Test of Concrete Cylinders; Calibration of Confined Concrete02 Material to Match the Slope of the Unconfined Concrete

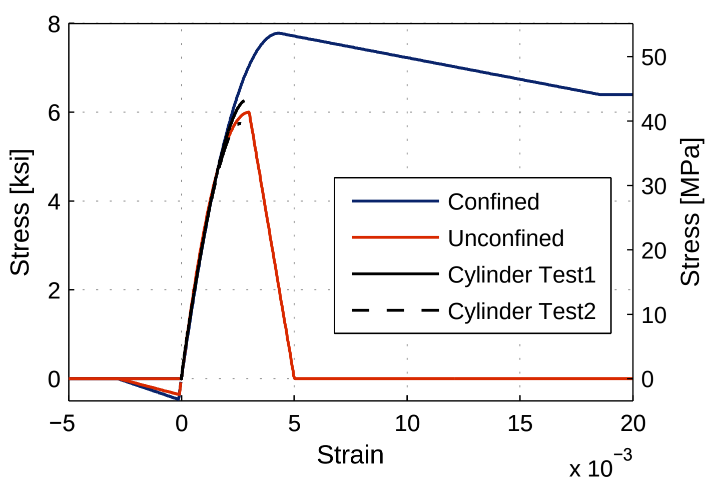

Figure 5. Calibration of the Steel02 and ReinforcingSteel Materials using Data from the Pull-Out Test of the Steel Coupons

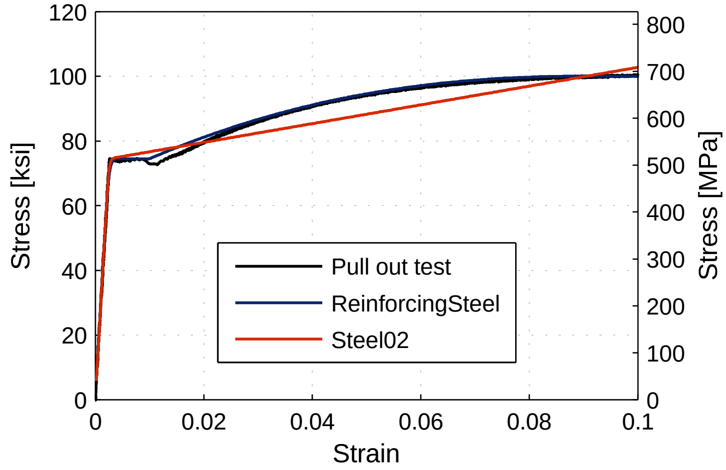

Table 1. Concrete01 Material Model Parameters

Material	f_c' [ksi]	ε_0	f_{cu}	ε_{cu}
Concrete cover	6.09[a]	$2f_c'/E_c$	0	0.005
Concrete core	f_{cc}'[b]	$2f_{cc}'/E_{cc}$	$0.2f_{cc}'$	ε_{cu}[c]

Note: E_c, E_{cc} = initial moduli of elasticity (calibrated to match test results of concrete cylinders); f_c' = compressive strength of concrete; ε_0 = concrete strain at maximum strength; f_{cu} = concrete crashing strength; ε_{cu} = concrete strain at crushing strength

[a] From test results on concrete cylinders; [b] Mander et al. (1988); [c] Terzic and Stojadinovic (2015)

Table 2. Concrete02 Material Model Parameters

Material	f_c' [ksi]	ε_0	f_{cu}	ε_{cu}	λ	f_t	E_{ts}
Concrete cover	6.09[a]	$2f_c'/E_c$	0	0.005	0.1	$0.05f_c'$	f_t/ε_0
Concrete core	f_{cc}'[b]	$2f_{cc}'/E_{cc}$	$0.2f_{cc}'$	ε_{cu}[c]	0.1	$0.05f_{cc}'$	f_t/ε_0

Note: E_c, E_{cc} = initial moduli of elasticity (calibrated to match test results of concrete cylinders); f_c' = compressive strength of concrete; ε_0 = concrete strain at maximum strength; f_{cu} = concrete crashing strength; ε_{cu} = concrete strain at crashing strength; λ = ratio between unloading slope at ε_{cu} and initial slope; f_t = tensile strength of concrete; E_{ts} = slope of the tension softening branch

[a] From test results on concrete cylinders; [b] Mander et al. (1988); [c] Terzic and Stojadinovic (2015)

Table 3. Steel02 Material Model Parameters

Material	f_y [ksi]	E_s [ksi]	b	R_0	c_{R1}	c_{R2}
Steel02	74.5[a]	29,000	0.01	15	0.925	0.15

Note: f_y = yield stress in tension; E_s = modulus of elasticity; b = strain hardening ratio; R_0, c_{R1}, c_{R2} = parameters that control the transition from elastic to plastic branches of the hysteretic curve
[a] From test results on steel coupons

Table 4. ReinforcingSteel Material Model Parameters

Material	f_y [ksi]	E_s [ksi]	f_{su} [ksi]	E_{sh}[ksi]	ε_{sh}	ε_{su}
ReinforcingSteel	74.5[a]	29,000	100[a]	725[a]	0.01[a]	0.09[a]

Note: f_y = yield stress in tension; E_s = modulus of elasticity; f_{su} = ultimate stress in tension; E_{sh} = tangent at initial strain hardening; ε_{sh} = strain corresponding to initial strain hardening; ε_{su} = strain at peak stress
[a] From test results on steel coupons

3.5 Parametric Study Results

While the prediction of the post-earthquake residual drift ratios was of the utmost importance in this phase of the research, the parametric study also aimed at developing modeling recommendations to predict the peak seismic drift ratios and accelerations, since they directly relate to the column deformations and forces. The parametric study had several stages; in one stage only one set of parameters (e.g., material models) was varied, while in the other, modeling parameters were fixed (e.g., element models and damping models). The seismic responses generated by varying the selected set of parameters, as well as the parameters that predicted the seismic response with the highest accuracy, were passed to the next stage of the parametric study. The accuracy of the seismic response predictions was judged by comparing the average prediction errors across a set of ground motions. For each earthquake imposed on the column, errors in predicting the positive and negative peaks (i.e., peaks in each direction of shaking) for the response quantity of interest were included when calculating the average error.

The parametric study included the following stages.

- ***Stage 1*: Selection of material models.** Different material models for concrete and reinforcing steel were evaluated while modeling the column with four DBEs where each element had three integration points. Damping was modeled with DM3 using a damping ratio of 2% and stiffness-proportional Rayleigh damping. The material models that predicted the seismic response of the column with the highest accuracy were selected and used in Stage 2.

- *Stage 2*: **Selection of element parameters.** Modeling parameters associated with different element formulations were explored while utilizing the concrete and reinforcing steel material models selected in Stage 1. Damping was modeled with DM3 using a damping ratio of 2% and stiffness-proportional Rayleigh damping. An optimal set of element parameters was selected for every element type considered and used in Stage 3 of the parametric study.
- *Stage 3*: **Selection of damping model parameters.** Different damping model implementations were explored for each element type, and the models that predicted the seismic response of the column with the highest accuracy were selected as the final damping models. Finally, three finite-element models of the bridge column were created using different element formulations (FBE, DBE, and BWHE).
- *Stage 4*: **Comparison of the simulation results for the three finite-element models.** The results of the response history analysis for the set of six consecutive ground motions, generated with three different finite-element models, were compared. Final modeling recommendations were formulated as part of this phase.

Response Predictions Considering Different Material Models

To evaluate different material models' capabilities to accurately predict the seismic response of the bridge column, four analytical models were created (designated as Analytical 1 through Analytical 4). Table 5 shows the concrete and reinforcing steel material models used for each of the analytical models. In this stage of analysis, the column was modeled with four DBEs, where each element had three integration points. Damping was modeled with DM3 using a damping ratio of 2% and stiffness-proportional Rayleigh damping.

Table 5. Analytical Models based on the Material Selection for Concrete and Reinforcing Bars

Material	Analytical 1	Analytical 2	Analytical 3	Analytical 4
Concrete model	Concrete01	Concrete01	Concrete02	Concrete02
Reinforcing steel model	Steel02	ReinforcingSteel	Steel02	ReinforcingSteel

Figure 6 compares the peak positive and negative experimental and simulated drift ratios and accelerations, highlighting the residual drifts (shown in white) after each of the simulated earthquakes. The results presented show the comparable ability of the considered material models in predicting peak drift ratios and accelerations. However, the analytical models that utilize ReinforcingSteel material to model reinforcing steel (Analytical 2 and Analytical 4) are better at predicting the residual drifts than the models that use the Steel02 material model (Analytical 1 and Analytical 3); the difference in prediction of residual drifts is especially noticeable for the first design-level earthquake (EQ3) and its aftershock (EQ4). While analytical models that use ReinforcingSteel generate a similar prediction of drift ratio, the model that used the Concrete02 material model to model concrete is somewhat better at predicting the acceleration. Therefore, ReinforcingSteel is selected for modeling reinforcing bars, and Concrete02 is selected for modeling concrete.

Figure 6. Comparison of Peak Positive and Negative Experimental and Simulated Responses using DBE, DM3, and Different Material Models for Reinforcing Steel and Concrete

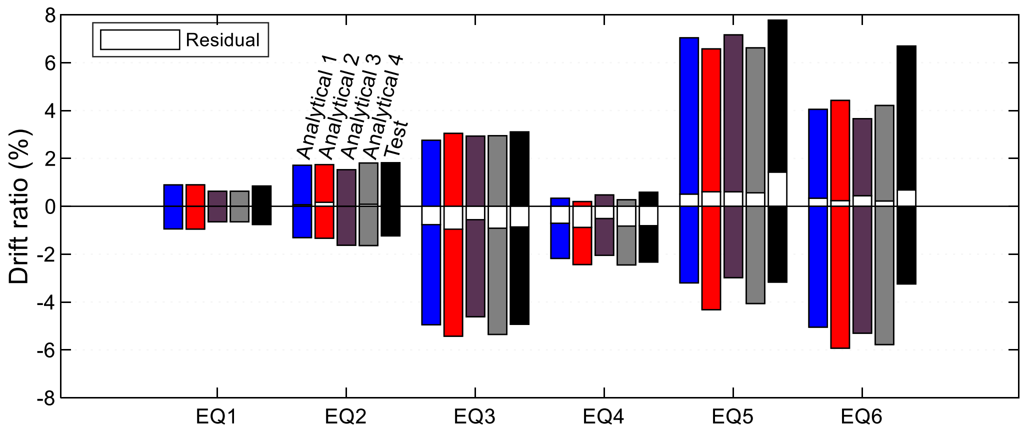

(a) Drift Ratio

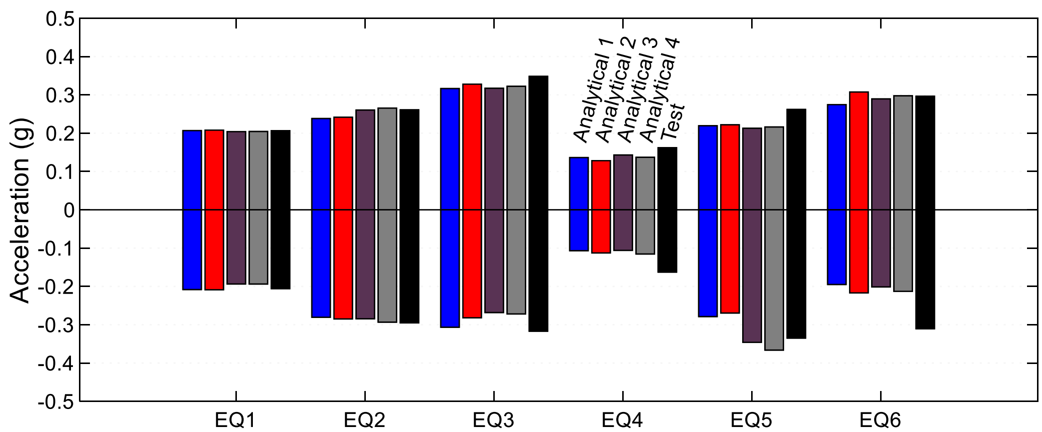

(b) Acceleration

Response Predictions Considering Different Element Types

In this stage of the parametric study, the number of elements and the number of integration points are varied for FBE and DBE, and the effective moment of inertia of the interior portion of the column is varied for the BWHE, which was modeled as elastic. Modeling parameters associated with different element formulations are explored while utilizing the Concrete02 and ReinforcingSteel material models. Damping is modeled with DM3 using a damping ratio of 2% and stiffness-proportional Rayleigh damping.

To evaluate the effect of the modeling parameters on the accuracy of prediction, the average error is calculated at different stages of the experiment: (1) after the first two earthquakes, when the column had very small plastic deformations, (2) after the first four earthquakes, at which point the column has experienced significant damage and has had a noticeable residual drift, and (3) at the end of the entire testing protocol that included six earthquakes, after the fifth earthquake has induced the largest damage and residual drifts. In this way, the researchers traced the accumulation of error in predicting the column response with the increase of shaking intensity.

Figure 7 shows the average error for the DBE modeled with 2, 4, 8, 12, and 16 elements with either 3 or 5 integration points at different stages during the experiment. The results show that if the number of elements used to model the DBE is larger than 4, irrespective of the number of integration points, the simulated seismic responses of the column after the first two earthquakes are about the same (Figure 7a). However, for the higher intensities of shaking that induce significant column damage and residual drifts, the DBE model with 4 elements and 3 integration points simulates the column response the most accurately. While this model provides sufficient accuracy in predicting the seismic response up to design-level earthquakes (Figure 7b), its accuracy in predicting the column's seismic response for a beyond-design-level earthquake is not adequate (Figure 7c).

Figure 8 shows the average error for the FBE modeled with 1, 2, 4, and 8 elements with either 3 or 5 integration points at different stages during the experiment. The results presented show almost equal accuracy in simulating the seismic responses when the element parameters are varied for small intensities of shaking (EQ1 and EQ2; Figure 8a). However, for the higher shaking intensities that induce significant column damage and residual drifts, the FBE model with 2 elements and 5 integration points simulates the column response the most accurately. While this model provides sufficient accuracy in predicting the seismic response up to design-level earthquakes (Figure 8b), its accuracy in predicting the column's seismic response for a beyond-design-level earthquake is not adequate (Figure 8c).

Figure 9 shows the average error for the BWHE, modeled with different effective moments of inertia of the interior portion of the column, ranging from 0.2 to 0.7 times the column cross-section's moment of inertia. The presented results show that the accuracy of the predicted results greatly depends on the effective moment of inertia, where its optimal values change with the increase of shaking intensity. These results indicate the need for a more sophisticated model that utilizes BWHE, where the effective moment of inertia is updated after each earthquake to properly model the state of the interior portion of the column. Therefore, an additional analysis was conducted to identify the optimal values of effective moments of inertia of the interior portion of the column for each earthquake. The following values were found to produce the best accuracy: 0.65 for EQ1, 0.5 for EQ2, 0.33 for EQ3 and EQ4, 0.25 for EQ5, and 0.2 for EQ6. The results indicate a notable reduction of the effective moment of inertia of the interior portion of the column after every earthquake.

Figure 7. The Average Error in Predicting Drift Ratio, Acceleration, and Residual Drift with DBE Modeled with Different Numbers of Elements and Integration Points

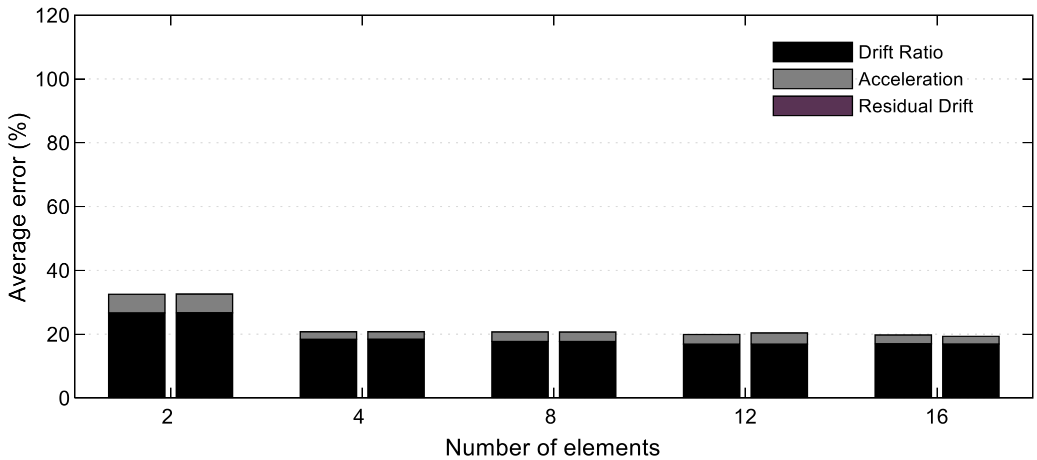

(a) First Two Earthquakes

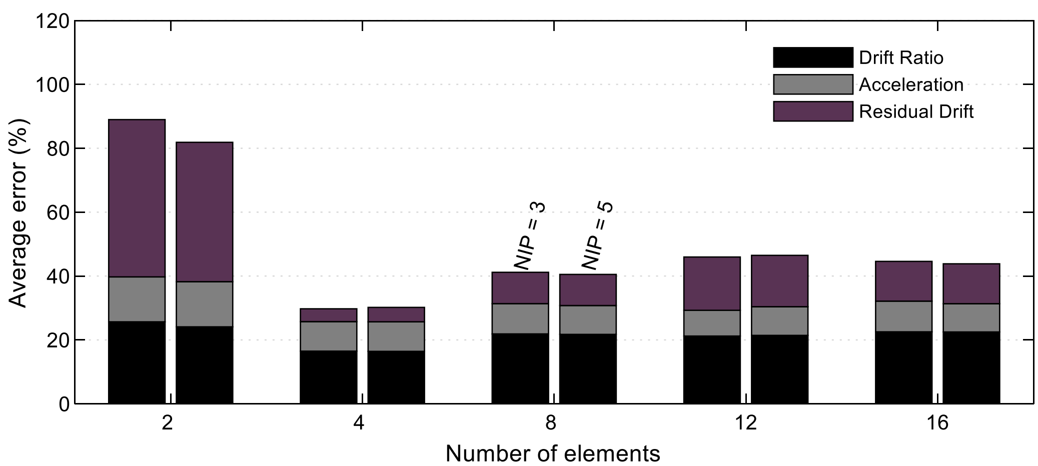

(b) First Four Earthquakes

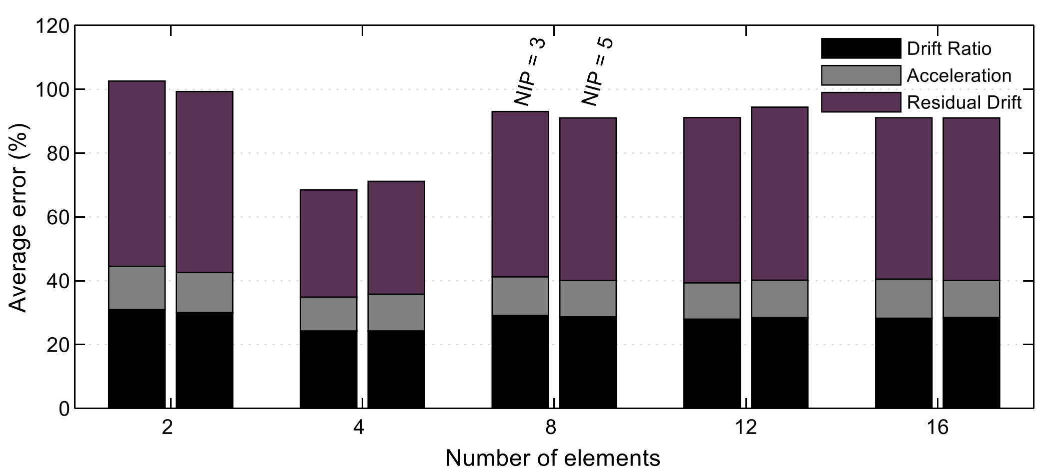

(c) All Six Earthquakes

Figure 8. The Average Error in Predicting Drift Ratio, Acceleration, and Residual Drift with FBE Modeled with Different Numbers of Elements and Integration Points

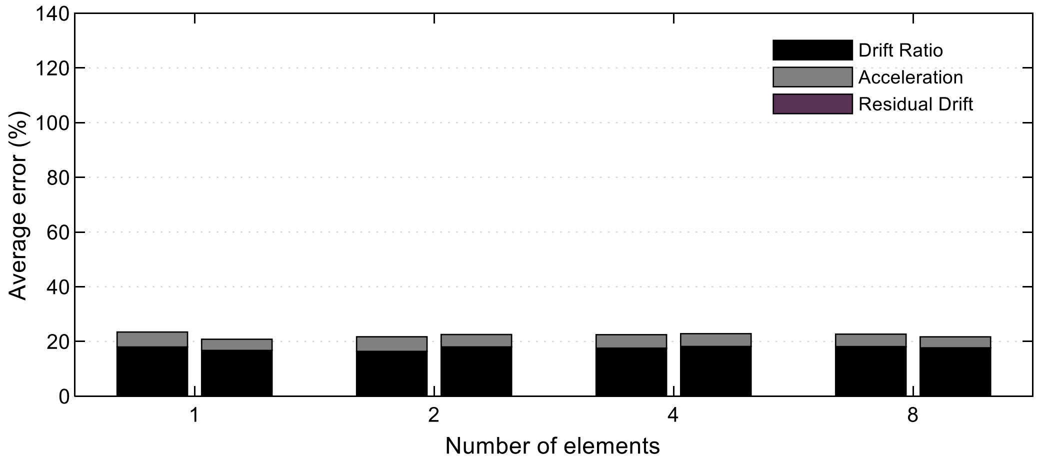

(a) First Two Earthquakes

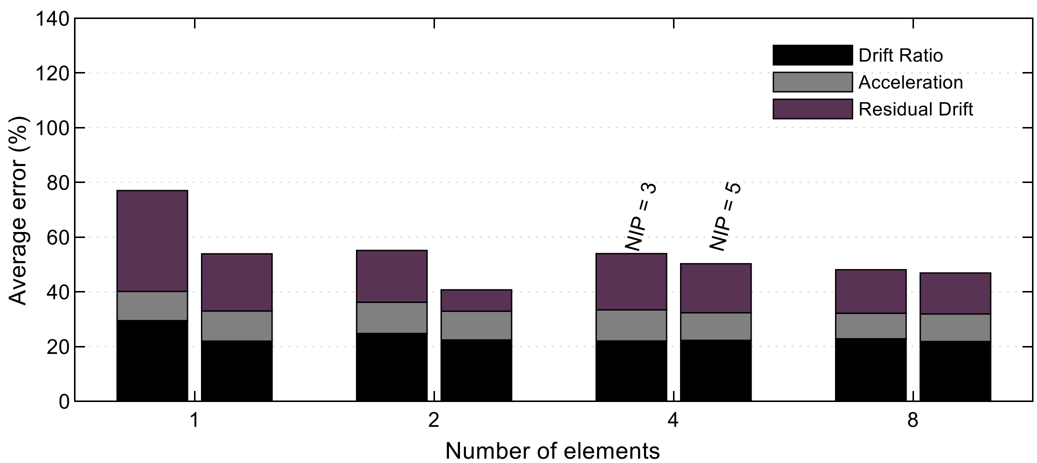

(b) First Four Earthquakes

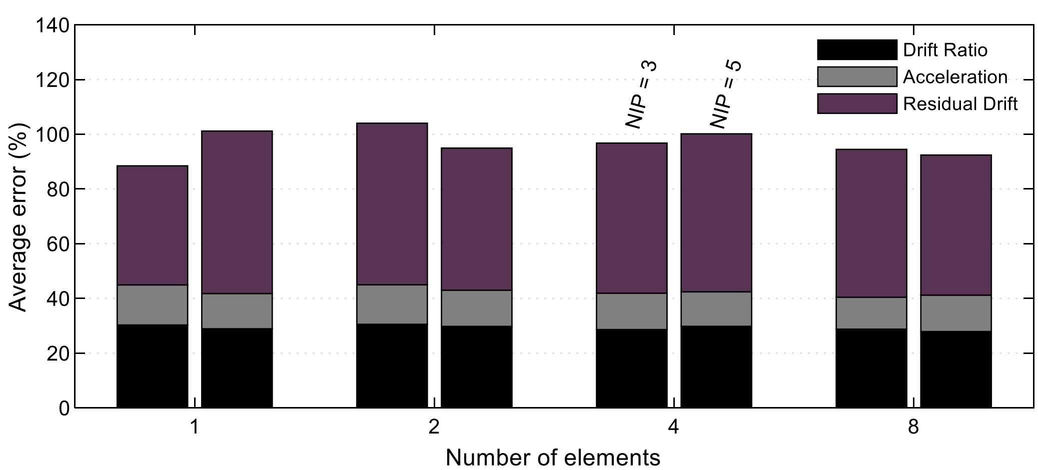

(c) All Six Earthquakes

Figure 9. The Average Error in Predicting Drift Ratio, Acceleration, and Residual Drift with BWHE Considering Different Effective Moments of Inertia of the Interior (Elastic) Portion of the Column

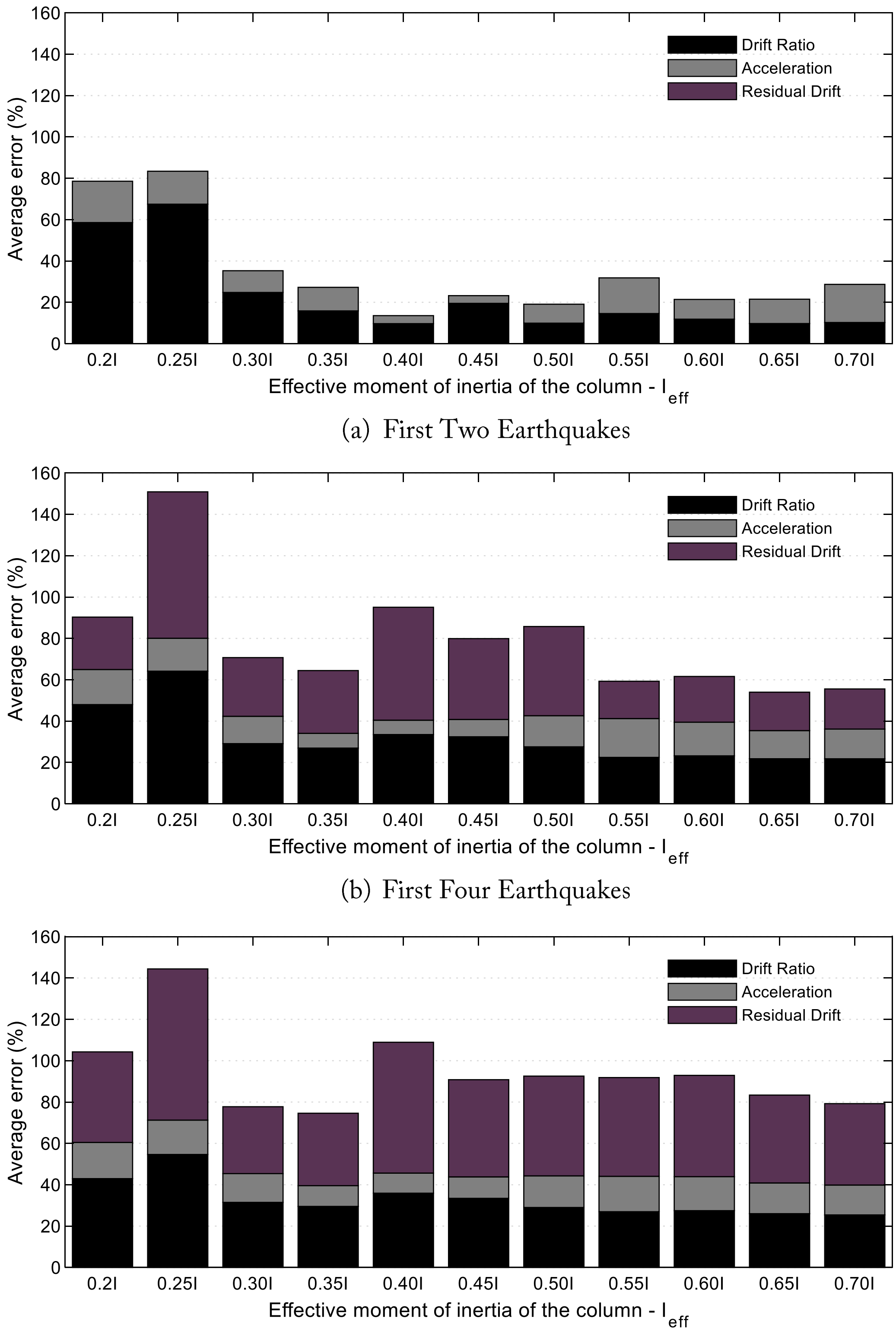

(a) First Two Earthquakes

(b) First Four Earthquakes

(c) All Six Earthquakes

Response Predictions Considering Different Damping Models

In this stage of the parametric study, different damping model implementations were explored for each element type. To model viscous damping of the system, the authors considered three implementations of the Rayleigh damping model: damping matrix based on the initial stiffness (DM1), damping matrix based on the tangent stiffness with Rayleigh proportionality constants updated before each earthquake (DM2), and damping matrix based on the tangent stiffness with Rayleigh proportionality constants updated after each step of the analysis (DM3). Furthermore, each of these damping model implementations was tested by assigning the damping ratios of 1%, 2%, or 3%, and by modeling damping as either stiffness-proportional (designated as "Kprop") or mass- and stiffness-proportional (designated as "MKprop"). The Concrete02 and ReinforcingSteel material models were used to model concrete and reinforcing steel, respectively. The DBE element was modeled with four elements and three integration points; the FBE element was modeled with two elements and five integration points. The interior portion of BWHE was modeled with the following values of the effective moment of inertia: 0.65 for EQ1, 0.5 for EQ2, 0.33 for EQ3 and EQ4, 0.25 for EQ5, and 0.2 for EQ6.

Average errors at different stages of the experiment are provided for DBE in Figure 10 for the "Kprop" damping model and Figure 11 for the "MKprop" damping model, for FBE in Figure 12 for the "Kprop" damping model and Figure 13 for the "MKprop" damping model, and for BWHE in Figure 14 for the "Kprop" damping model and Figure 15 for the "MKprop" damping model. Observations common to all three element types are as follows.

- The accuracy of the predicted seismic responses changes significantly with the change of the damping model parameters.
- "MKprop" damping model provides higher accuracy in predicting the column seismic response than "Kprop."
- DM2 and DM3 (which are based on tangent stiffness) provide significantly higher accuracy in the prediction of the column seismic response than DM1 (which is based on the initial stiffness).
- Damping ratios of 1% and 2% generate smaller errors than a damping ratio of 3%.
- The smallest error is generated by DM3 with a damping ratio of 1%, where Rayleigh damping is modeled as mass- and stiffness-proportional (i.e., "MKprop").

Comparing the capabilities of three finite-element models of the bridge column which utilize different element types and the most accurate damping model (DM3, "MKprop" with a damping ratio of 1%), the following is observed.

- FBE and DBE predict the column response with comparable accuracy. While they predict the column responses with sufficient accuracy up to the design-level earthquake, their accuracy in predicting the column's seismic response beyond the design-level earthquake is not adequate.

- BWHE predicts the column response with sufficient accuracy at all intensities of shaking.

Figure 10. The Average Error in Predicting Drift Ratios, Accelerations, and Residual Drifts with DBE Considering Different Damping Models that Utilize Damping Ratios of 1%, 2%, and 3% and "Kprop" Implementation

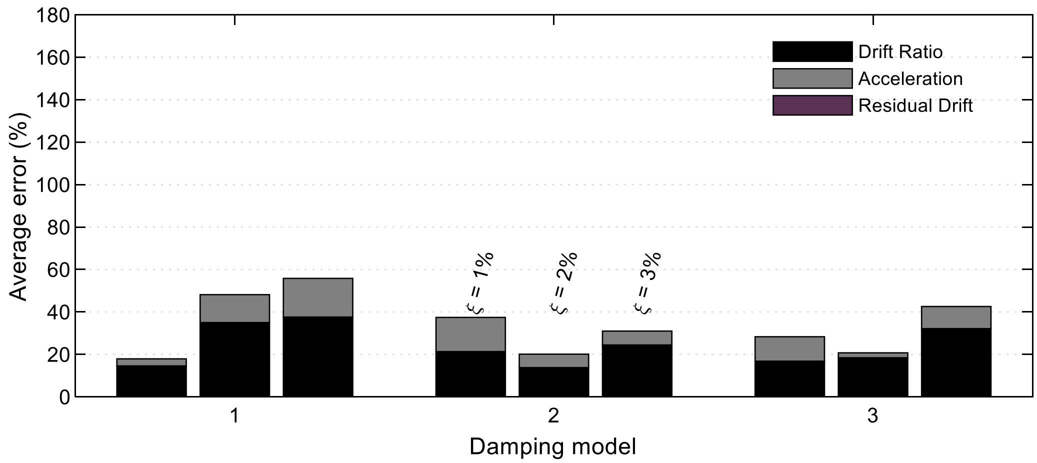

(a) First Two Earthquakes

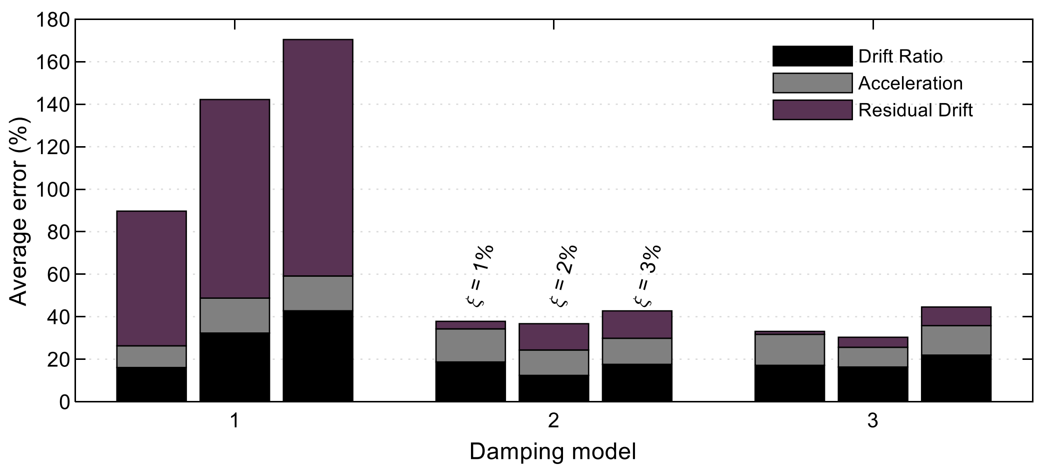

(b) First Four Earthquakes

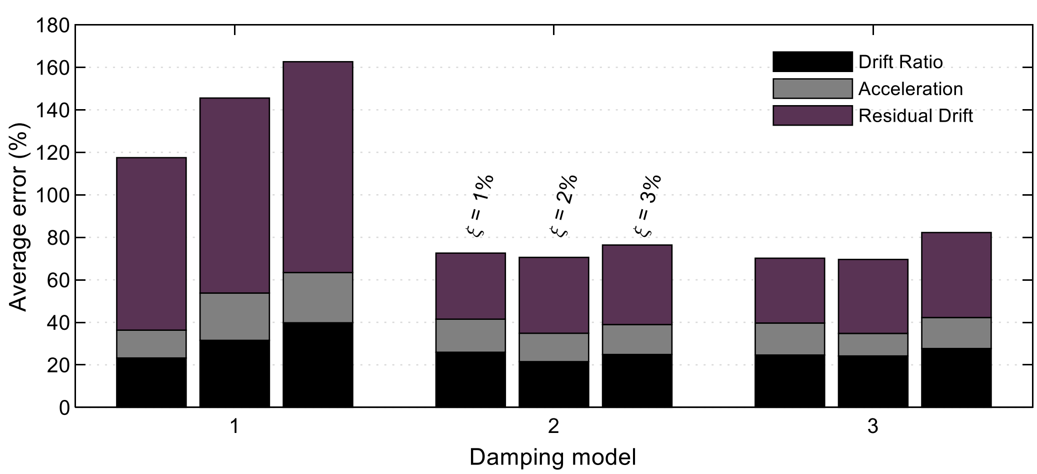

(c) All Six Earthquakes

Figure 11. The Average Error in Predicting Drift Ratios, Accelerations, and Residual Drifts with DBE Considering Different Damping Models that Utilize Damping Ratios of 1%, 2%, and 3% and "MKprop" Implementation

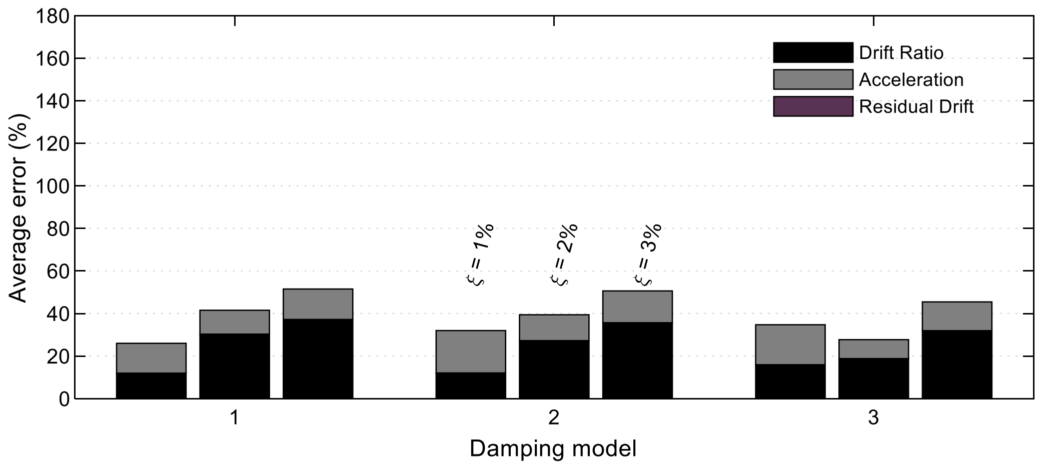

(a) First Two Earthquakes

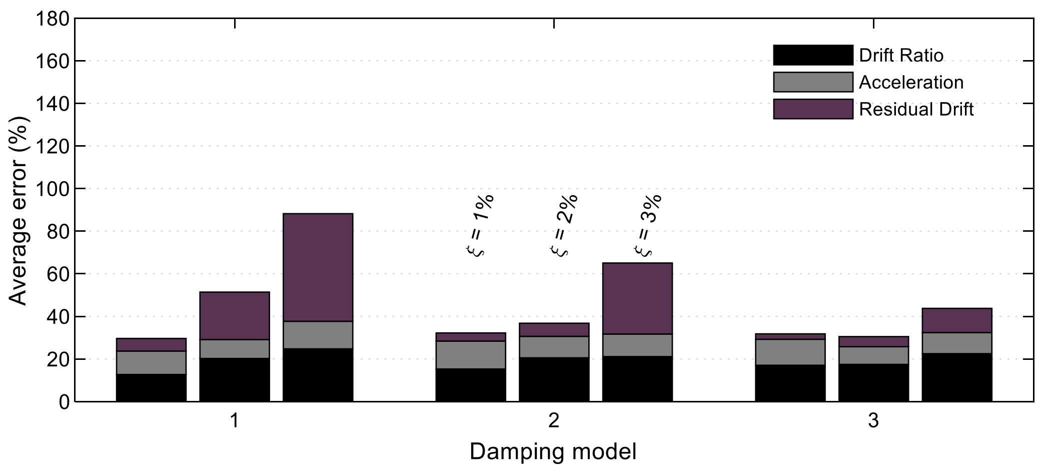

(b) First Four Earthquakes

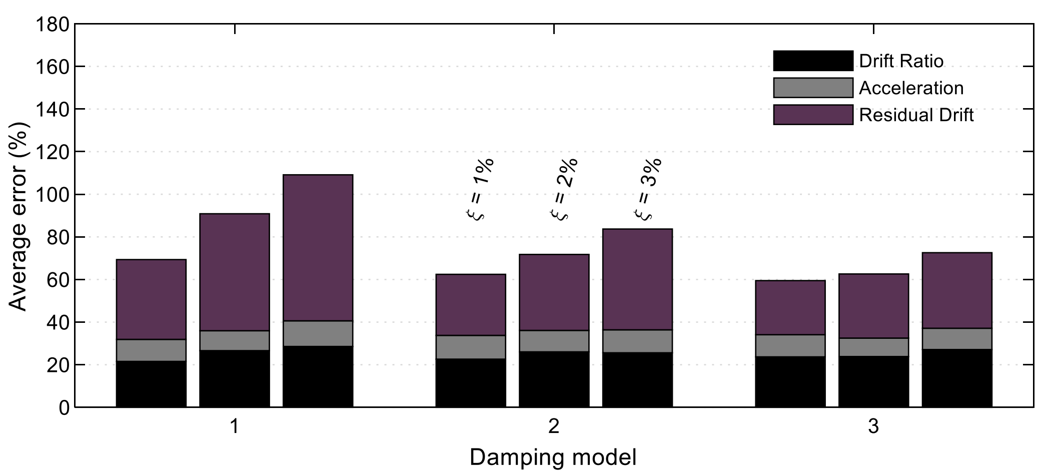

(c) All Six Earthquakes

Figure 12. The Average Error in Predicting Drift Ratios, Accelerations, and Residual Drifts with FBE Considering Different Damping Models that Utilize Damping Ratios of 1%, 2%, and 3% and "Kprop" Implementation

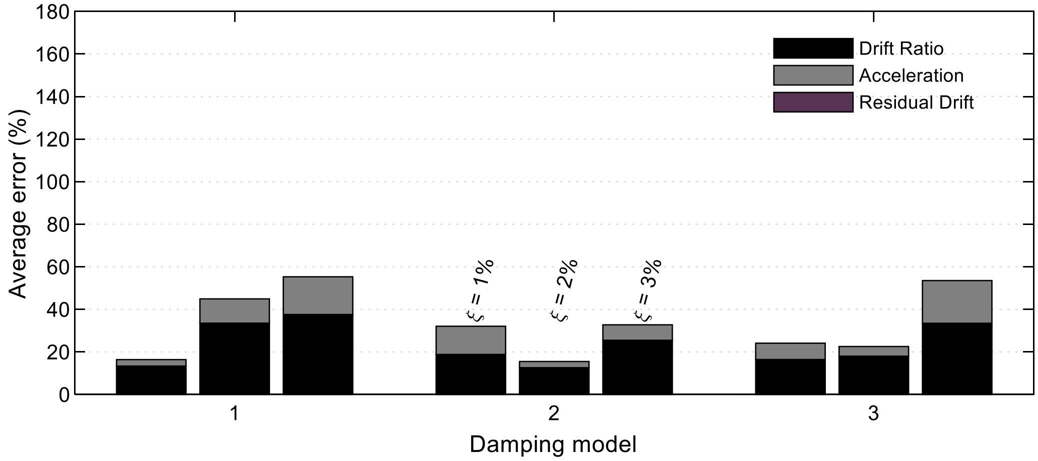

(a) First Two Earthquakes

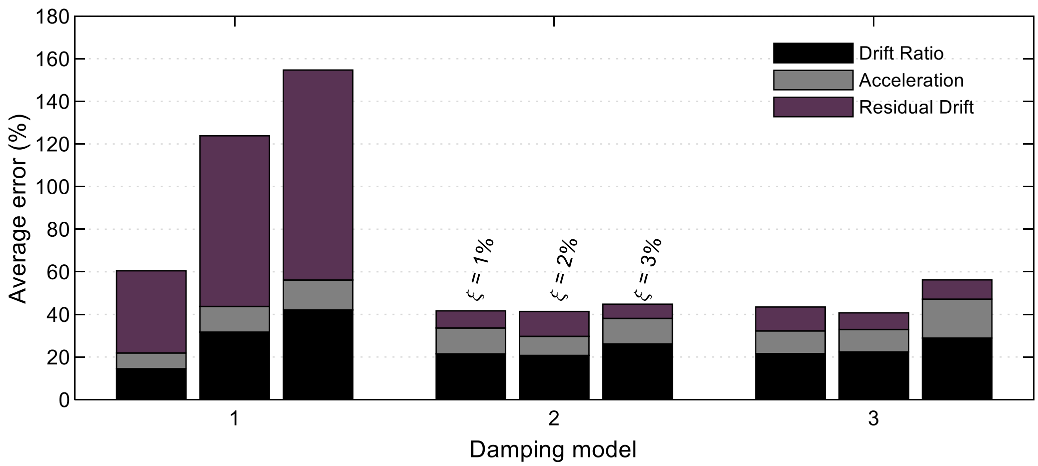

(b) First Four Earthquakes

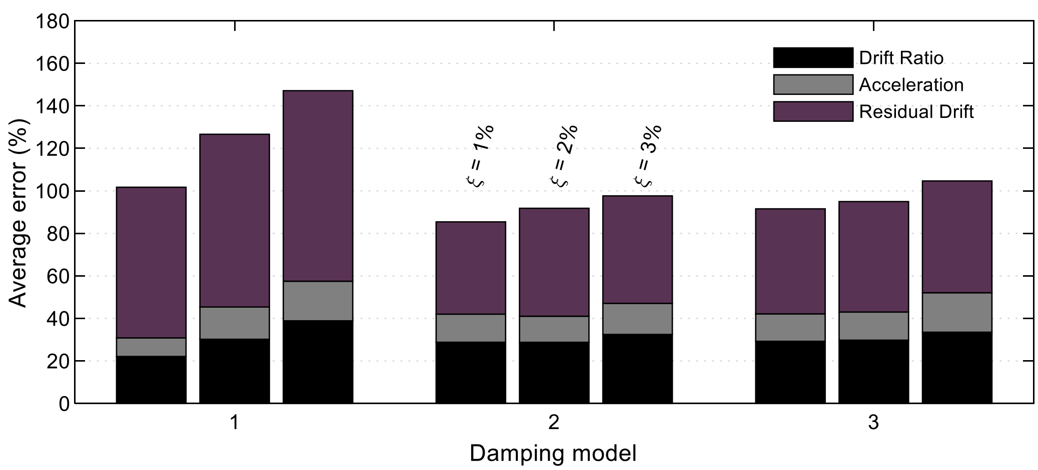

(c) All Six Earthquakes

Figure 13. The Average Error in Predicting Drift Ratios, Accelerations, and Residual Drifts with FBE Considering Different Damping Models that Utilize Damping Ratios of 1%, 2%, and 3% and "MKprop" Implementation

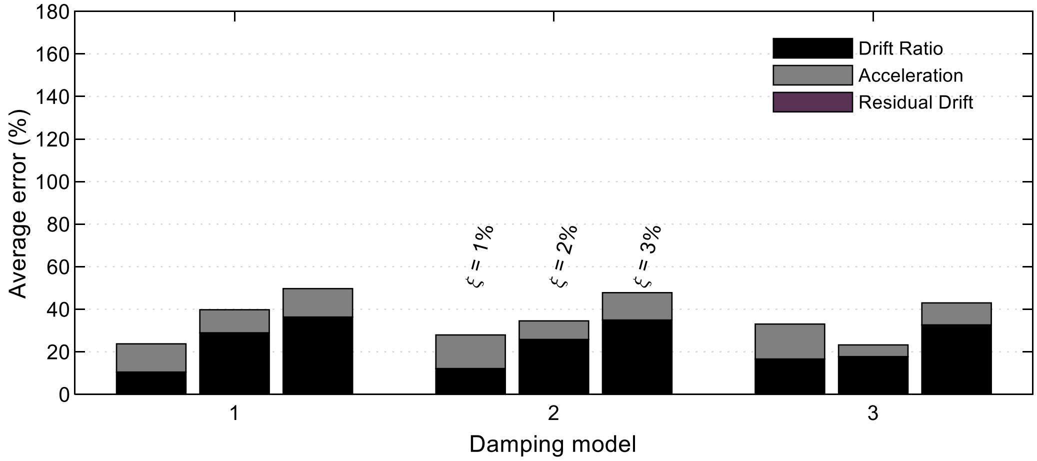

(a) First Two Earthquakes

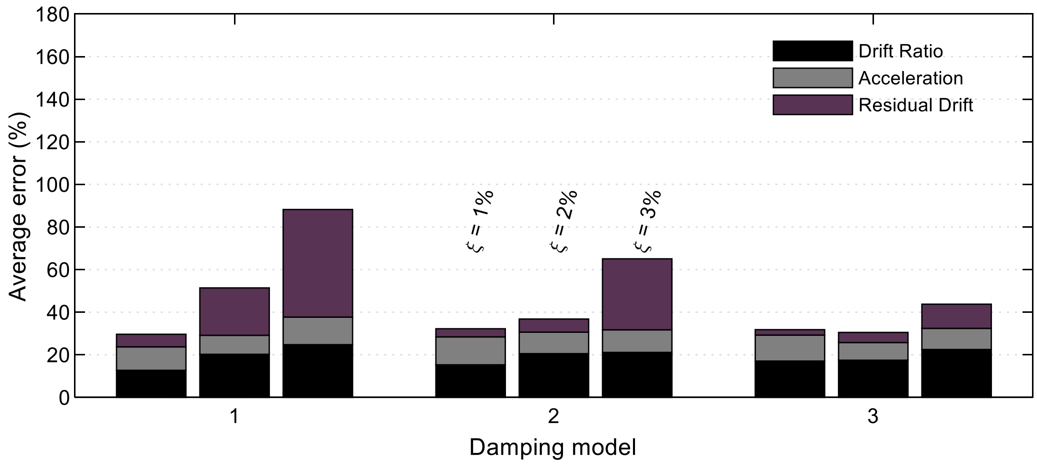

(b) First Four Earthquakes

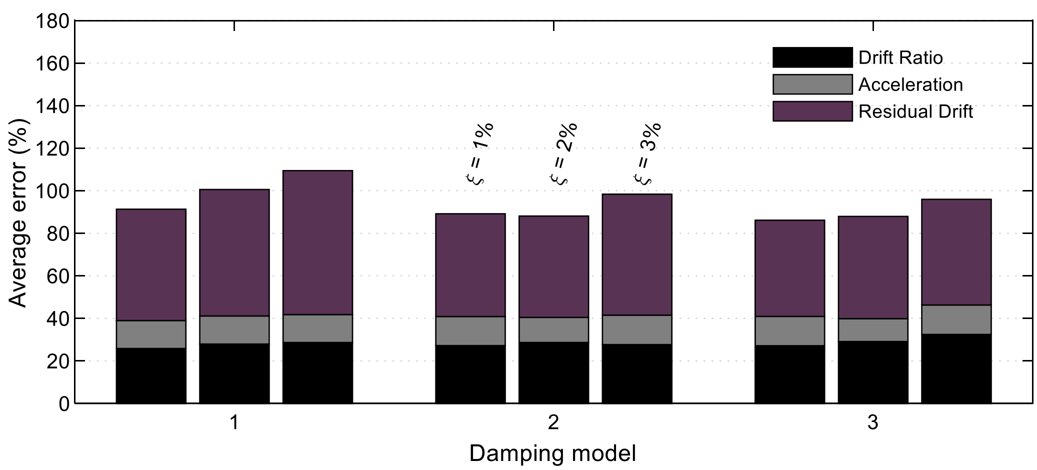

(c) All Six Earthquakes

Figure 14. The Average Error in Predicting Drift Ratios, Accelerations, and Residual Drifts with BWHE Considering Different Damping Models that Utilize Damping Ratios of 1%, 2%, and 3% and "Kprop" Implementation

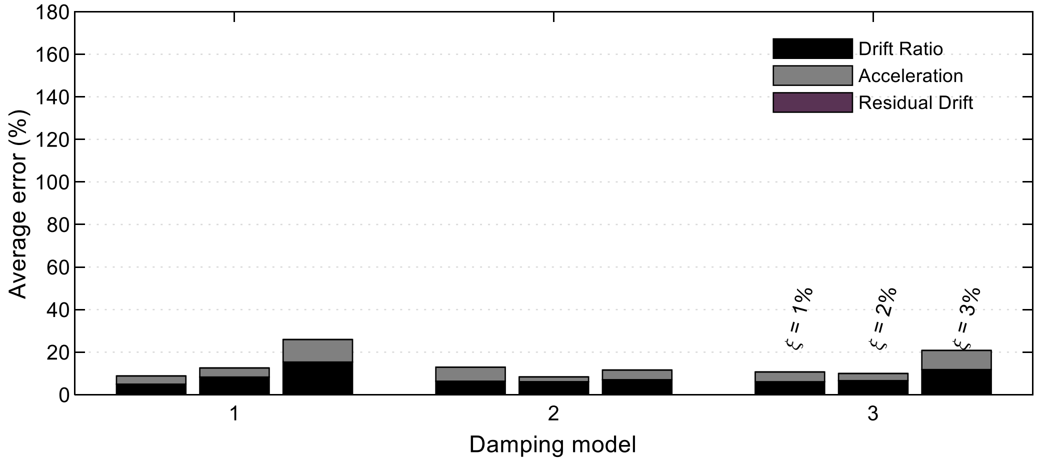

(a) First Two Earthquakes

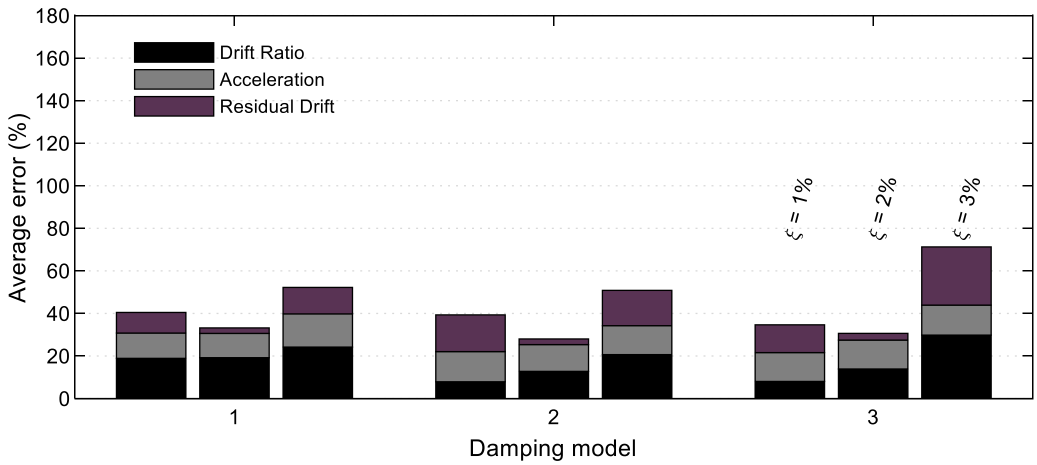

(b) First Four Earthquakes

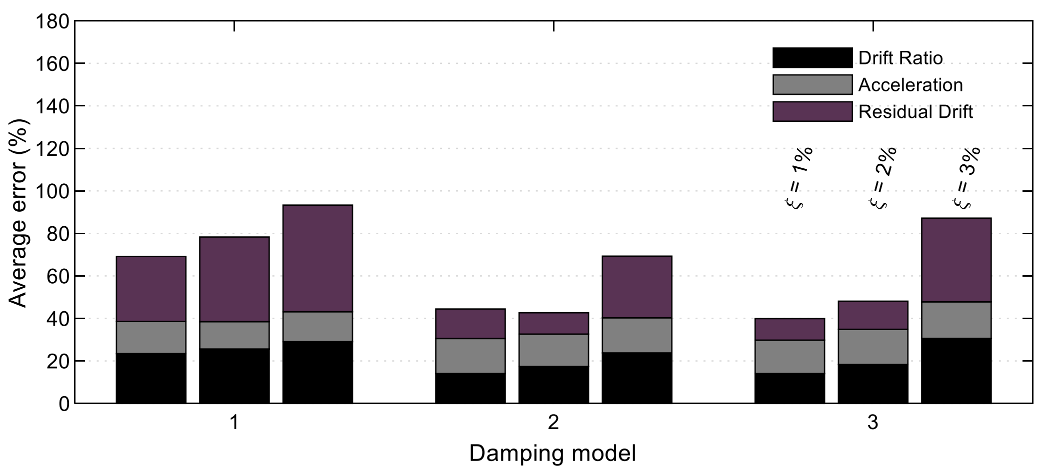

(c) All Six Earthquakes

Figure 15. The Average Error in Predicting Drift Ratios, Accelerations, and Residual Drifts with BWHE Considering Different Damping Models that Utilize Damping Ratios of 1%, 2%, and 3% and "MKprop" Implementation

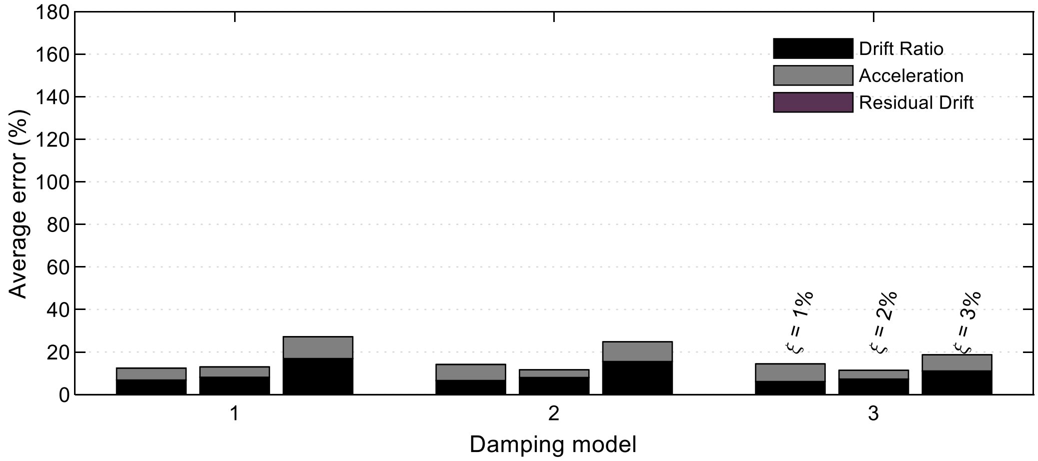

(a) First Two Earthquakes

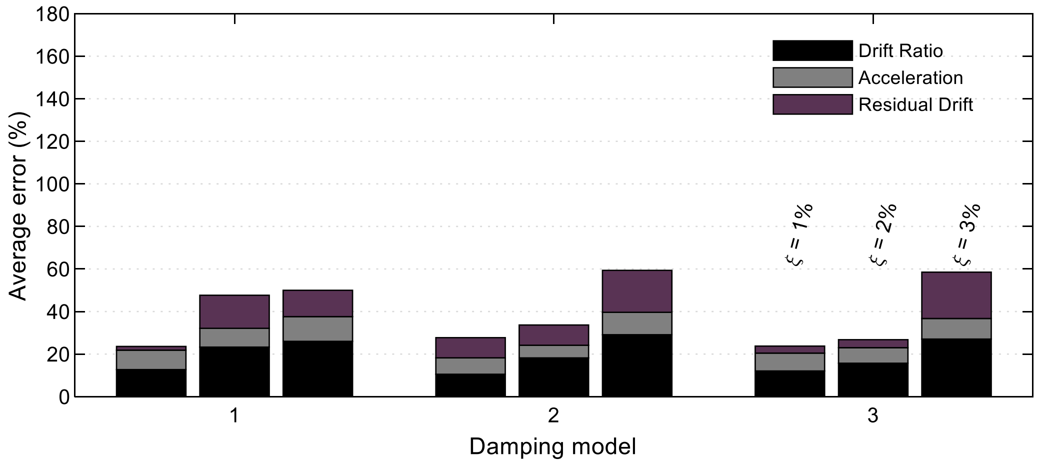

(b) First Four Earthquakes

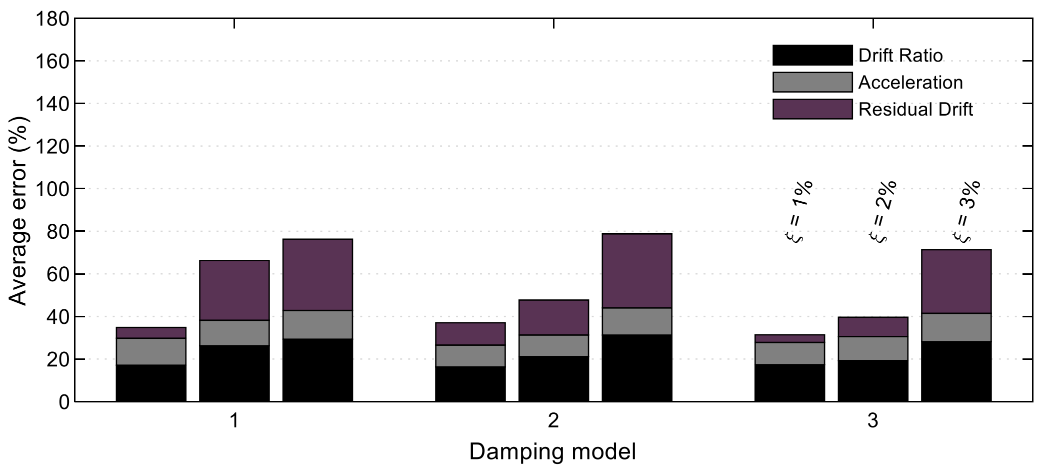

(c) All Six Earthquakes

3.6 Seismic Responses Predicted with Finite-Element Models of the Bridge Column that Utilize Different Element Formulations

Using the experimental data, the research team calibrated three finite-element models of the bridge column utilizing different element formulations, namely FBE, DBE, and BWHE. All finite-element models utilized the same material models and a damping model. Concrete02 was used to model the concrete material, and ReinforcingSteel was used to model the reinforcing bars. The material model parameters were derived from the compression cylinder tests of concrete and pull-out tests of the reinforcing bar coupons. Damping was modeled with mass- and stiffness-proportional Rayleigh damping using the damping ratio of 1%, the first two modes of vibration, and the tangent stiffness of the column that was updated at every step of the analysis. The DBE element was modeled with 4 elements and 3 integration points; the FBE element was modeled with 2 elements and 5 integration points. The interior portion of BWHE was modeled with the following values of the effective moment of inertia expressed as a ratio to the total moment of inertia: 0.65 for EQ1, 0.5 for EQ2, 0.33 for EQ3 and EQ4, 0.25 for EQ5, and 0.2 for EQ6.

Figure 16 compares the peak positive and negative experimental and simulated drift ratios, residual drift ratios, and accelerations, considering different column models. While the three models predict the column responses with comparable accuracy up to EQ4, BWHE predicts the column responses at EQ5 and EQ6 with higher accuracy than FBE and DBE. Furthermore, Figure 17 shows drift ratio histories, and Figure 18 shows acceleration histories for six consecutive earthquakes predicted with the three finite-element models of the bridge column. The simulated response histories compare well with the experimental data, especially in the case of BWHE, demonstrating high fidelity of the finite-element models considered. Due to its capability of predicting softening responses, BWHE predicts residual drifts accurately at all levels of shaking, which yields a more accurate prediction of drift ratio histories for a beyond-design-level earthquake (EQ5) and for a repeated design-level earthquake (EQ6).

Figure 16. Comparison of Peak Positive and Negative Experimental and Simulated Responses Considering Different Column Models

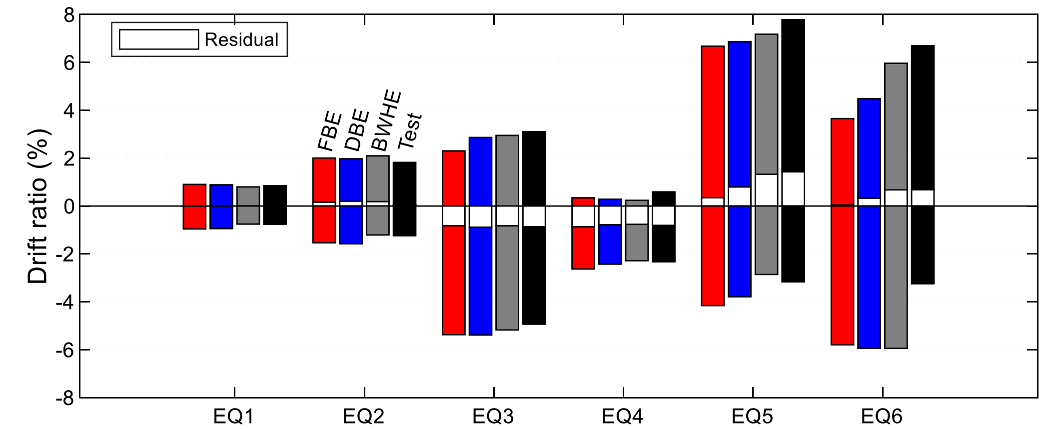

(a) Drift Ratios

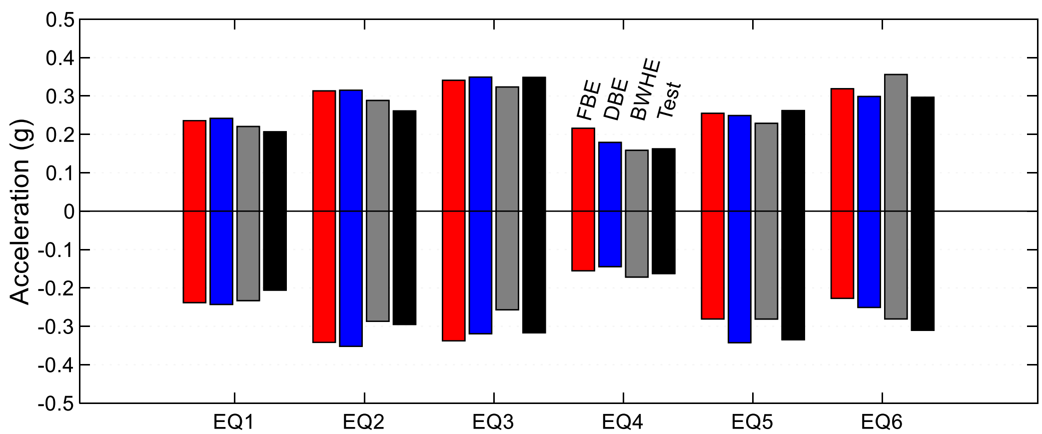

(b) Accelerations

Figure 17. Comparison of Experimental and Simulated Drift Ratio Histories (Finite-Element Model) for FBE, DBE, and BWHE

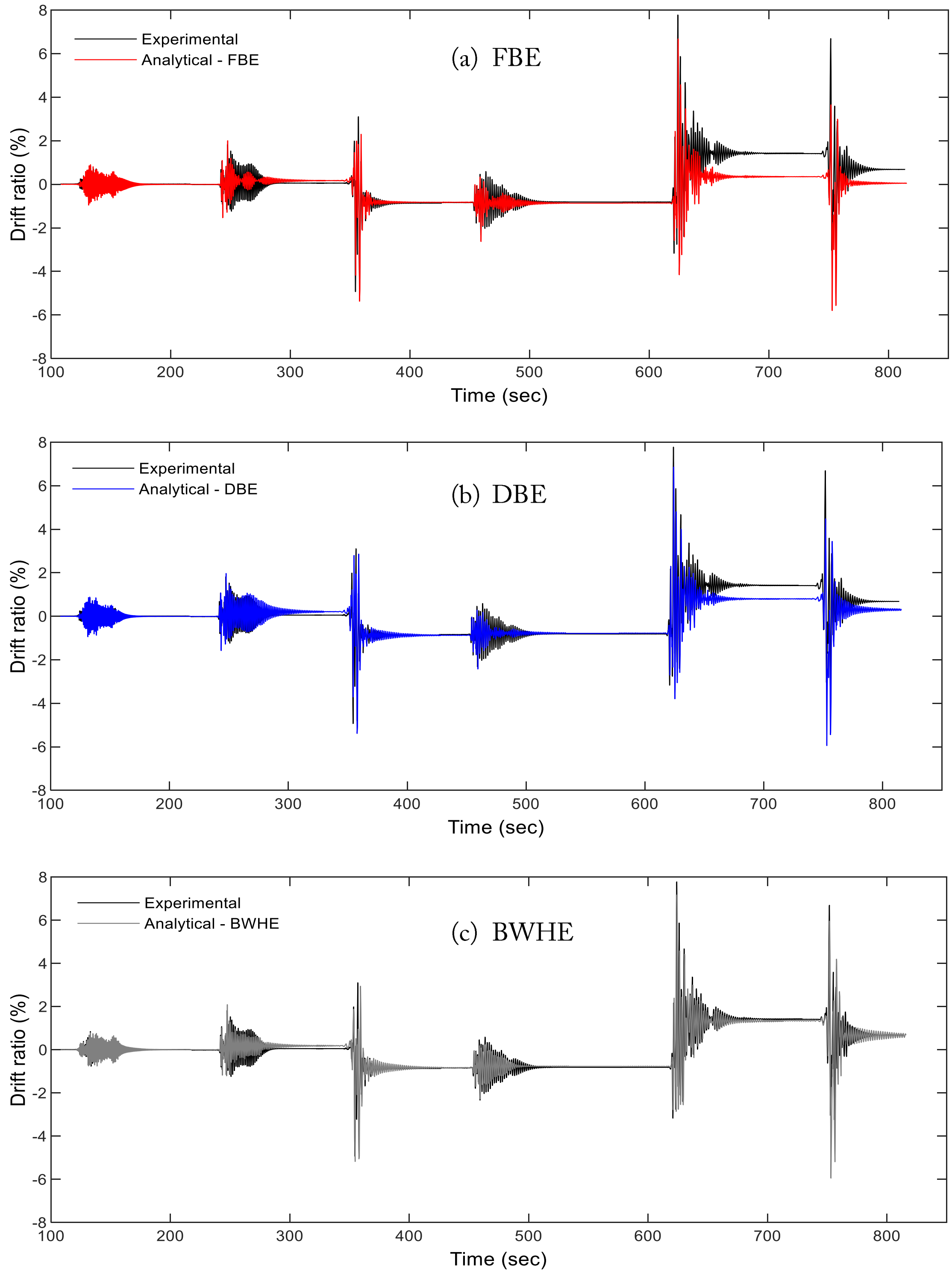

Figure 18. Comparison of Experimental and Simulated Acceleration Histories (Finite-Element Model) for FBE, DBE, and BWHE

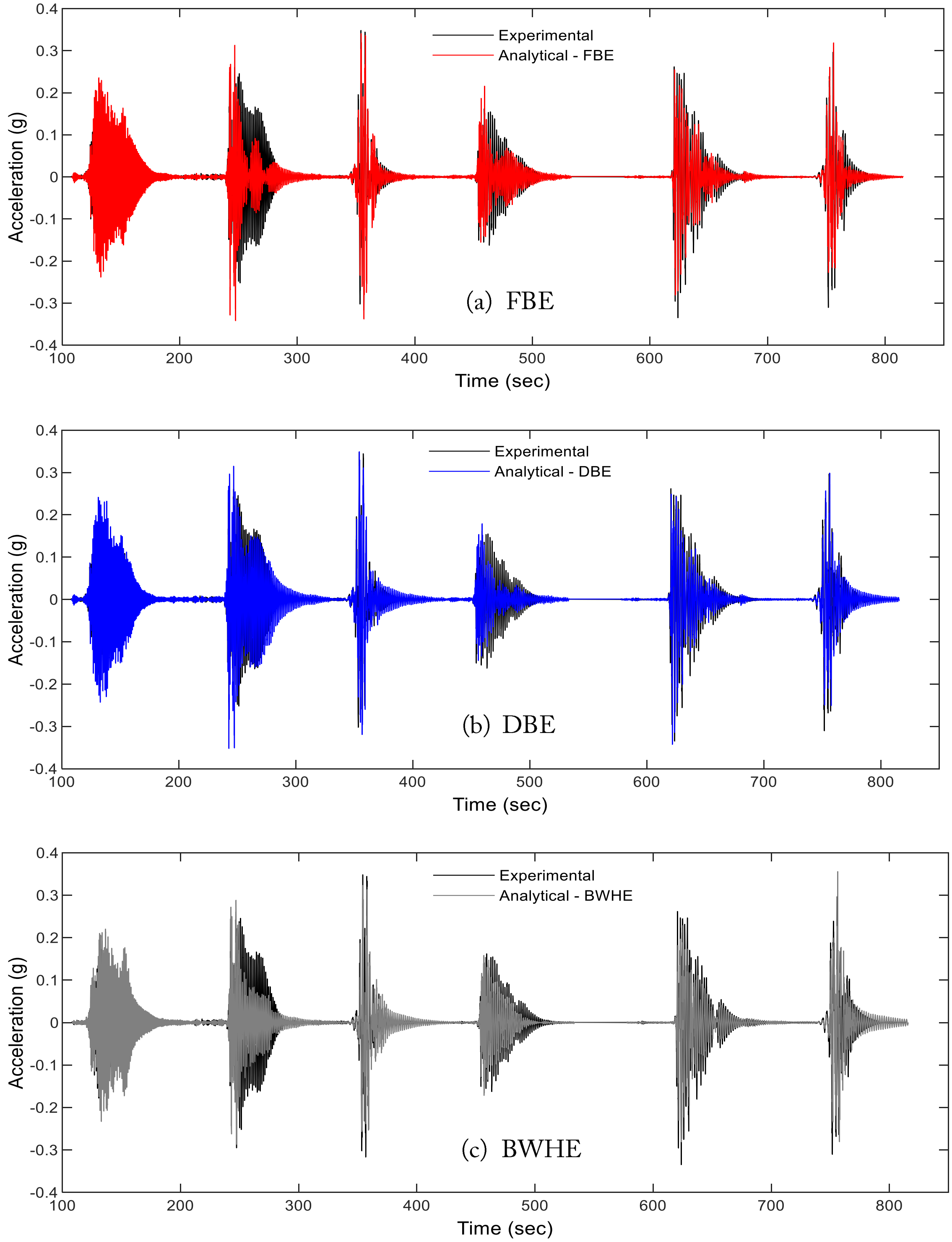

3.7 Column Model for Evaluating Post-Earthquake Axial Load-Carrying Capacity

The model developed to simulate the seismic response of the bridge column is expanded to enable an evaluation of the axial load-carrying capacity of damaged columns. Experimental data provided by Terzic and Stojadinovic (2015a,b) from the crushing tests on the columns with earthquake-induced damage are used to support this phase of the project.

Terzic and Stojadinovic (2015a,b) conducted a research program to investigate the relationship between earthquake-induced damage in reinforced concrete bridge columns and the axial capacity of the columns in their damaged condition. Their experimental program comprised quasi-static cyclic tests and monotonic axial load tests. In the first stage of Terzic and Stojadinovic's experimental program, three column specimens were tested by applying a bidirectional quasi-static incremental lateral displacement protocol with circular orbits of displacement up to the predetermined displacement ductility targets of 1.5, 3, and 4.5. In the second stage of their testing procedure, an undamaged column specimen and the three damaged specimens (with no permanent drifts) were subjected to a monotonically increasing axial force up to failure. The specimens are listed in Table 6.

Table 6. Test Matrix (Terzic and Stojadinovic, 2015a)

Specimen Designation	Ductility Target	Test Sequences
Base0	0	Axial
Base15	1.5	Lateral and axial
Base30	3.0	Lateral and axial
Base45	4.5	Lateral and axial

Based on the test results, Terzic and Stojadinovic (2015b) provided recommendations for modeling the axial load capacity of damaged columns using the ReinforcingSteel material model for reinforcing bars, the Concrete02 material model for concrete core and cover, and a force-based beam-column element (FBE) for the bridge column. The first phase of the present research has demonstrated the limitations of an FBE model in adequately simulating peak drift ratios and residual drift ratios in the case of a beyond-design-level earthquake (Figure 17b). Moreover, the present study also demonstrates that BWHE can simulate residual and story drifts with sufficient accuracy even in the case of beyond-design-level earthquakes (Figure 17c). Therefore, this phase of development of the analytical model of a bridge column aimed at evaluating the capability of BWHE to predict the axial load capacity of a damaged bridge column.

To support the present study, BWHE utilized the same material models for concrete and reinforcing bars as FBE (presented in Terzic and Stojadinovic 2014). However, the interior portion of the BWHE element is modeled as elastic, where the modulus of elasticity of the interior portion of the element is calibrated from the axial test of the undamaged column specimen (Base0) to match the slope of the axial force-displacement curve. The effective moment of inertia of the interior portion of BWHE was calibrated from the lateral-load tests. It was determined that the effective moments of inertia, expressed as a ratio to the total moment of inertia, I, are 0.30 for the Base15 test and 0.35 for the Base30 and Base45 tests. These values of the effective moment of inertia align well with Caltrans SDC (2013) recommendations.

The experimental protocol used by Terzic and Stojadinovic (2015a) included many cycles of loading prior to the first yield of reinforcement (especially for Base15), generating numerous micro-cracks. To simulate the pre-yield response of the column with the FBE (which utilizes the same nonlinear cross-section across the entire element height), Terzic and Stojadinovic (2015a) demonstrated that it was necessary to reduce the modulus of elasticity of concrete to adequately capture the column stiffness. However, to capture the pre-yield stiffness of the column utilizing BWHE, the present study determined that the nonlinear plastic hinges shall be modeled using the experimentally observed modulus of elasticity of concrete, and the interior portion of the column (which is modeled as elastic) shall be modeled with the effective (reduced) moment of inertia to account for cracking of concrete prior to the yielding of steel. Figure 19, Figure 20, and Figure 21 show the lateral force-displacement response curves of the tested specimens and the analytically simulated column responses (FBE and BWHE) for the three quasi-static tests: Base15, Base30, and Base45, respectively. Responses obtained with FBE and BWHE agree well with the experimental results.

Furthermore, Terzic and Stojadinovic (2015a) found out that the post-peak degrading stiffness of confined concrete core has significant influence on the accuracy in predicting the axial load capacity of damaged columns. They also reported that the post-peak degrading stiffness depends on the modeling approach used. Therefore, this study has calibrated the post-peak degrading stiffness for the BWHE that utilizes ReinforcingSteel and Concrete02 material models and has determined that the post-peak degrading slope of confined concrete of $0.05E_{cc}$ provides the highest accuracy in predicting the axial load capacity of damaged columns (Figure 22).

The calibrated column model that utilizes BWHE (presented here) is used in the subsequent section of this report to support the evaluation of the post-earthquake traffic load capacities of bridges with well-confined reinforced concrete columns.

Figure 19. Comparison of Experimental and Simulated Lateral Force-Displacement Response Curves for Test Base15 and Analytical Models FBE [(a) X-direction; (b) Y-direction] and BWHE [(c) X-direction; (d) Y-direction]

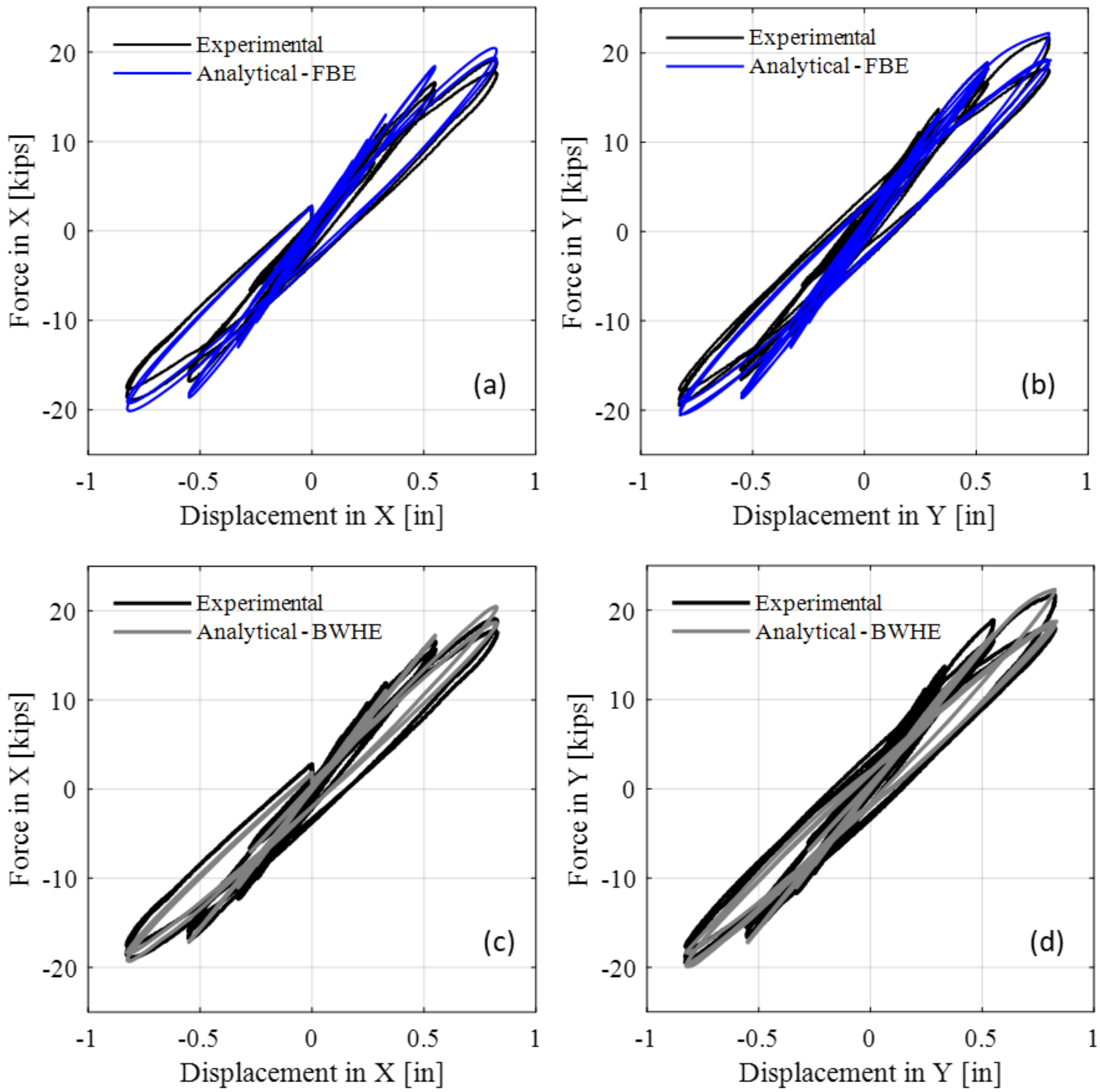

Figure 20. Comparison of Experimental and Simulated Lateral Force-Displacement Response Curves for Test Base30 and Analytical Models FBE [(a) X-direction; (b) Y-direction] and BWHE [(c) X-direction; (d) Y-direction]

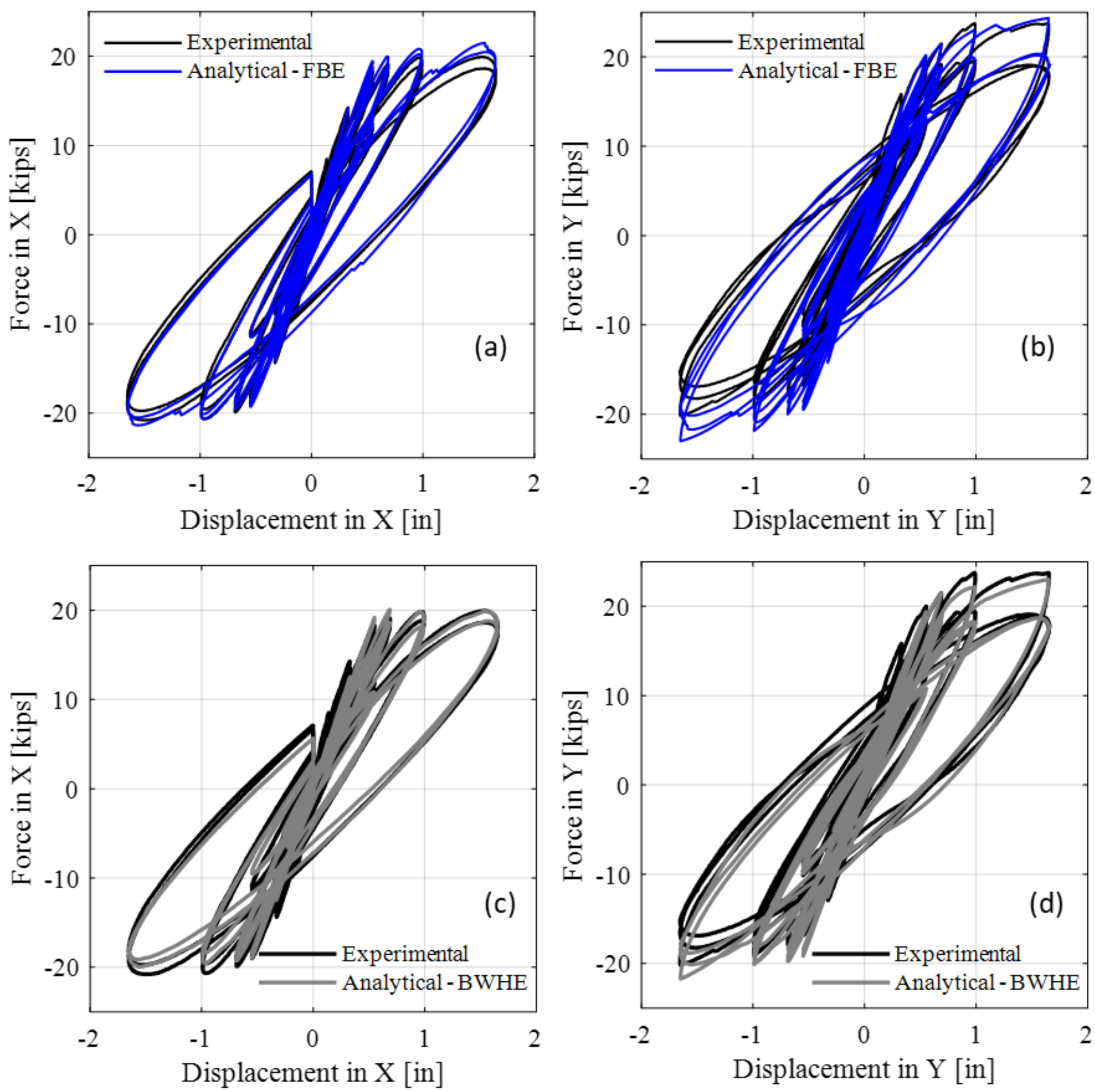

Figure 21. Comparison of Experimental and Simulated Lateral Force-Displacement Response Curves for Test Base45 and Analytical Models FBE [(a) X-direction; (b) Y-direction] and BWHE [(c) X-direction; (d) Y-direction]

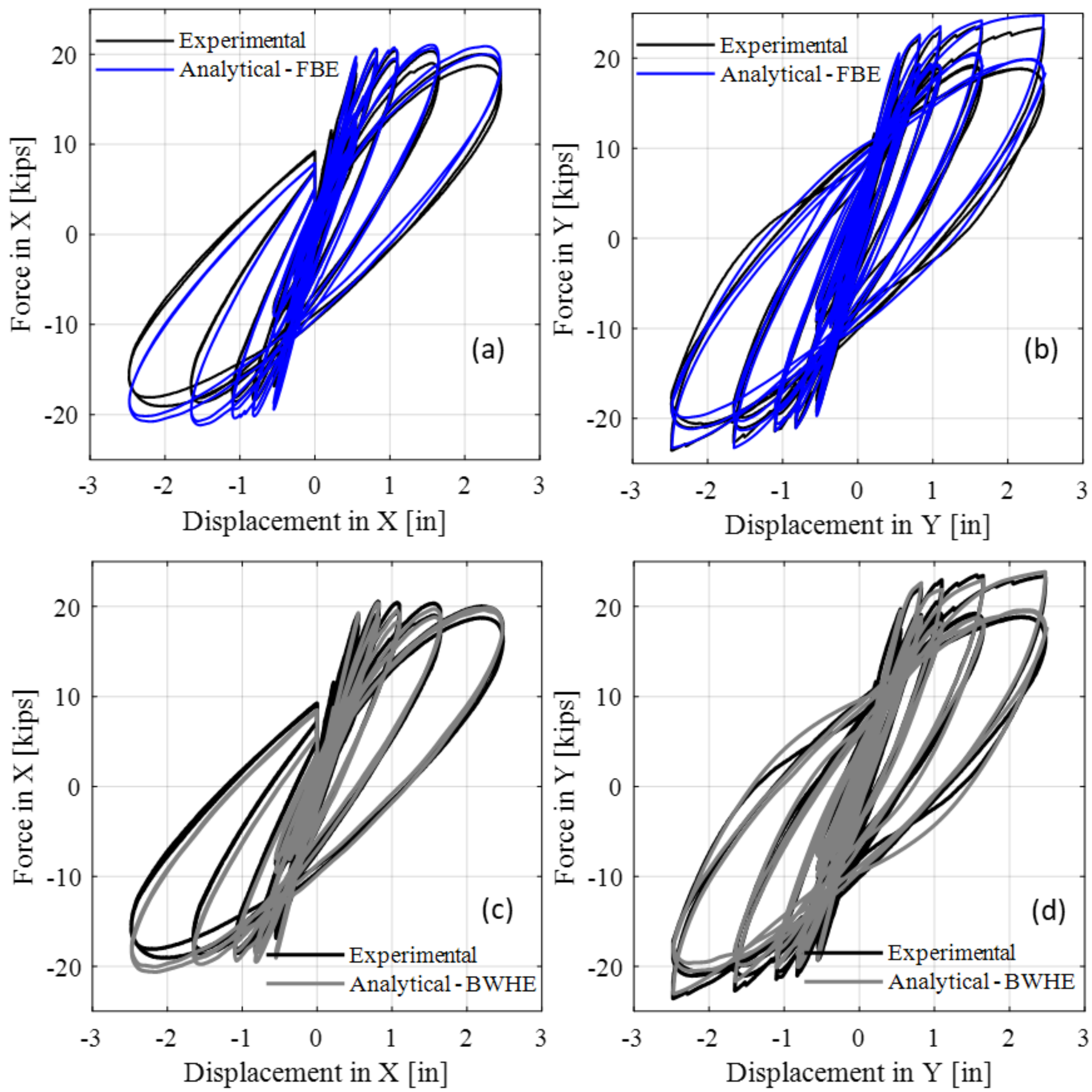

Figure 22. Comparison of Experimental and Simulated Axial Force-Displacement Relationships: (a) Base0; (b) Base15; (c) Base30; (d) Base45

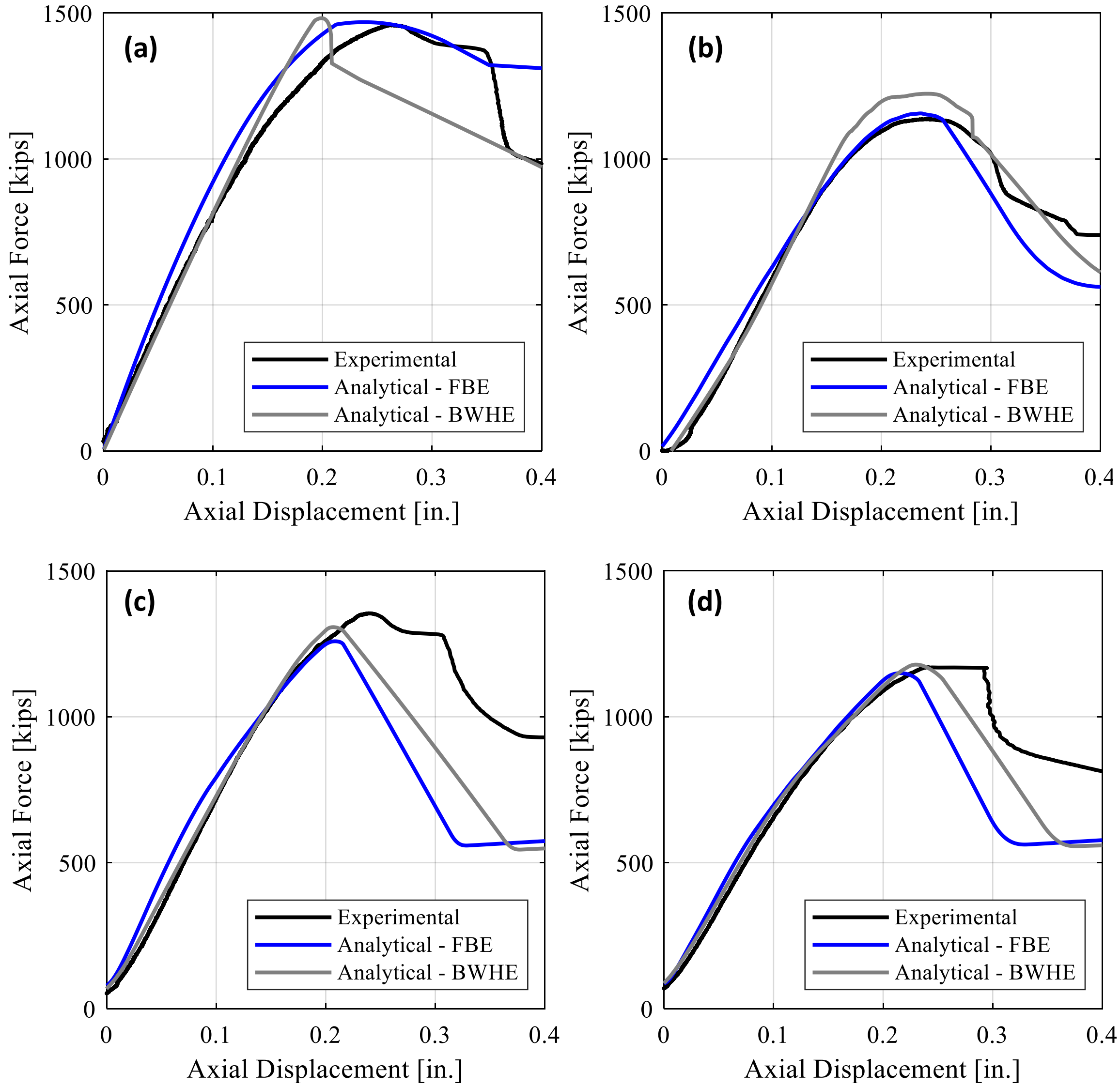

IV. Post-Earthquake Traffic Capacity and Functionality State of a Bridge

The goal of this chapter is to develop a direct evaluation method for the post-earthquake traffic capacity and associated functionality state of the bridge. While the previous studies have provided methods for determining the post-earthquake functionality of a bridge based on the highest level of damage of individual component types, the new method presented here provides quantifiable links between earthquake intensity, component-level EDPs, and system-level traffic capacity and associated functionality. The unique features of the proposed method are a consideration of the post-earthquake residual drift of a bridge when evaluating the functionality state of the bridge and a direct evaluation of the post-earthquake traffic capacity of the bridge considering realistic traffic load scenarios. The main outcome of the method is a reliable estimate of the probability that a traffic loading associated with the considered functionality limit state of the bridge can be safely accommodated following an earthquake event. In addition to presenting the proposed method, this section includes an original case study that provides an application of the proposed method.

4.1 Method for Evaluating the Post-Earthquake Traffic Capacity and Associated Functionality State

This section presents a method for evaluating the post-earthquake traffic capacity and functionality of a reinforced-concrete highway overpass bridge. The method includes a definition of the functionality limit states (FLSs) of the bridge, recommendations for modeling a bridge structure, definition of realistic traffic load scenarios that correspond to different traffic load restrictions, an evaluation of the post-earthquake traffic capacity for a selected FLS, an evaluation of correlations between the engineering demand parameters (EDPs, i.e., structural responses) and traffic capacity, and finally an evaluation of post-earthquake functionality through a comparison of traffic capacity with traffic demand. Distinguishing features of the method are the quantitative links between the earthquake intensity, component-level EDPs, and system-level traffic capacity. The presented method can be used for any type of reinforced-concrete highway overpass bridge, although certain aspects may need to be re-evaluated and adjusted based on the type of bridge under consideration. A subsequent section presents case studies that demonstrate one application of the method.

Functionality Limit States

The functionality of a bridge represents the level of traffic that can safely pass over the bridge, and functionality limit states represent different possible levels of post-earthquake functionality. To support this study, the functionality limit state definitions are adopted from earlier studies by Mackie and Stojadinovic (2006) and DesRoches et al. (2012), presented in Table 7. The functionality limit state FLS-0 is characterized by no loss in bridge functionality; the bridge is open to normal levels of traffic (i.e., no vehicle restrictions) when there is a minor or no observable damage of critical bridge components. On the other end of the spectrum, the functionality limit state FLS-3 is characterized by the full loss of functionality; the bridge is closed to all traffic due to extensive damage of critical bridge components. The intermediate functionality limit states FLS-1 and FLS-2 represent minor to major losses in functionality and include restrictions on the number of vehicles that can pass over the bridge due to moderate damage to critical bridge components.

Table 7. Functionality Limit States (FLSs)

Functionality Limit State Classification	**FLS-0**	**FLS-1**	**FLS-2**	**FLS-3**
Damage level	Low	Medium	High	Extensive
Loss in functionality	No loss	Minor loss	Major loss	Full loss
Functionality	Open to normal traffic (no restrictions)	Open to limited traffic (speed/weight/ lane restrictions)	Open to emergency vehicles only	Full closure (all vehicles restricted)

Defining these functionality limit states is an important first step in determining the system-level traffic capacity of a bridge, because the FLS is what determines the permitted traffic load on the bridge after an earthquake. Each of the presented functionality limit states is characterized by unique traffic load scenarios/restrictions that are to be accounted for when deriving the post-earthquake traffic capacity of the bridge. Different traffic load scenarios are explored further in the following subsections.

Modeling

With the FLSs defined, the next step towards the evaluation of the post-earthquake bridge traffic capacity is the development of a finite-element model of a bridge. As demonstrated by Terzic and Stojadinovic (2010a,b), the bridge components that affect the traffic capacity the most are columns and abutments; they are the primary components of the lateral load-resisting system of the bridge and are designed to dissipate the earthquake's energy through controlled damage accumulation.

A high-fidelity nonlinear analytical model of a bridge column that accurately predicts seismic response and the axial load capacity of a damaged column is developed and proposed in Section III of this report. The proposed bridge column model is recommended for use in studies that aim at evaluating the bridge's post-earthquake traffic capacity.

Numerous high-fidelity abutment models are currently available (e.g., Aviram et al. 2008, DesRoches et al. 2012, Shamsabadi et al. 2010, Kaviani et al. 2012, Xie et al. 2019). An appropriate abutment model shall be selected based on the specificities of the considered bridge. The secondary bridge components (e.g., bridge superstructure, foundation, bearings, restrainers) which are expected to remain elastic under a design-level earthquake shaking shall be modeled following the recommendations by Aviram et al. (2008) and DesRoches et al. (2012).

Analysis

After a bridge model is developed, the next step is a site-specific scenario or intensity-based ground motion selection and a definition of the traffic load protocols for each of the FLSs under consideration. The traffic load protocols shall include the definition of the magnitude and location of the vehicle loads on the bridge. The load protocols should follow the FHWA LRFD Reference Manual for Highway Bridge Superstructures (Grubb et al. 2015), which is used by Caltrans engineers to determine the loading scenarios for the design of highway overpass bridges. Determinations of the loading protocols for different FLSs are demonstrated through the case study.

With the ground motions selected and the loading protocols established, the gravity load analysis is conducted first; it is followed by the response history analysis for ground motion and a free vibration analysis until the post-earthquake state of the bridge is established; the analysis is concluded with the traffic load analysis, whereby the load corresponding to a selected traffic load protocol is incrementally increased until the bridge model reaches its maximum traffic capacity. This process is repeated for all selected ground motions and traffic load scenarios.

Traffic Capacity Evaluation

Following the completion of the analysis for one earthquake and traffic load scenario, the traffic capacity of the bridge is evaluated by measuring the axial forces in the columns and vertical reactions of the abutments at the time the bridge reaches its maximum traffic capacity. The bridge is supposed to reach its maximum traffic capacity for ground motion and a loading scenario when a critical column reaches its axial load-carrying capacity. The critical column is a column with the highest axial force among all bridge columns. The axial load capacity of the critical column is determined as a minimum of the following three values: (1) axial force that corresponds to the peak moment on the axial force versus bending moment curve, (2) peak axial force on the axial force versus displacement curve, and (3) axial force at the time the maximum strain in longitudinal rebars exceeds the suggested allowable level per Caltrans SDC recommendations (Caltrans 2013). The process for determining the axial load capacity of a critical column, as well as the process for evaluating the corresponding bridge traffic capacity, is explained further in the case study section of this report.

Correlation Between EDPs and Bridge Traffic Capacity

Many studies utilize the EDPs (i.e., structural responses) of bridge components to evaluate damage states (DSs) of bridge components, where DS-0 and DS-1 typically represent no damage and minor damage of the component and DS-4 or DS-5 typically represent extensive component damage. These damage states are probabilistic lognormal functions defined with a median and a dispersion of a considered EDP.

A study conducted by Vosoochi and Saiidi (2010) evaluates many EDPs for bridge columns, including maximum drift ratio, residual drift ratio, frequency ratio, damage index (inelasticity index), and maximum longitudinal and transverse steel strain. They propose the use of either maximum drift ratio or damage index as an EDP to relate the column response to its damage state. Furthermore, the studies conducted by DesRoches et al. (2012) and Saini and Saiidi (2013) propose EDPs of damage states for abutments and many of the secondary components, including joint separation in abutments and superstructure, displacements in bearings and shear keys, displacement and rotation in foundations, and many more.

After traffic capacities are determined for all earthquakes representative of a scenario or an intensity level and all traffic load scenarios, the analytical data enable a determination of the correlation between the component-level EDPs and system-level traffic capacity for each FLS of the bridge. By comparing correlation coefficients for different EDPs of a component, the EDPs with the strongest correlation with the bridge traffic capacity can be identified. It is also useful to evaluate the correlation between EDPs of different components to understand the relationship between damage states of different components and their combined effect on the post-earthquake traffic capacity.

Evaluation of Post-Earthquake Functionality

The traffic capacity values, which are evaluated for an earthquake intensity level considering a traffic load scenario representative of an FLS, are used to develop a traffic capacity fragility (TCF) value. These TCFs, which show the probability that a certain traffic capacity will be achieved, are then compared with the traffic demand fragility (TDF), which represents the probability that a certain traffic loading on the bridge will be reached for the FLS under consideration. The demand and capacity fragilities are plotted on the same graph to find the probability that the capacity is greater than the demand (intersecting point of the two fragilities) for the considered earthquake intensity level and the FLS of the bridge. In other words, the intersecting point of the two fragilities represents the probability that a traffic loading associated with the considered FLS of the bridge can be safely accommodated after the bridge has experienced an earthquake representative of the considered intensity.

4.2 Case Study: Post-Earthquake Traffic Capacity and Functionality States for a Single-Column Bent Bridge

The method for determining the post-earthquake traffic capacity and functionality states of the bridge is demonstrated in a case study considering a modern single-column bent bridge. The case study evaluates bridge functionality at three levels of earthquake intensity and two functionality limit states of the bridge: FLS-0, bridge open to normal traffic, and FLS-2, bridge open only for one emergency vehicle at a time.

Bridge Description

The bridge selected for this study is the Type 11 prototype bridge from Ketchum et al. (2004). While Ketchum et al. (2004) offer several typical Caltrans bridges, which are designed with sufficient detail, the Type 11 bridge was chosen as it represents a type of highway overpass bridge with tall columns common in California. It is to be noted that the selected prototype bridge is not designed for a specific location (site) but for a selected set of design parameters representative of many locations in California. The selected bridge is a straight, cast-in-place box girder bridge with five spans and single column bents. The bridge has three internal spans of 150 ft, two external spans of 120 ft, a 39-ft-wide deck, and 50-ft-tall circular columns 6.25 ft in diameter (Figure 23). The superstructure is a pre-stressed (CIP/PS) two-cell box girder supported on neoprene bearing pads under each of the three-box webs. The reinforcement of the column consists of longitudinal bars placed around its perimeter and a continuous spiral encasing the longitudinal bars. Each column has 34 longitudinal No. 11 reinforcing bars and a No. 8 spiral with a center-to-center spacing of 6 inches. This reinforcement layout gives a longitudinal reinforcement ratio of 1.2% and a transverse reinforcement ratio of 0.75%. The cover is 2 inches all around.

Figure 23. Type 11 Prototype Bridge (Terzic and Stojadinovic 2010a)

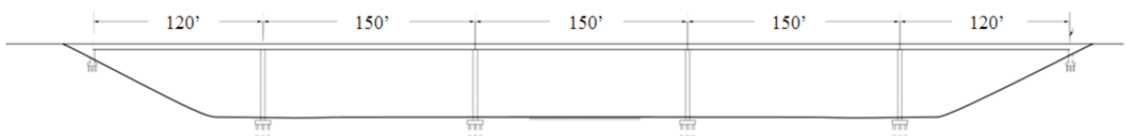

(a) Bridge Elevation

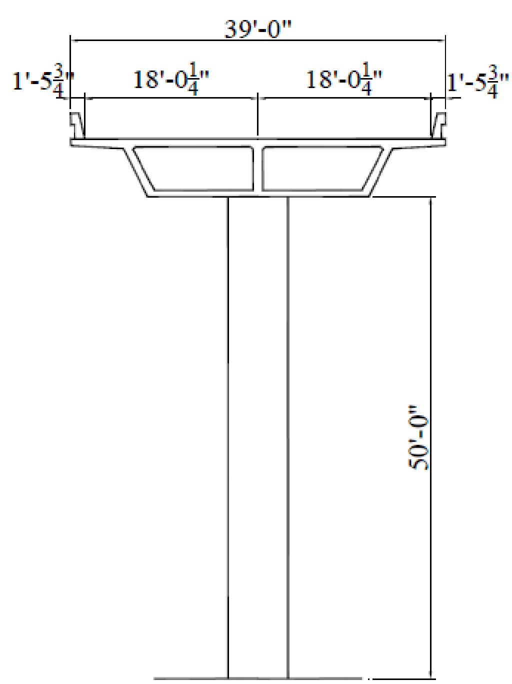

(b) Column and Superstructure Section

Analytical Model of the Bridge

In the present study, the bridge is modeled as a three-dimensional nonlinear finite-element model using the computational platform OpenSees (McKenna, 1997). The bridge is modeled as a spine model with line elements located at the centroids of the cross-sections. The bridge deck and columns are modeled with three-dimensional beam-column elements with corresponding cross-sectional properties. All six degrees of freedom were restrained at the base of the columns.

The bridge deck is modeled with elastic elements. To accurately represent the mass distribution of the deck, each span of the bridge deck is modeled with at least ten elements. At every node of the deck, the lumped masses associated with the tributary lengths of deck elements are assigned in the three global directions of the bridge (longitudinal, transverse, and vertical). In addition, the rotational mass (mass moment of inertia) is assigned at each deck node.

The columns are modeled with two types of elements. The top of the column, representing the portion of the column embedded in the superstructure, is modeled as a rigid link. The remainder of the column is modeled with a nonlinear beam with hinges element (BWHE), following the modeling recommendations presented in Section III. A fiber cross-section, assigned to each integration point of the element, was generated to explicitly account for longitudinal reinforcing bar placement and the effects of unconfined and confined concrete. Each material in the cross-section was assigned a uniaxial stress-strain relationship, where reinforcing bars were modeled with the ReinforcingSteel material and the confined core and unconfined cover were modeled with Concrete02 material. The following material properties were used to define the steel and concrete: the compressive strength of the unconfined concrete, f_c', was 5.0 ksi; the modulus of elasticity of concrete was calculated as $57{,}000\sqrt{f_c'}$ psi (Caltrans 2013); the yield strength of steel was 68 ksi (Caltrans 2013); the ultimate tensile stress of steel was 95 ksi (Caltrans 2013). All other material properties were adopted from Section III. Although the effect of shear is not significant in tall columns reinforced following SDC, it is nevertheless accounted for through aggregation of an elastic-plastic shear force-deformation relationship with the fiber column section at each integration point of the beam-column elements. The shear strength and stiffness are calculated following equations from Section 3.6 in Caltrans SDC (Caltrans 2013).

Abutment modeling plays a significant role when determining the post-earthquake bridge traffic load capacity. Two simple abutment models that generate the upper and lower bounds of the bridge response for the earthquake and traffic load are considered in this study. The actual response of the bridge lies between these two abutment models. The first abutment model, designated as Rx1, consists of a simple boundary condition module that applies single point constraints against displacement in the vertical direction (vertical support) and rotation about the superstructure longitudinal axis (full deck torsion restraint). The second abutment model, designated as Rx0, applies single point constraints against displacement in the vertical direction, representing a roller boundary condition at the superstructure ends.

Based on findings presented in Section III, the damping is modeled with the mass- and stiffness-proportional Rayleigh damping model utilizing the damping ratio of 1% for the first transverse and the first longitudinal modes of vibration. The damping matrix was based on the tangent stiffness, and Rayleigh proportionality constants were updated after each step of the analysis.

The effects of column axial loads acting through large lateral displacements, known as P-Δ, are included while analyzing the bridge system. The consideration of P-Δ effects helps identify the structural instability hazard of the bridge by capturing the degradation of strength and the amplification of the demand on the column bents caused by the relative displacement between the column top and bottom.

Ground Motion Selection

Since the Type 11 bridge from Katchum et al. (2004), which is investigated in this study, does not have a specific location (site), it is not possible to select the ground motion intensity such that it has a certain probability of being exceeded in a given period. Therefore, ground motion intensity levels for the study are selected to generate different damage states of the bridge. They are adopted from Baker (2010), which has provided the site-specific ground motions representative of the hazard at the site of the I880 viaduct in Oakland, California. Baker selected forty ground motions for each of three hazard levels: 50% in 50 years, 10% in 50 years, and 2% in 50 years. In this study, the selected ground motions that correspond to the three hazard levels will be designated as frequent, rare, and very rare earthquakes. Given that the selected site in Oakland is close enough to the Hayward fault to potentially experience directivity effects, a number of the selected ground motions had velocity pulses in the fault-normal component of the recording (7 out of 40 frequent earthquakes, 16 out of 40 rare earthquakes, and 19 out of 40 very rare earthquakes).

Traffic Capacity and Functionality Evaluation for FLS-2: Traffic Load Scenarios

To evaluate the traffic capacity of the bridge, it is necessary to define the loading scenarios for the functionality limit state under consideration. In the case of FLS-2, only one emergency vehicle is allowed to pass over the bridge at any given time. To simulate the vehicle load on the bridge, a standard HL-93 truck was chosen as the typical truck vehicle (see Section 3.4.2.2 of FHWA LRFD Reference Manual for Highway Bridge Superstructures: Grubb et al. 2015). It is a three-axle truck (Figure 24) with a fixed spacing of 14 ft between the first two axles and variable spacing of 14 to 30 ft between the last two. The spacing between the two rear axles of 14 ft was chosen, as this spacing will produce the largest axial forces and bending moments in the bridge columns.

Figure 24. Standard HL-93 Design Truck (Grubb et al. 2015)

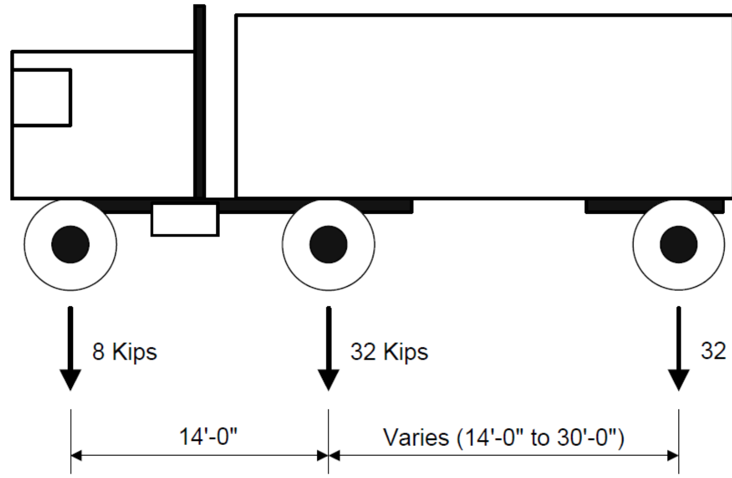

The truck load on the bridge was simulated by two sets of forces—vertical and torsional—applied at superstructure elements. The vertical set of forces corresponds to the truck weight applied at its axle locations: this involves three concentric forces with magnitudes that follow the ratio 1:4:4. Given that the truck is positioned on the bridge in the conventional traffic lanes at some distance from the bridge deck centerline (Figure 25), it will generate the torsional moments that correspond to axle loads placed eccentrically with respect to the bridge deck centerline.

Figure 25. Two Considered Cases of Truck Position Relative to Superstructure Centerline (Terzic and Stojadinovic 2010a)

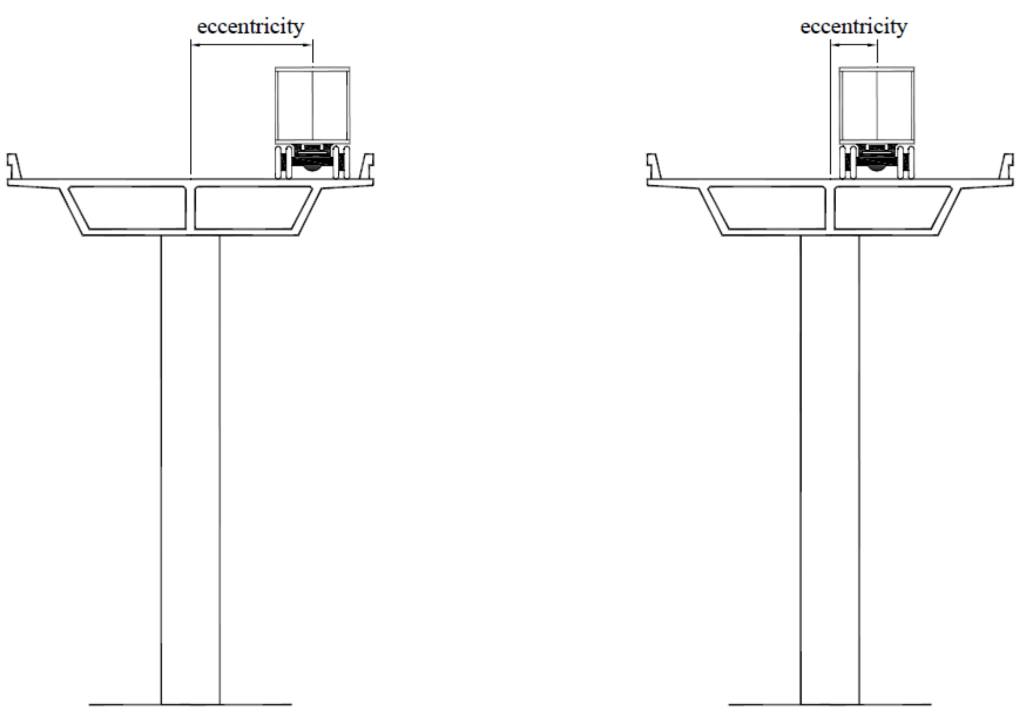

(a) Truck in the Curb Lane (b) Truck in the Fast Lane

Modern bridges in California (designed following the capacity design approach), when damaged in an earthquake, can experience one of two possible failure modes when exposed to the traffic load: bending failure or axial failure of the bridge columns. Influence lines for the axial load and the bending moments in the columns were examined by Terzic and Stojadinovic (2010a) to find the critical positions of the truck along the bridge superstructure. Those authors analyzed the damaged bridge for the critical truck positions to find the position that would first induce the failure of a column. In the process of analyzing a damaged bridge under the truck load, the loads representing the truck load in the specific position on the bridge were increased monotonically from zero until they induced the failure of a column. Two positions of the truck on the bridge relative to the superstructure centerline were considered. The first position of the truck considered a scenario where the truck uses the fast lane, the lane closest to the superstructure centerline (Figure 25b), and the second position considered a scenario where the truck uses the curb lane, furthest from the superstructure centerline (Figure 25a).

The critical failure mode of the bridge was found to be the bending failure of the end column when the truck was positioned to induce the largest bending moment in the column (Terzic and Stojadinovic, 2010a). Depending on whether residual drifts after an earthquake were positive or negative in the transverse bridge direction, two positions of the truck along the bridge (corresponding to the failure mode) are adopted for further analyses of the post-earthquake traffic capacity in the present study. Position 1 (Figure 26a) of the truck corresponds to the case when residual drifts are in the positive transverse bridge direction, and Position 2 (Figure 26b) corresponds to the negative direction.

Figure 26. Critical Positions of the Truck on the Bridge (Terzic and Stojadinovic 2010a)

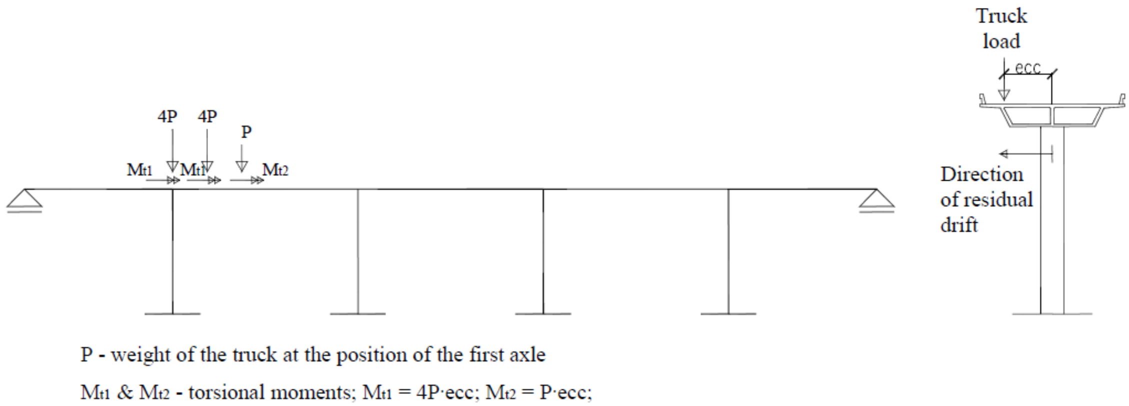

(a) Truck Position 1 and Corresponding Truck Forces

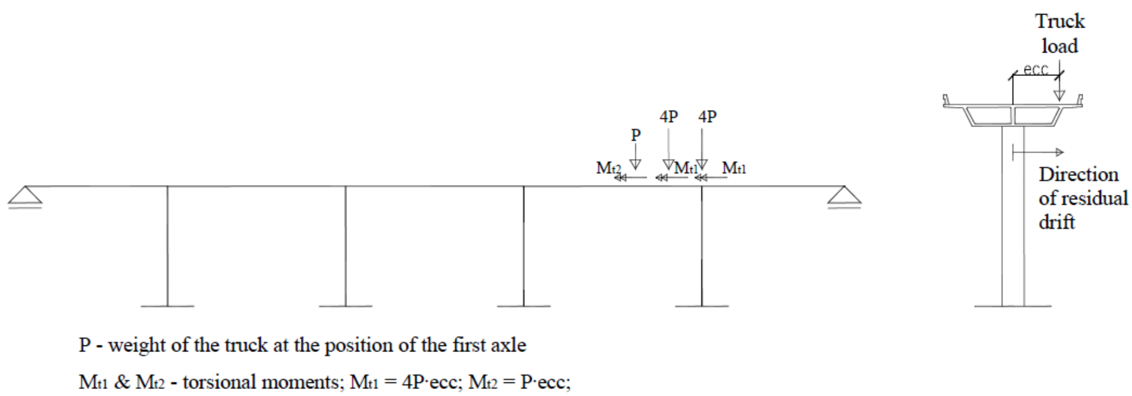

(b) Truck Position 2 and Corresponding Truck Forces

Traffic Capacity Evaluation

In the present study, the traffic capacity of the bridge is conservatively evaluated as the axial load capacity of the bridge column positioned directly below the truck—either the left or right exterior column. The axial load capacity of the critical column was determined by considering three criteria. The first criterion considered the relationship between the axial force and bending moment at the bottom of the column (Figure 27a). In this case, the axial load capacity of the column is the axial load which corresponds to the maximum bending moment in the column. The axial force-bending moment interaction diagram for the bridge column, which does not include the strain hardening of steel, is also shown in Figure 27a. Although it provides a conservative estimate of the column capacity, it serves as a reference point for the evaluation of the results. The next criterion considered the relationship between the axial force at the bottom of the column and the axial displacement of the top of the column (Figure 27b). The axial load capacity was selected as the axial load in the column at the instance of a significant change of the axial stiffness of the column. The last criterion was based on whether the maximum strain in the most critical longitudinal rebar exceeded the Caltrans suggested limit of 0.06 (Figure 27c). The axial force corresponding to the point where the rebar strain first reaches the strain limit (either positive or negative) represents the axial load capacity for that criterion. This criterion was not considered for those cases where the maximum strain never reached the strain limit. Finally, the axial load capacity of the critical column is determined as a minimum of the three capacities evaluated with the aforementioned criteria.

Figure 27. Example Graphs of Criteria for Determining Columns' Axial Load-Carrying Capacity (earthquake #4 for ground motion set representative of very rare earthquakes, abutment type Rx1, and truck in the fast lane)

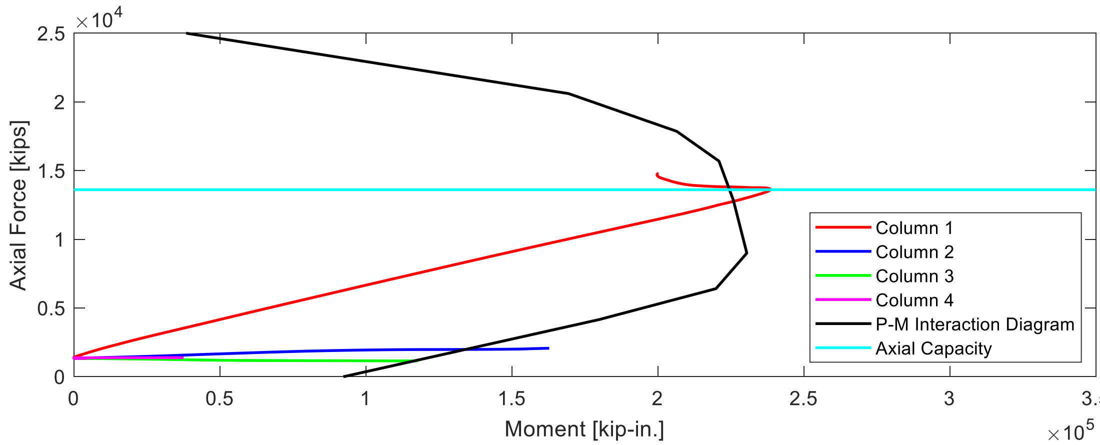

(a) Axial Force vs. Bending Moment

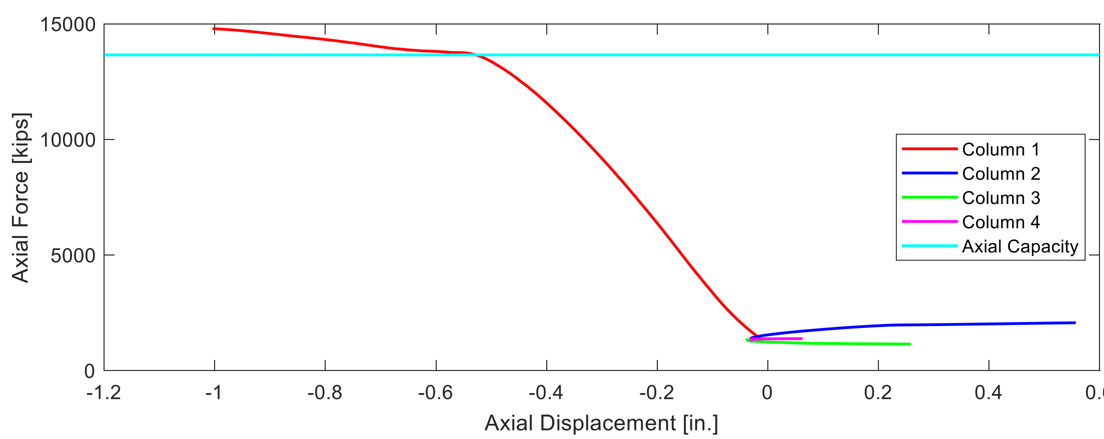

(b) Axial Force-Displacement Relationship

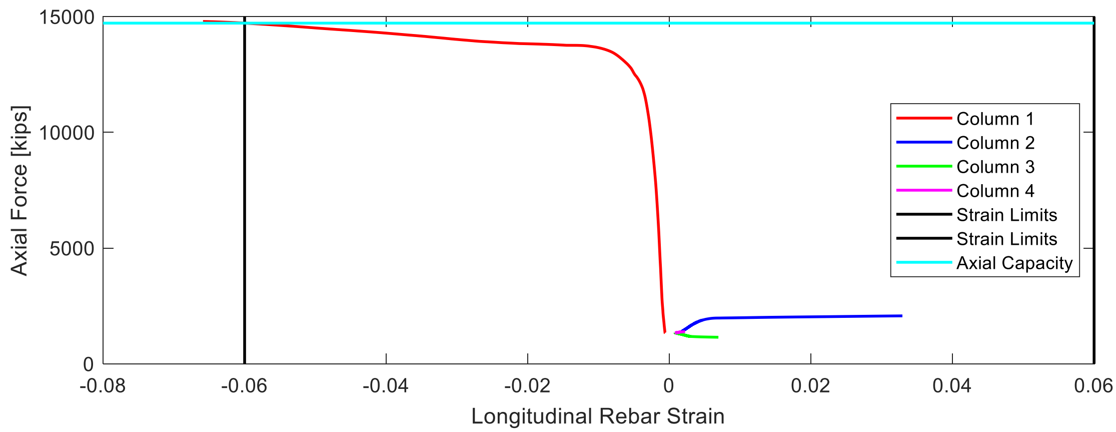

(c) Axial Force vs. Strain in Longitudinal Rebar

Correlations between EDPs and Bridge Traffic Capacity

The EDPs that were considered in the case study are the column's maximum drift ratio (MDR), residual drift ratio (RDR), and damage index (DI). The maximum drift ratio and residual drift ratio represent the maximum column displacement and the residual displacement divided by the height of the column. The damage index represents the difference between the maximum earthquake displacement and the yield displacement of the column divided by the difference between the ultimate displacement capacity and yield displacement of the column. DI is considered to be a good measure of damage in columns because it is a measure of the lost plastic deformation capacity (Saini and Saiidi 2013).

Preceding the evaluation of the traffic capacity of the bridge in the damaged condition, the post-earthquake damage state of the bridge columns is evaluated. To allow for this evaluation at different hazard levels, Figure 28 shows the fragilities for the three considered EDPs (MDR in Figure 28a, DI in Figure 28b, and RDR in Figure 28c) along with the damage states that correspond to five levels of column damage (DS-1 through DS-5) developed by Vosooghi and Saiidi (2010). These damage states are flexural cracks (DS-1), first spalling and shear cracks (DS-2), extensive cracks and spalling (DS-3), visible lateral and/or longitudinal bars (DS-4), and the start of core damage indicating imminent failure of the column (DS-5). Note that the column responses for the rare and very rare earthquakes are presented separately for sets of ground motions with velocity pulses and those without velocity pulses (Figure 28).

By comparing the EDP fragilities with the DS fragilities, we see that DI suggests a smaller level of column damage than MDR, and furthermore, MDR suggests a smaller level of damage than RDR. The observed differences in the column damage states predicted with different EDPs are more pronounced for the ground motion sets with velocity pulses than for those without velocity pulses. For the considered hazard levels, the following damage levels are expected (based on MDR fragilities): for frequent earthquakes, no visible damage is expected; for rare earthquakes without pulses, flexural cracks with a chance of spalled concrete are expected; for rare earthquakes with pulses and very rare earthquakes without pulses, the damage levels are very similar and are characterized by spalling of concrete and the presence of shear cracks; for very rare earthquakes with pulses, it is expected that the reinforcing bars will become exposed with a possibility of column failure.

Figure 28. Structural Response Fragilities (abutment type Rx1) for the Three Considered Hazard Levels

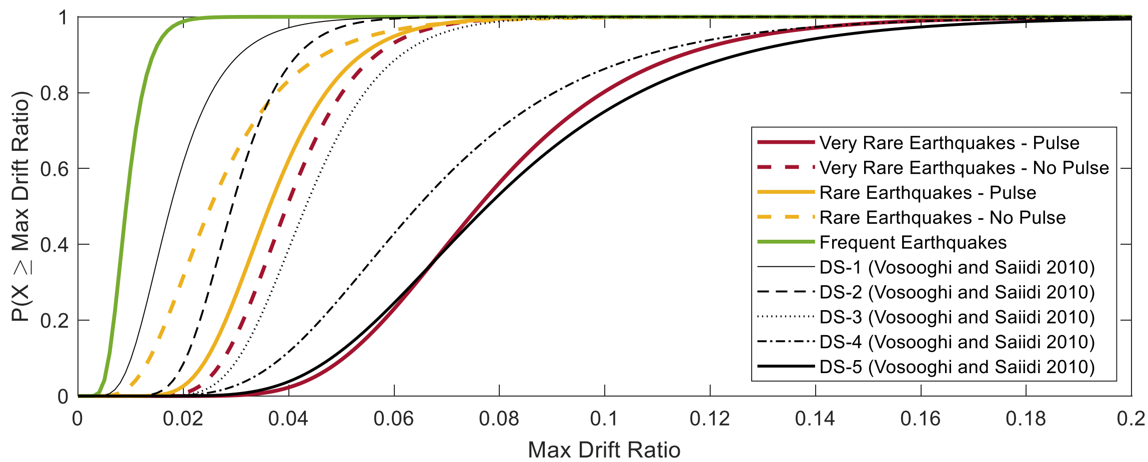

(a) MDR Fragilities

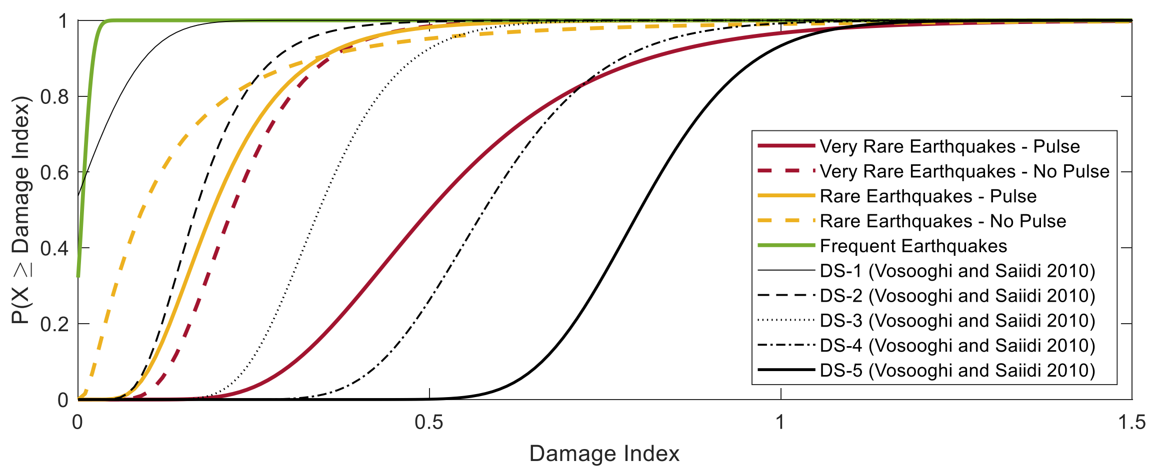

(b) DI Fragilities

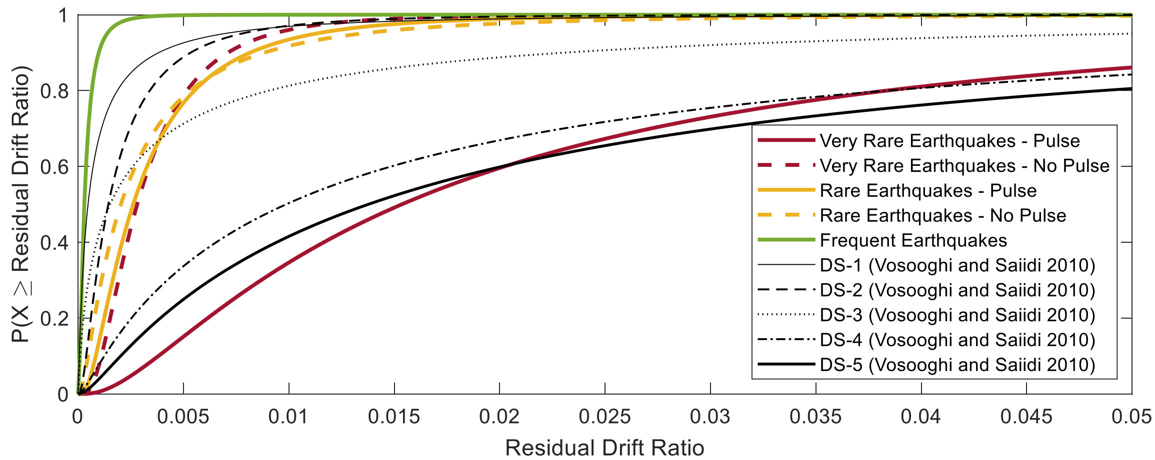

(c) RDR Fragilities

Example plots of the correlations between traffic capacity and the EDPs considered in this case study are presented in in Figure 29 for the following scenario: very rare earthquakes, abutment type Rx1, and truck in the fast lane. The left y-axis shows the post-earthquake traffic capacity values, and the right y-axis shows the traffic capacity ratio values, where the traffic capacity ratio is the post-earthquake traffic capacity divided by the pre-earthquake traffic capacity. The pre-earthquake capacity was determined with the same criteria as the post-earthquake capacity, but the bridge was not subjected to any ground motions. For very rare earthquakes, the correlation coefficient for MDR and DI was found to be -0.958, suggesting that there is a very strong negative correlation between traffic capacity, MDR, and DI. The values are the same because both parameters are a function of the maximum displacement of the top of the critical column. The correlation coefficient between traffic capacity and RDR was found to be -0.981, suggesting that there is an even stronger correlation between traffic capacity and RDR than between traffic capacity and MDR or DI. These strong correlations are evident from the plots, and they suggest that as the EDPs increase (i.e., the damage in the components increases), the post-earthquake traffic capacity decreases.

As can be seen in Figure 30, there were some cases where the traffic capacity ratio slightly exceeded a value of one, meaning that the post-earthquake capacity was found to be slightly larger than the pre-earthquake capacity. As noted earlier, the critical position of the truck load on the bridge tends to generate bending failure of the column. In some cases when the residual drift ratios are very low, the decrease in the bending moment capacity of the damaged column could be accompanied by the increase of the corresponding axial load capacity relative to its pre-earthquake capacities. This phenomenon is depicted in Figure 30, which provides a comparison of the pre-earthquake and post-earthquake axial force and bending moment capacities of the critical column. As can be seen in Figure 30, a column with a relatively small level of earthquake-induced damage might see an increase of the axial load capacity due to an interaction between axial force and bending moment.

Figure 29. Traffic Capacity vs. EDPs for Very Rare Earthquakes (abutment type Rx1, truck in fast lane)

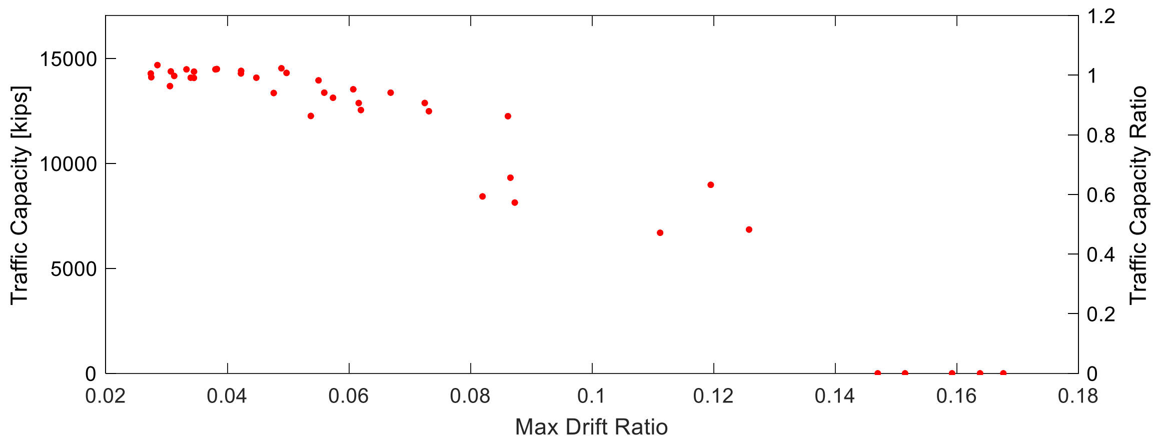

(a) EDP is the Maximum Drift Ratio

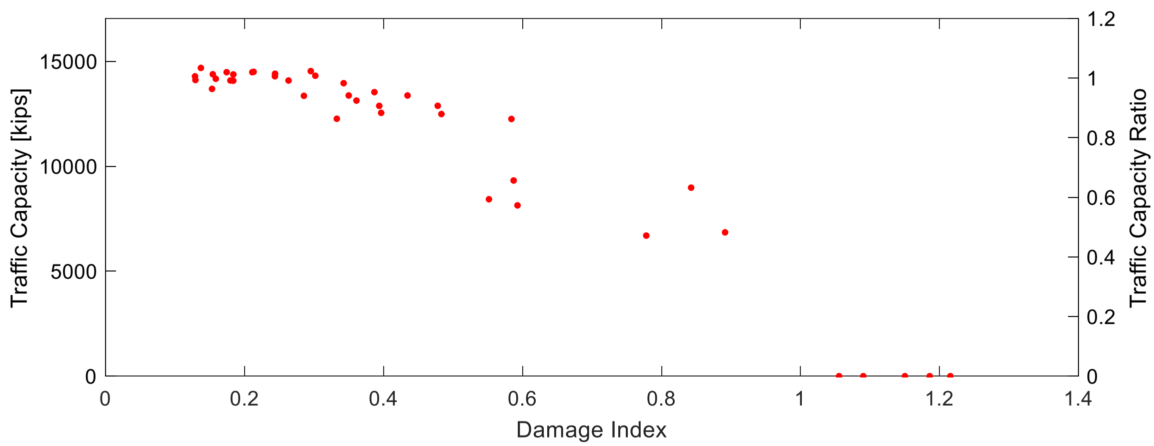

(b) EDP is the Damage Index

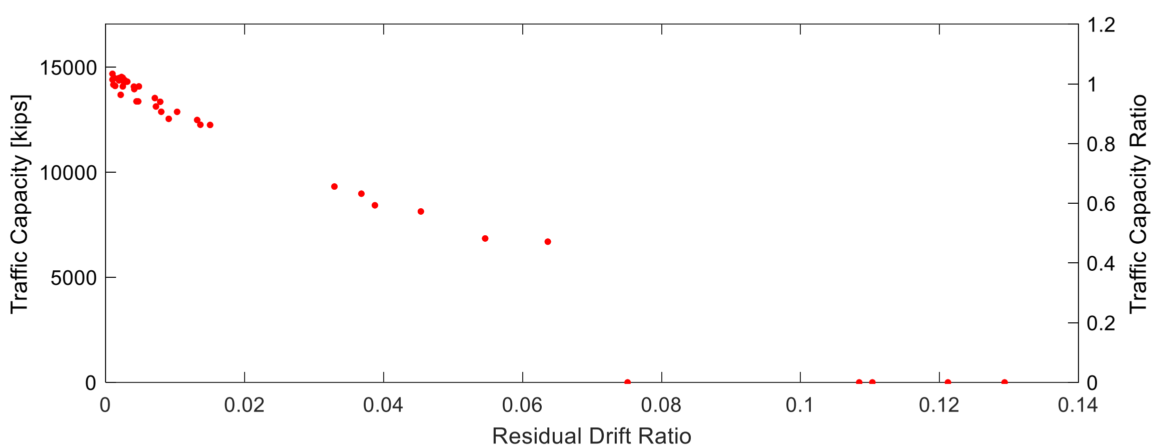

(c) EDP is the Residual Drift Ratio

Figure 30. Pre-Earthquake vs. Post-Earthquake Capacity (abutment type Rx1, truck in fast lane) and Axial Force vs. Bending Moment Relationship

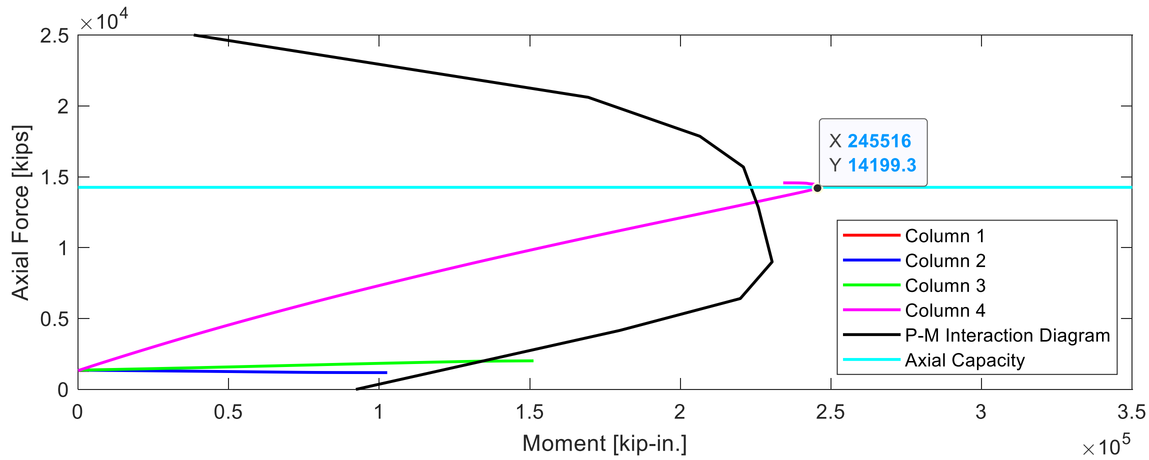

(a) Pre-Earthquake Capacity

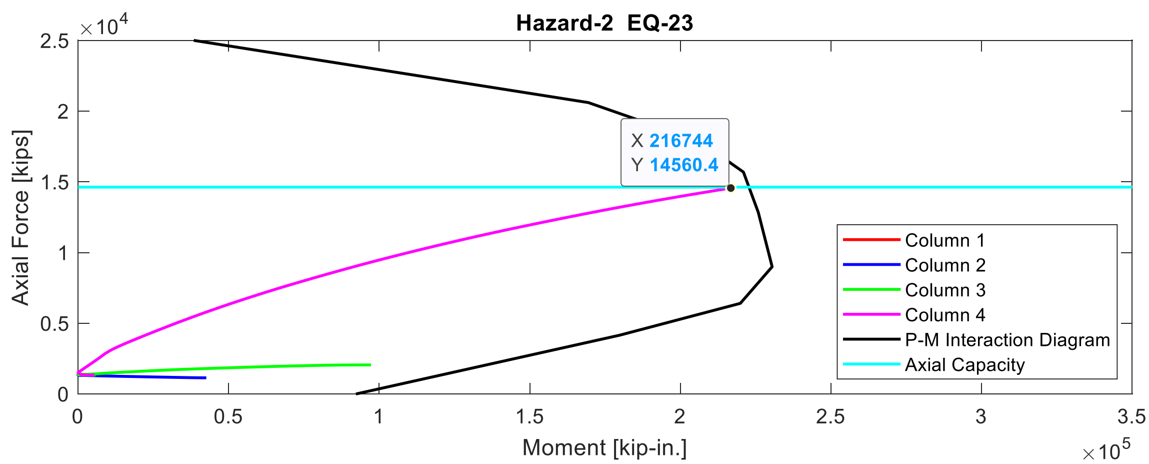

(b) Post-Earthquake Capacity (hazard level: very rare earthquakes, earthquake #23)

Evaluation of Post-Earthquake Functionality

Traffic capacity fragilities associated with the FLS-2 (designated as TCF-2) are presented in Figure 31 for the two types of abutment models (Rx0 and Rx1), two positions of the truck load on the bridge (fast lane and curb lane), and three hazard levels (frequent, rare, and very rare earthquakes). Figure 31 also includes the traffic demand fragility (designated as TDF-2), which was determined based on the actual truck loading on the bridge using the criteria from the FHWA LRFD Reference Manual for Highway Bridge Superstructures (Grubb et al. 2015). To find the median of the TDF-2, the truck loading (represented by the HL-93 truck axle loads in Figure 24) is multiplied by the multiple presence factor and dynamic load allowance factor. The multiple presence factor (per section 3.4.1.2 in Grubb et al. 2015) depends on the total number of lanes that are being loaded. For the FLS-2, where only one lane is loaded, the multiple presence factor is 1.2. The dynamic load allowance (per section 3.4.8 from FHWA LRFD Reference Manual for

Highway Bridge Superstructures: Grubb et al. 2015) is defined as an increase in the applied traffic loading to account for the dynamic interaction between the bridge and the moving vehicles. For the bridge columns, which are used to evaluate the traffic capacity, the dynamic load allowance is 33%, meaning that the dynamic load allowance factor is 1.33. The dispersion of the TDF-2 (represented by the possible range in the weight of the vehicles) is chosen to be 0.3, as there would be a relatively low level of dispersion in the possible weight of the truck.

For frequent earthquakes, Figure 31a shows significantly higher traffic capacity than the traffic demand for FLS-2 for the two abutment conditions (Rx0 and Rx1) and for both truck positions (curb lane and fast lane). There is total certainty that the bridge will be safe to support one emergency vehicle at a time. By comparing the two abutment conditions and the two truck positions on the bridge, we see that in the case when abutments provide full torsional restraint for the deck (Rx1) and when the truck is in the fast lane (the closest to the deck centerline), the traffic capacity is about four times larger than in the case when the abutments do not provide torsional restraint for the deck (Rx0) and when the truck is in the curb lane (the furthest from the deck centerline). The presented results clearly depict the effect of the abutment model and the position of the truck load on the TCF-2.

For rare and very rare earthquakes, as presented in Figure 31b and Figure 31c, there are instances of zero traffic capacities: these represent cases of bridge collapse during an earthquake. To depict the effect of the ground motions with velocity pulses on the probability of collapse, the results are presented separately for sets of ground motions with velocity pulses and those without velocity pulses. The sets of ground motions with velocity pulses generate a significantly larger probability of collapse than those without velocity pulses; for example, for very rare earthquakes and the Rx1 abutment model, the probability of collapse in the case of pulses is 25%, otherwise, it is 0%. Furthermore, the probability of collapse is significantly larger for the case of the Rx0 abutment model than for the Rx1 model. Finally, it is important to note that when the analyzed bridge did not collapse, it showed sufficient capacity to support one emergency vehicle at a time.

The intersecting point of the TCF-2 and TDF-2 represents the probability that a traffic loading associated with the FLS-2 (i.e., one emergency vehicle) can be safely accommodated after the bridge has experienced an earthquake representative of the intensity under consideration. If we designate this probability of FLS-2 as PFLS-2, then the probability of bridge closure after an earthquake that corresponds to FLS-3 (i.e., PFLS-3) can be calculated as one minus PFLS-2.

Figure 31. Traffic Capacity Fragilities (TCF-2) vs. Traffic Demand Fragility (TDF-2) for the Three Considered Hazard Levels, Two Abutment Types (Rx0 and Rx1), and Two Truck Load Positions (fast lane and curb lane)

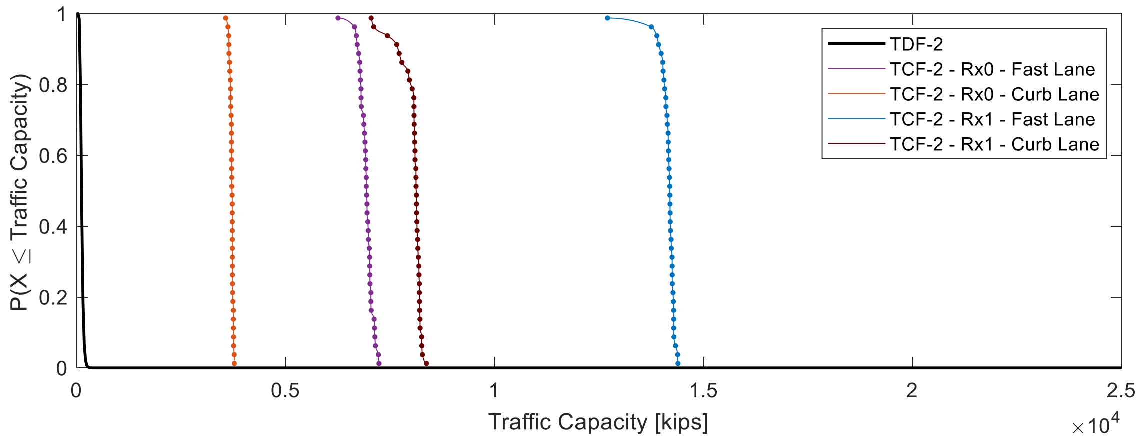

(a) Frequent Earthquakes

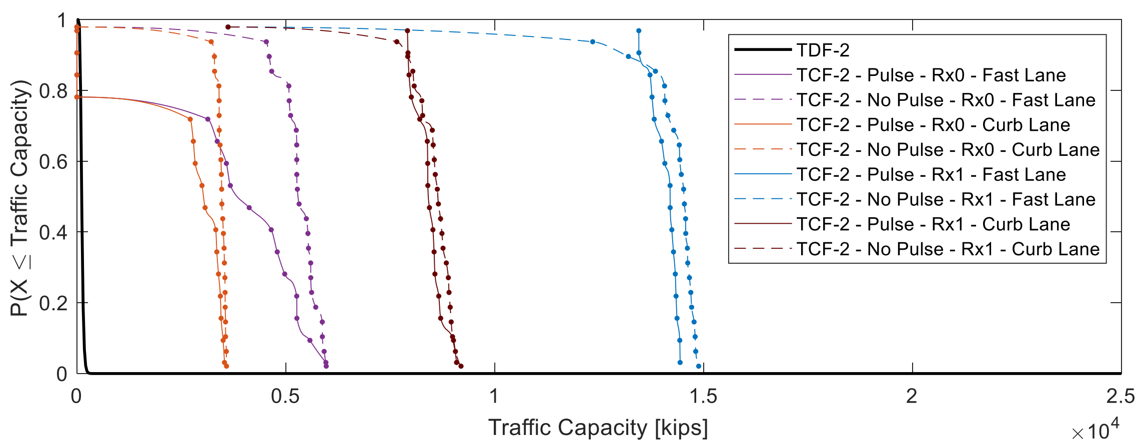

(b) Rare Earthquakes

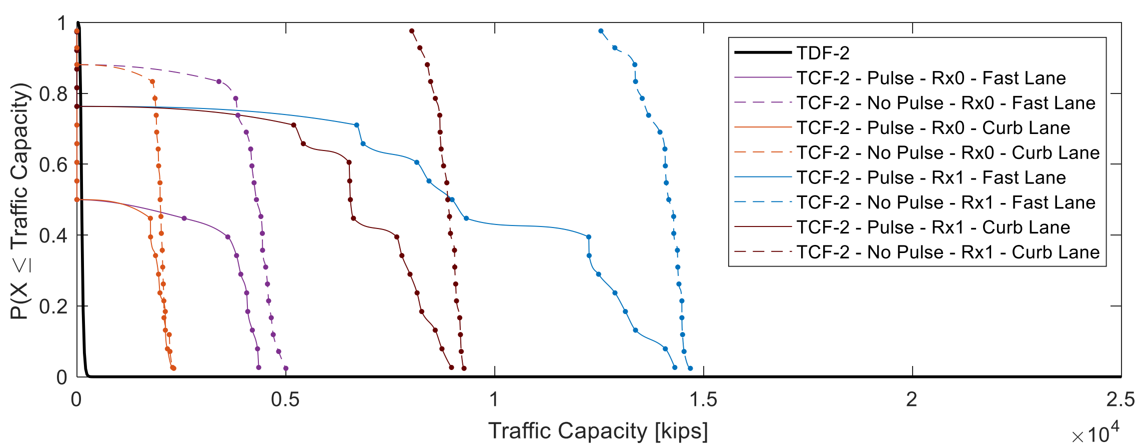

(c) Very Rare Earthquakes

Traffic Capacity and Functionality Evaluation for FLS-0: Traffic Load Scenarios

To further evaluate the post-earthquake functionality state of the bridge, the appropriate traffic loading scenarios were established for the FLS-0 and used to generate the corresponding TCFs and TDFs.

In the case when there are no traffic restrictions (FLS-0), two extreme distributions of vehicles on the bridge are considered: all lanes in one direction of travel are fully loaded with vehicles, while all lanes in the opposite direction of travel are empty (loading scenario 1, which maximizes the bending moments in the columns), and all lanes in both directions of travel on the bridge are fully loaded with vehicles (loading scenario 2, which maximizes the axial forces in the columns). To induce the largest forces in the bridge columns, the bridge is loaded with standard HL-93 trucks, where one truck on the bridge is positioned directly above the exterior column (as shown in Figure 26) and all other trucks are spaced 50 feet from each other (i.e., the distance between the rear axle of one truck and the front axle of another is 50 feet per section 3.4.3.1 of the FHWA LRFD Reference Manual for Highway Bridge Superstructures: Grubb et al. 2015). In loading scenario 1, when the traffic loading is applied on the half of the bridge (one travel direction), the truck load is applied on the side of the bridge deck with permanent displacements in the transverse direction. Each ground motion analysis is repeated several times to cover a range of loading scenarios and abutment restraint conditions (Rx1 and Rx0).

Traffic Capacity Evaluation

Given that the entire bridge is loaded with the maximum expected load on the bridge, the traffic capacity of the bridge is evaluated by measuring the axial forces in the columns and vertical reactions of the abutments at the time the bridge reaches its maximum traffic capacity. The bridge reaches its maximum traffic capacity for the ground motion and loading scenario when a critical column reaches its axial load-carrying capacity, where the critical column is a column with the highest axial force among all bridge columns. The axial force in each column is determined as a minimum of the following two values: axial force that corresponds to the peak moment on the axial force-bending moment curve, and the peak axial force on the axial force-displacement curve. In the case of FLS-0, the criterion for evaluating the axial force based on the rebar strain was not considered, as the columns continued to retain their strength even as the strain limits were exceeded (Figure 32c, Figure 33c). Figure 32(a,b) presents an example for determining the axial force of each column based on the two criteria for loading scenario 1, and Figure 33 (a,b) presents an example for loading scenario 2. It can be seen from these figures that when the bending moment of a column was maximized (loading scenario 1) the column had a relatively small axial load-carrying capacity, and when the axial force of a column was maximized (loading scenario 2), it resulted in a relatively large axial load-carrying capacity, as the bending moment of the column was relatively small.

Figure 32. Example Graphs of Criteria for Determining Axial Load-Carrying Capacity of Columns (earthquake #1 from set of very rare earthquakes, abutment type Rx1, and loading scenario 1)

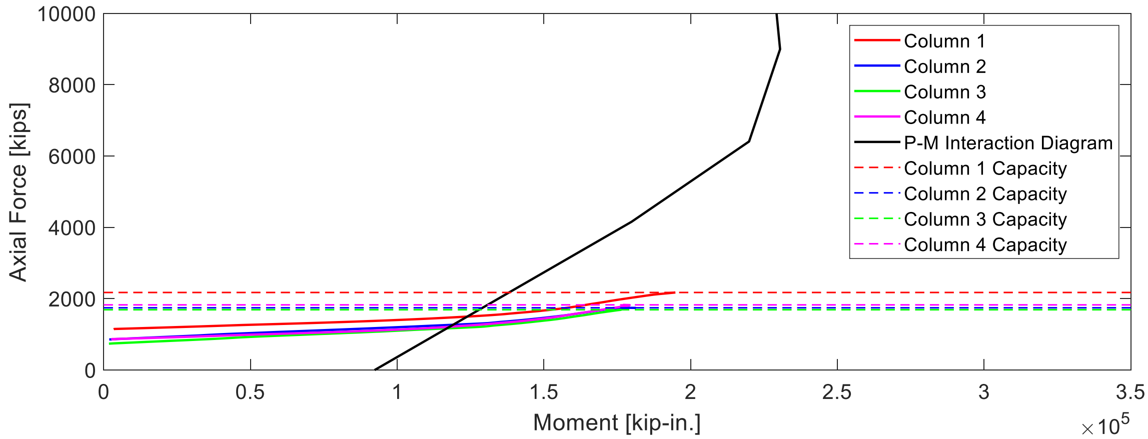

(a) Axial Force vs. Bending Moment

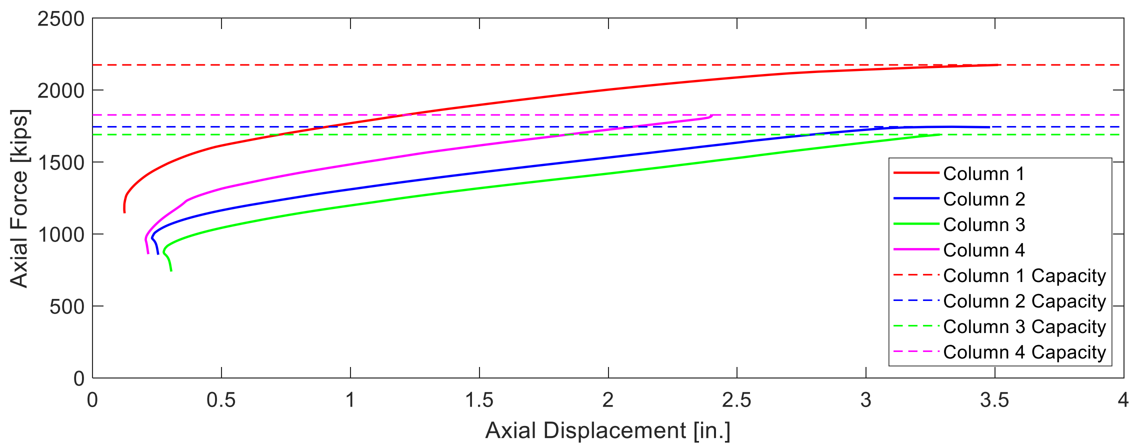

(b) Axial Force vs. Axial Displacement

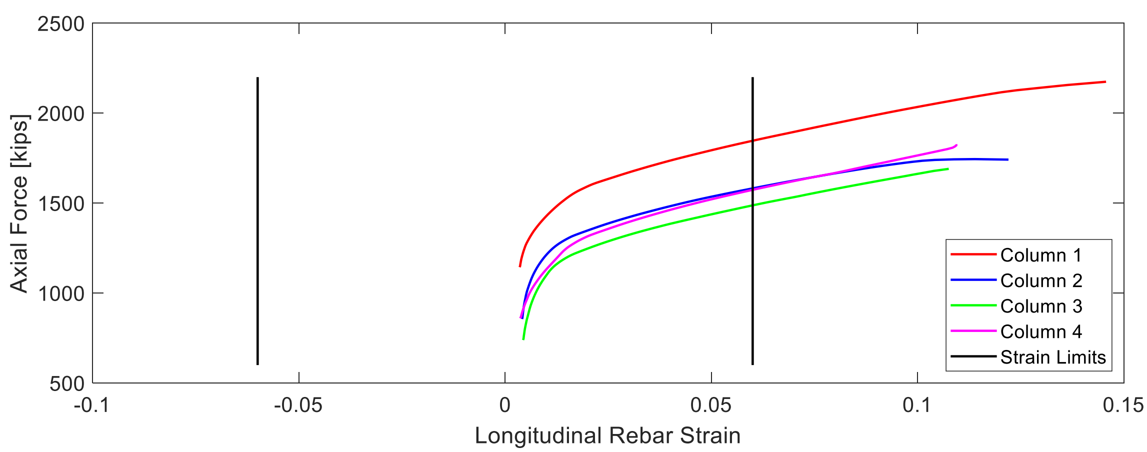

(c) Axial Force vs. Strain in Longitudinal Rebar

Figure 33. Example Graphs of Criteria for Determining Axial Load-Carrying Capacity of Columns (earthquake #1 from set of very rare earthquakes, abutment type Rx1, and loading scenario 2)

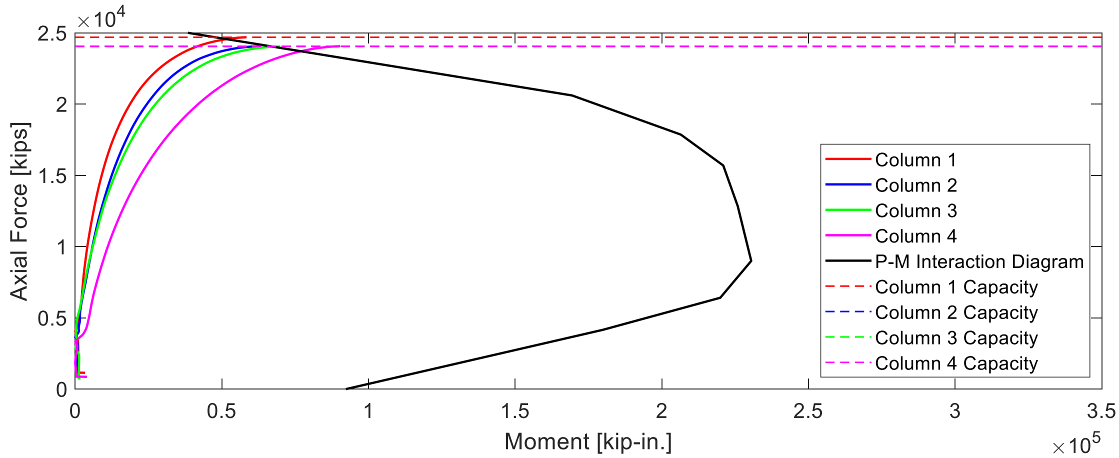

(a) Axial Force vs. Bending Moment

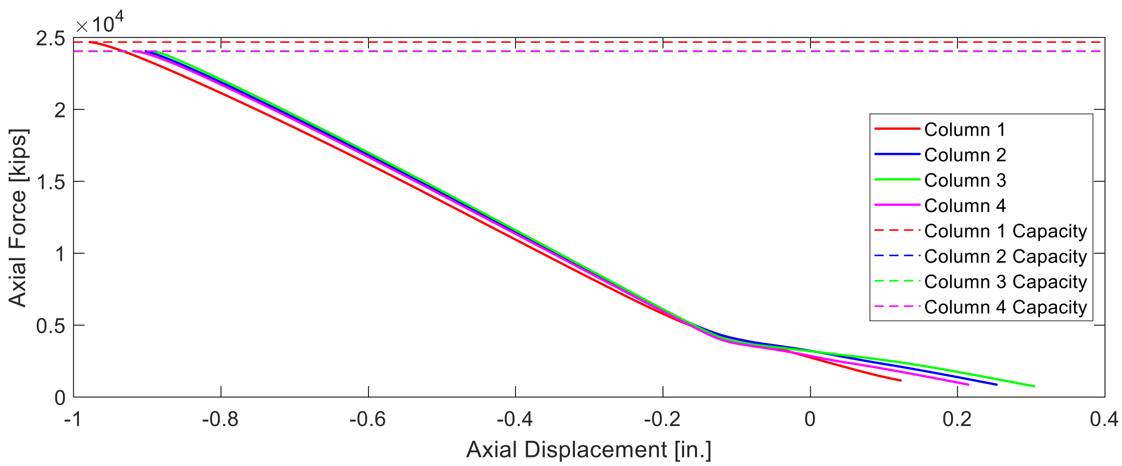

(b) Axial Force vs. Axial Displacement

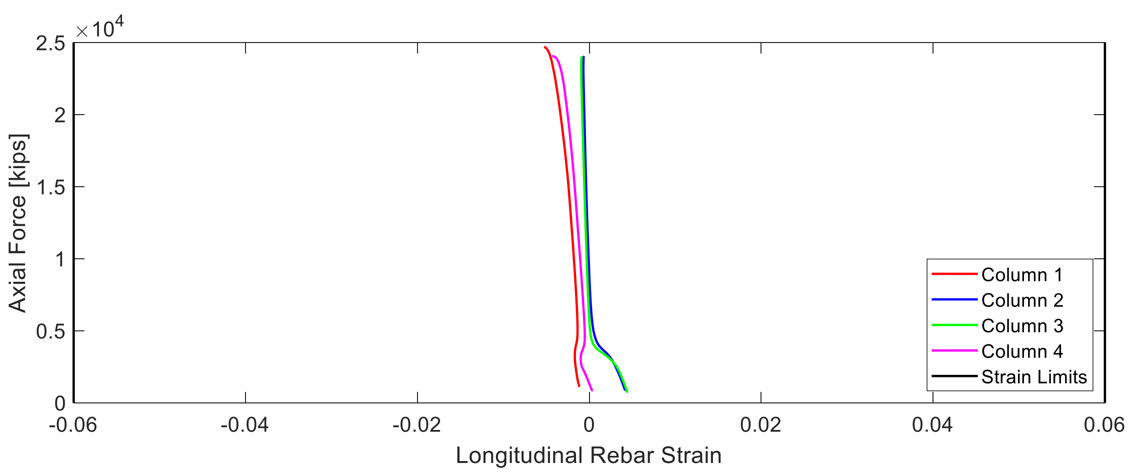

(c) Axial Force vs. Strain in Longitudinal Rebar

Correlations between EDPs and Bridge Traffic Capacity

Example plots of the correlations between traffic capacity and the EDPs considering FLS-0 are presented for very rare earthquakes and abutment type Rx1 in Figures 34 and 35 for loading scenarios 1 and 2, respectively. The left y-axis shows the post-earthquake traffic capacity values, and the right y-axis shows the traffic capacity ratio values, where the traffic capacity ratio is the post-earthquake traffic capacity divided by the pre-earthquake traffic capacity. The pre-earthquake capacity was determined through the same criteria as the post-earthquake capacity, but the bridge was not subjected to any ground motion.

For very rare earthquakes and loading scenario 1, where half of the bridge deck is loaded with trucks (i.e., vehicles in one travel direction) resulting in a bending failure of a critical column, at least 80% of the traffic load capacity is maintained even for very high values of EDPs (Figure 34). In this case, the traffic capacity of the bridge is relatively low compared to the traffic loading scenario 2 (Figure 35), as the bending capacity of the column is reached at a low level of axial force (Figure 32a). In the case of loading scenario 2, where the bridge deck is fully loaded (both travel directions) resulting in the axial failure of the critical column, we see a pronounced loss in the bridge's traffic capacity with the increase of RDRs (Figure 35c). While at least 70% of the traffic capacity is maintained if residual drift ratios are below 1%, only 20% to 30% of traffic capacity is maintained if drift ratios are larger than 2% and if the bridge did not collapse during an earthquake.

Figure 34. Traffic Capacity vs. EDPs for Loading Scenario 1 and Very Rare Earthquakes (abutment type Rx1)

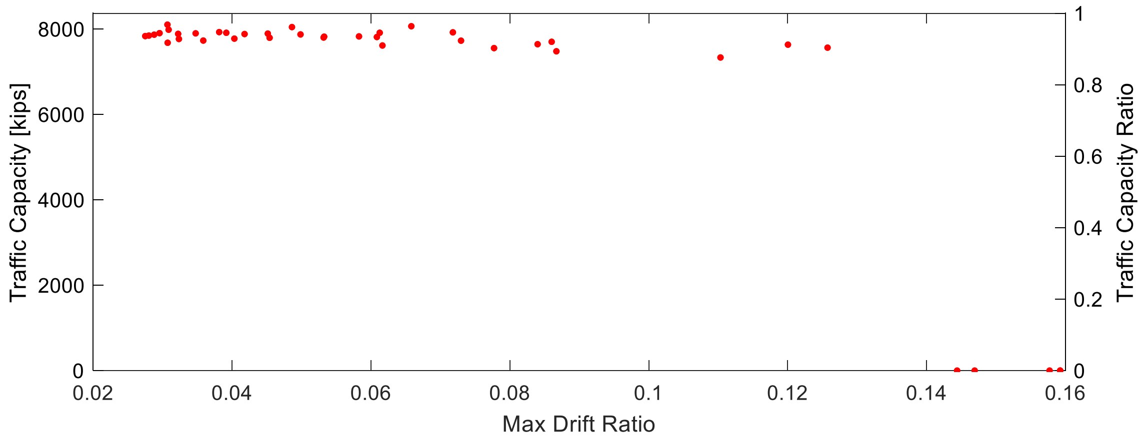

(a) Traffic Capacity vs. Max Drift Ratio

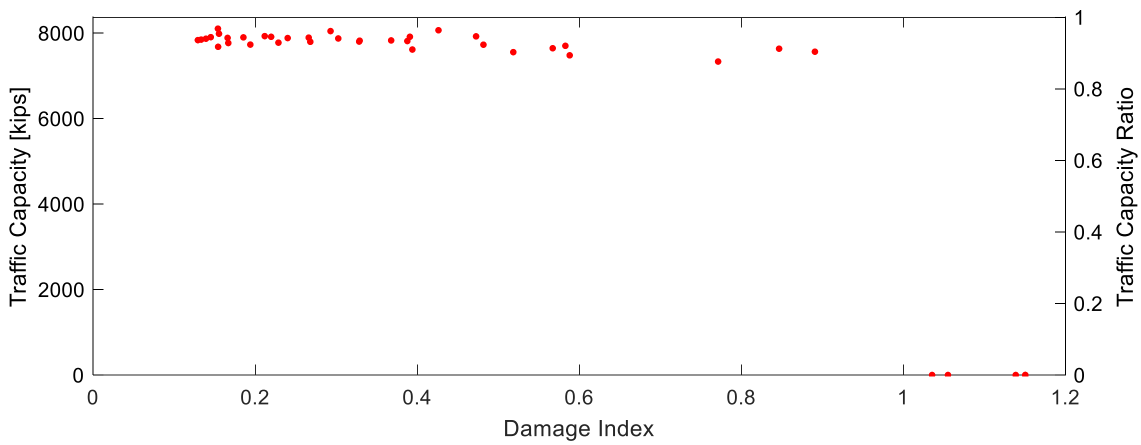

(b) Traffic Capacity vs. Damage Index

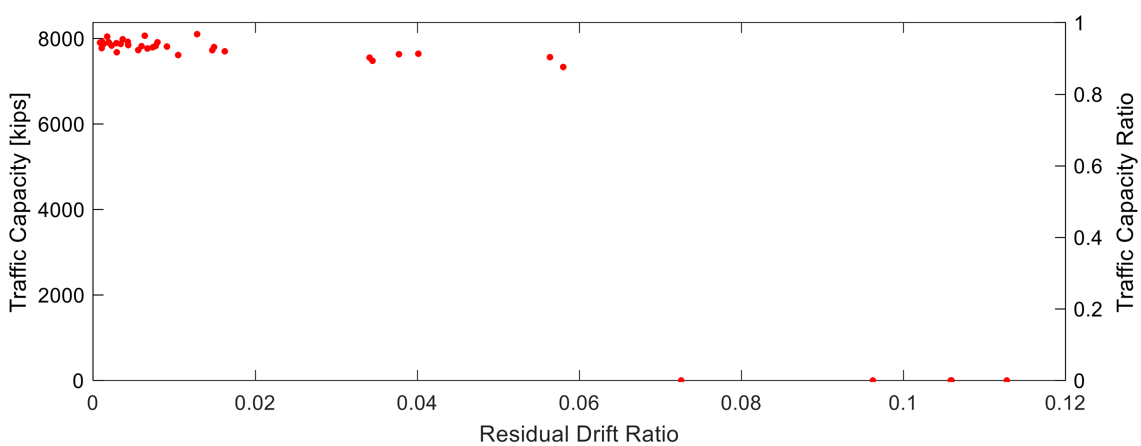

(c) Traffic Capacity vs. Residual Drift Ratio

Figure 35.   Traffic Capacity vs. EDPs for Loading Scenario 2 and Very Rare Earthquakes (abutment type Rx1)

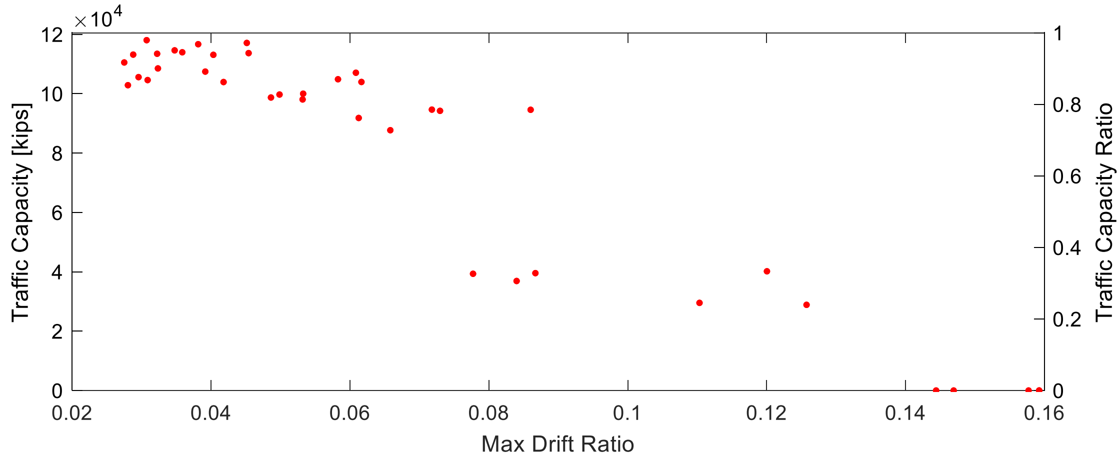

(a) Traffic Capacity vs. Max Drift Ratio

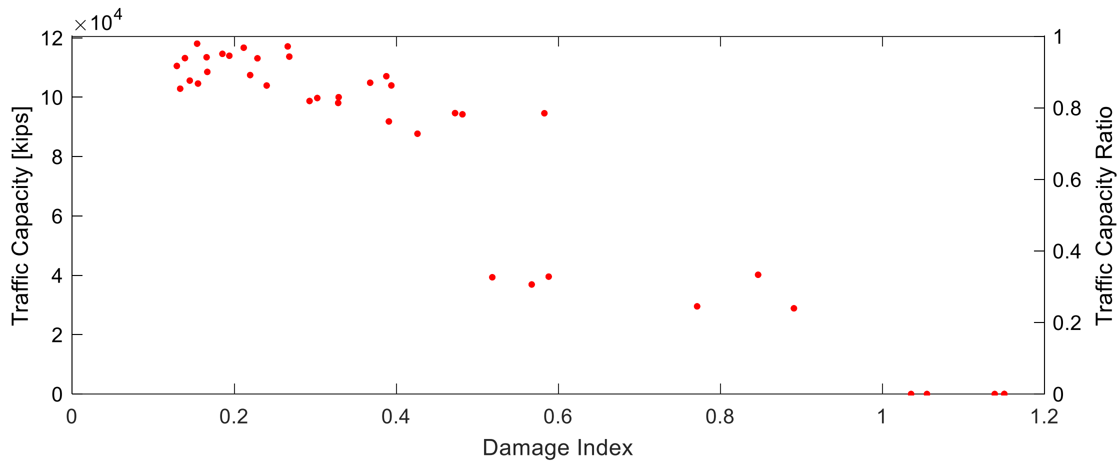

(b) Traffic Capacity vs. Damage Index

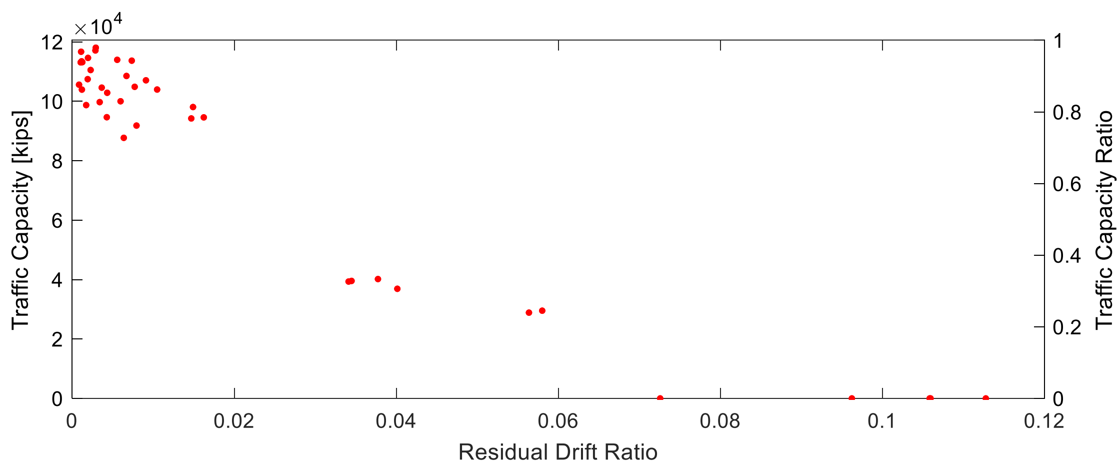

(c) Traffic Capacity vs. Residual Drift Ratio

Evaluation of Post-Earthquake Functionality

Traffic capacity fragilities associated with the FLS-0 (designated as TCF-0) and loading scenario 1 are presented in Figure 36 for three hazard levels (frequent, rare, and very rare earthquakes) and two types of abutment models (Rx0 and Rx1). The figure also includes the traffic demand fragility (designated as TDF-0), which was determined based on the truck loading on half of the bridge deck (i.e., one loading direction). The presented results show that when the bridge did not collapse, it had sufficient capacity to support the full traffic load in one travel direction for all hazard levels considered. Furthermore, we see significantly larger bridge traffic capacity for the case when abutments provide torsional restraint for the deck (Rx1) compared to when they do not (Rx0), demonstrating the great effect of abutments on the traffic capacity.

Lastly, Figure 37 presents traffic capacity and demand fragilities for loading scenario 2. In this case, traffic demand fragility is established by considering the fully loaded bridge. We see that the traffic capacity is significantly higher than demand, suggesting that the bridge can remain fully open unless it has collapsed during an earthquake.

Figure 36. Traffic Capacity Fragilities (TCF-0) vs. Traffic Demand Fragility (TDF-0) for Loading Scenario 1; Three Hazard Levels and Two Abutment Types (Rx0 and Rx1)

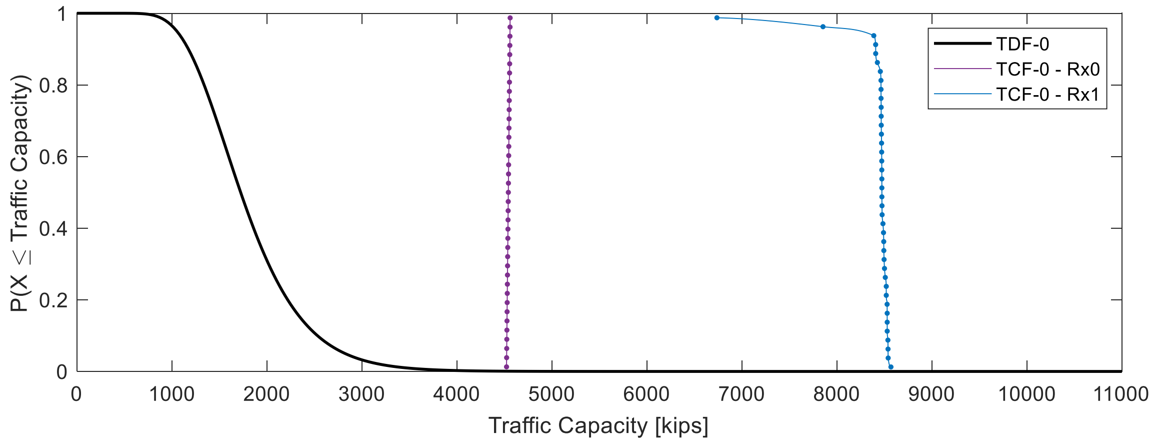

(a) Frequent Earthquakes

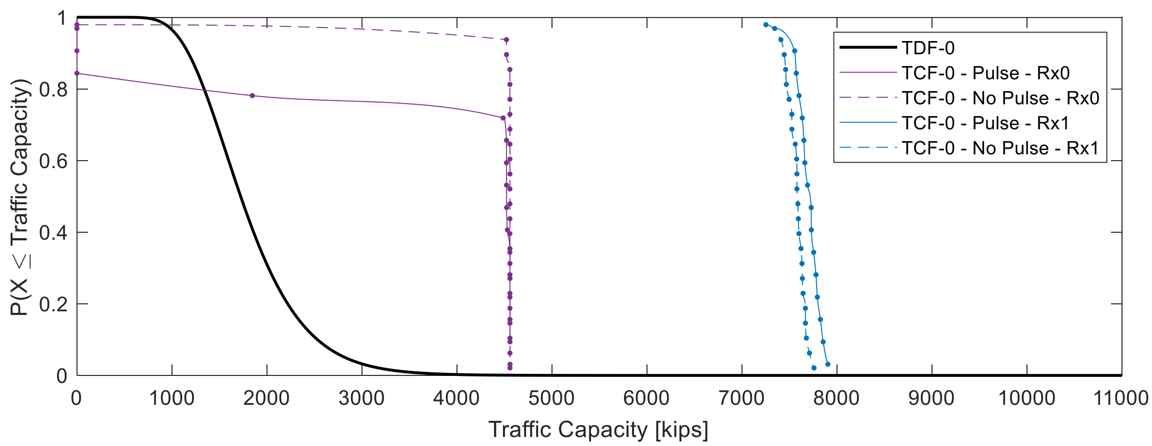

(b) Rare Earthquakes

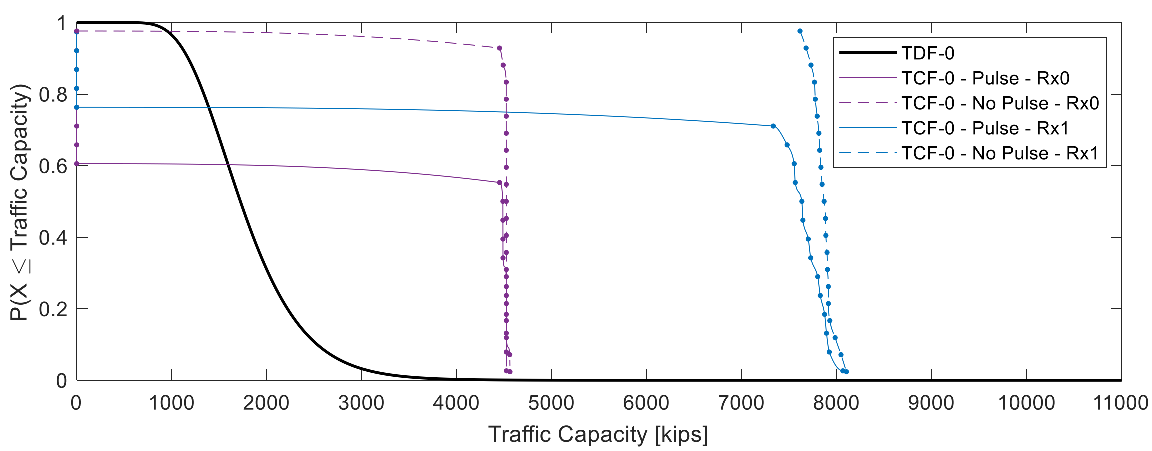

(c) Very Rare Earthquakes

Figure 37. Traffic Capacity Fragilities (TCF-0) vs. Traffic Demand Fragility (TDF-0) for Loading Scenario 2; Three Hazard Levels and Two Abutment Types (Rx0 and Rx1)

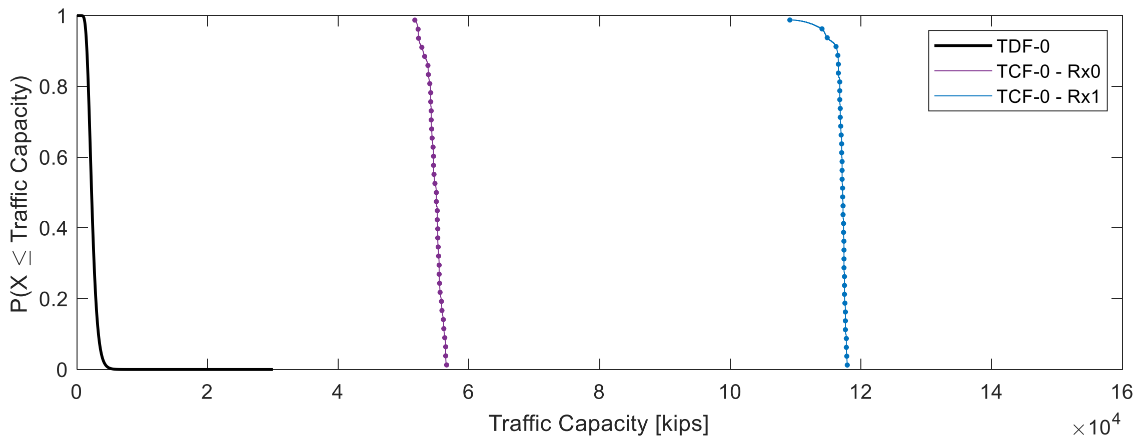

(a) Frequent Earthquakes

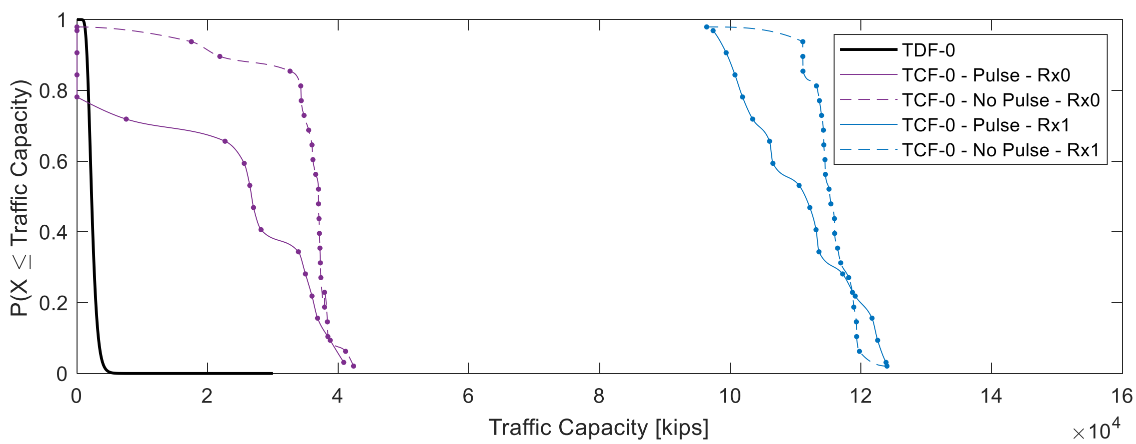

(b) Rare Earthquakes

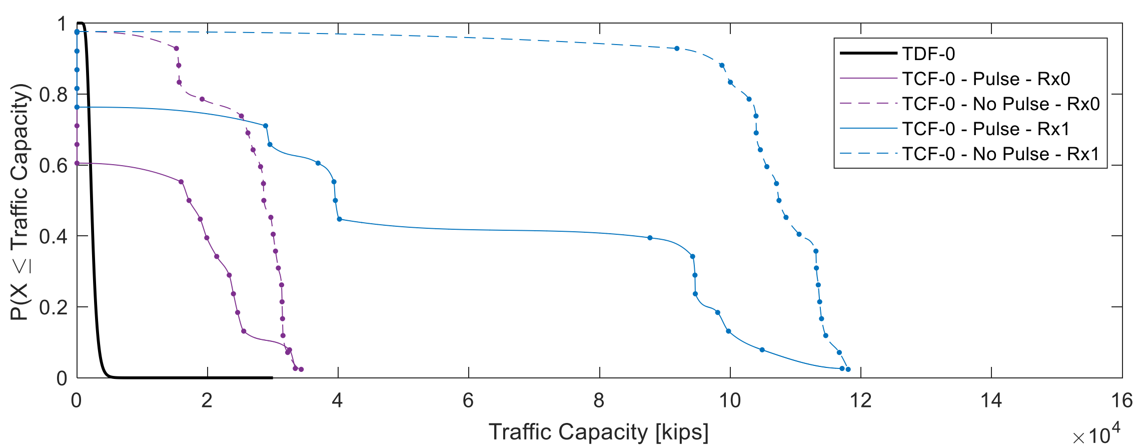

(c) Very Rare Earthquakes

4.3 Summary of Results of the Case Studies

The method for determining the post-earthquake traffic capacity and functionality states of the bridge is demonstrated above in a case study considering a modern single-column bent bridge. The case study evaluated bridge functionality at three levels of earthquake intensity and two functionality limit states of the bridge: FLS-0, a bridge open to normal traffic, and FLS-2, a bridge open only for one emergency vehicle at a time. While the bridge model utilizes a high-fidelity column model developed in the research presented in this report, the abutments are modeled using two simple models that are expected to generate the upper and lower bounds of the bridge response for the earthquake and traffic capacity.

The major findings of the case study are the following.

- The developed method for evaluating the post-earthquake bridge functionality state provides an opportunity to understand the relationship between the damage sustained by bridge components and traffic capacity.
- Traffic capacity of the bridge is highly correlated with the residual drift ratio of the bridge.
- The abutment model has a significant effect on the bridge traffic capacity suggested by the model outputs. To accurately evaluate the post-earthquake bridge functionality, it is important to use high-fidelity abutment models.
- Ground motions with velocity pulses generate a significant reduction of traffic capacity when compared to ground motions of similar intensity without velocity pulses.
- Increasing levels of damage at higher intensities of ground motions generate a reduction of the traffic load capacity.
- For the bridge considered in the case study, traffic capacity fragilities were significantly higher than traffic demand fragilities for all considered FLSs and earthquake hazard levels, implying full functionality of the bridge at all hazard levels—unless the bridge has collapsed during an earthquake.

V. Summary and Conclusions

In California, modern highway bridges designed using the Caltrans Seismic Design Criteria are expected to maintain bridge integrity and provide safety in the event of a design-level earthquake. However, their functionality will likely be compromised in case of a design-level or beyond-design-level earthquake that may generate excessive residual drifts. Prior to this research, there was no validated, quantitative approach for estimating the functionality level of the bridge after an earthquake due to the difficulty of accurately simulating the residual drifts of the bridge columns. This research develops a novel method for probabilistically evaluating the post-earthquake functionality state of the bridge; this assessment is founded on an explicit evaluation of residual drifts and associated traffic capacity by considering realistic traffic load scenarios.

To accurately simulate the post-earthquake residual drifts, this research proposes a high-fidelity finite-element model for bridge columns, which was developed and calibrated utilizing existing experimental data from shake table tests of a full-scale bridge column. This finite-element model of the bridge column was further expanded to enable evaluation of the axial load-carrying capacity of damaged columns, which is critical for an accurate evaluation of the traffic capacity of the bridge. Existing experimental data from the crushing tests on the columns with earthquake-induced damage were utilized to support this phase of the finite-element model development.

The finite-element model of the bridge column was developed in OpenSees. To accurately simulate the post-earthquake residual drifts and axial load-carrying capacity of damaged bridge columns, the finite-element model utilized a nonlinear beam with a hinge element—an extension of the force-based element formulation where the locations and weights of integration points are based on plastic hinge integration, allowing for an explicit definition of plastic hinge lengths at the element ends. The reinforced concrete section in the plastic hinge regions was modeled as a fiber section that accounts for the axial-bending interaction. The fiber section was divided into three parts: concrete cover, concrete core, and reinforcing steel, where fibers of the concrete cover (unconfined concrete) and concrete core (confined concrete) were modeled using Concrete02 material, and reinforcing steel fibers (longitudinal bars) were modeled using ReinforcingSteel material. To accurately simulate the axial load-carrying capacity of the damaged column, the post-peak degrading slope of confined concrete was set to 5% of its initial modulus of elasticity. The interior portion of the beam with the hinges element was modeled as elastic, where the effective moment of inertia, expressed as a ratio to the total moment of inertia, was 0.35 for the design-level earthquake and 0.25 for the beyond-design-level earthquake. Damping was modeled with a mass- and stiffness-proportional Rayleigh damping model using the damping ratio of 1%, the first two modes of vibration, and tangent stiffness of the column updated at every step of the analysis.

To properly evaluate the post-earthquake operational level of the bridge, the realistic traffic loadings representative of different bridge conditions (e.g., immediate access, emergency traffic only, closed) were applied in the proposed finite-element bridge model following an earthquake simulation. The traffic loadings in the finite-element models considered the distribution of the vehicles on the bridge inducing the largest forces in the bridge columns.

This research next proposed a method for directly evaluating the post-earthquake traffic capacity and functionality of a reinforced concrete highway overpass bridge through finite-element simulations. The method includes a definition of the functionality limit states (FLSs) for the bridge (full traffic, limited traffic, emergency vehicles only, no traffic), recommendations for modeling a bridge structure by incorporating the proposed bridge column model, a definition of realistic traffic load scenarios that correspond to different traffic load restrictions, evaluation of the post-earthquake traffic capacity for a selected FLS, and finally, evaluation of post-earthquake functionality through comparison of traffic capacity with the traffic demand. Distinguishing features of the method are the quantitative links between the earthquake intensity, component-level EDPs, and system-level traffic capacity. The main outcome of the method is a reliable estimate of the probability that a traffic loading associated with the considered functionality limit state of the bridge can be safely accommodated following an earthquake event.

The method for determining a bridge's post-earthquake traffic capacity and functionality states has been applied in a case study considering a modern single-column bent bridge. The case study showcased that the method also provides an opportunity to understand the relationship between the damage sustained by bridge components and the bridge traffic capacity. The major findings of the case study are: (1) that traffic capacity of the bridge is highly correlated with the residual drift ratio, damage state of columns, and damage state of abutments; (2) that ground motions with velocity pulses generate a significant reduction of traffic capacity when compared to ground motions of similar intensity without velocity pulses; and (3) that there is a high probability that the modern single-column bent bridges will remain fully functional after a major earthquake event.

The information on the post-earthquake functionality state of the bridge generated with the proposed method can be effectively used to support bridge maintenance decision-making processes by enabling an identification of retrofit needs that will generate long-term benefits to transportation agencies through reduced business interruptions. Furthermore, an objective evaluation of the post-earthquake bridge functionality may be used in place of current practices to improve public safety and to minimize economic impact caused by disruption of the transportation network from possibly unnecessary bridge closures.

Abbreviations and Acronyms

BWHE	Beam with Hinges Element
Caltrans	California Department of Transportation
DBE	Displacement-Based Element
DI	Damage Index
DS	Damage State
FBE	Force-Based Element
FHWA	Federal Highway Administration
FLS	Functionality Limit State
LRFD	Load and Resistance Factor Design
MDR	Maximum Drift Ratio
NGA	Next Generation Attenuation
PEER	Pacific Earthquake Engineering Research Center
RDR	Residual Drift Ratio
Rx0	Abutment with Rotational Restraint Designation
Rx1	Abutment without Rotational Restraint Designation
SDC	Seismic Design Criteria
TCF	Traffic Capacity Fragility
TDF	Traffic Demand Fragility

Bibliography

Aviram, A., A. Aviram, K. Mackie, K. Mackie, B. Stojadinovic, and B. Stojadinovic. "Guidelines of Nonlinear Analysis of Bridge Structures in California." *Report PEER 2008/03*. Berkeley, CA: Pacific Earthquake Engineering Research Center, University of California, 2008.

Baker, Jack. 2010. "DRAFT: PEER Site_specific Ground Motions for Oakland: Record Selection Notes."

Caltrans. "Bridge Design Specifications." California Department of Transportation, Sacramento, CA, 2004.

Caltrans. "Seismic Design Criteria." California Department of Transportation, Sacramento, CA, 2006.

Caltrans. "Seismic Design Criteria." California Department of Transportation, Sacramento, CA, 2013.

Caltrans. "California Transportation Asset Management Plan." California Department of Transportation, Sacramento, CA.

DesRoches, Reginald, Jamie Padgett, Karthik Ramanath, and Jazalyn Dukes. "Feasibility Studies for Improving Caltrans Bridge Fragility Relationships." *Report CA 12-1775*. California Department of Transportation, Sacramento, CA, 2012.

FEMA P-58. 2018. "Seismic Performance Assessment of Buildings - Methodology." *FEMA P-58-1*.

Field, Edward H., Ramon J. Arrowsmith, Glenn P. Biasi, Peter Bird, Timothy E. Dawson, Karen R. Felzer, David D. Jackson, et al. "Uniform California Earthquake Rupture Forecast, Version 3 (UCERF3): The Time-Independent Model." *Bulletin of the Seismological Society of America* (2014).

Grubb, Michael A., Kenneth E. Wilson, Christopher D. White, and William N. Nickas. "Load and Resistance Factor Design (LRFD) For Highway Bridge Superstructures: Reference Manual." *Report FHWA-NHI-15-047*. Federal Highway Administration, Washington, DC, 2015.

Guerrini, Gabriele, José I. Restrepo, Milena Massari, and Athanassios Vervelidis. "Seismic Behavior of Posttensioned Self-Centering Precast Concrete Dual-Shell Steel Columns." *Journal of Structural Engineering* 141, no. 4 (2015).

Jeong, Hyung Il, Junichi Sakai, and Stephen a Mahin. "Shaking Table Tests and Numerical Investigation of Self-Centering Reinforced Concrete Bridge Columns Shaking Table Tests and Numerical Investigation of Self-Centering Reinforced Concrete Bridge

Columns." *Report PEER 2008/06*. Berkeley, CA: Pacific Earthquake Engineering Research Center, University of California, 2008.

Jones, Lucile M., Richard Bernknopf, Dale Cox, James Goltz, Kenneth Hudnut, Dennis Mileti, Suzanne Perry, et al. "The ShakeOut Scenario." *USGS Open File Report 2008, 1150*. 2008.

Karsan, I. D., and James Jirsa. "Behavior of Concrete Under Compressive Loadings." *Journal of the Structural Division* (1969).

Kaviani, Peyman, Farzin Zareiana, and Ertugrul Taciroglu. "Seismic Behavior of Reinforced Concrete Bridges with Skew-Angled Seat-Type Abutments." *Engineering Structures* 45 (2012): 137–150.

Kent, D., and R. Park. 1971. "Flexural Members with Confined Concrete." *Journal of the Structural Division* 97, ST7 (1971): 1969–1990.

Ketchum, M., V. Chang, and Thomas Shantz. "Influence of Design Ground Motion Level on Highway Bridge Costs." *Report PEER 6D01*. Berkeley, CA: Pacific Earthquake Engineering Research Center, University of California, 2004.

Kunnath, Sashi K., Yeongae Heo, and Jon F. Mohle. "Nonlinear Uniaxial Material Model for Reinforcing Steel Bars." *Journal of Structural Engineering* 135, no. 4 (2009).

Mackie, Kevin R., John-Michael Wong, and Bozidar Stojadinovic. "Integrated Probabilistic Performance-Based Evaluation of Benchmark Reinforced Concrete Bridges." *Report PEER 2007/09*. Berkeley, CA: Pacific Earthquake Engineering Research Center, University of California, 2007.

Mackie, Kevin, and Bozidar Stojadinovic. "Residual Displacement and Post Earthquake Capacity of Highway Bridges." In *Proceedings of the 13th World Conference on Earthquake Engineering*. Vancouver, BC, Canada, 2004.

Mackie, Kevin, and Bozidar Stojadinovic. "Post-Earthquake Functionality of Highway Overpass Bridges." *Earthquake Engineering and Structure Dynamics* 35 (2006): 77–93.

Mander, J. B., M. J. Priestley, and R. Park. 1988. "Theoretical Stress-Strain Model for Confined Concrete." *Journal of Structural Engineering* 114, ST8 (1988): 1804–1826.

McKenna, Frank T. "Object-Oriented Finite Element Programming: Frameworks for Analysis, Algorithms and Parallel Computing." PhD Dissertation, University of California, Berkeley, 1997.

Menegotto, M., and P. E. Pinto. "Method of Analysis for Cyclically Loaded R.C. Plane Frames Including Changes in Geometry and Non-Elastic Behaviour of Elements under Combined Normal Force and Bending." *Symposium on the Resistance and Ultimate Deformability of*

Structures Acted on by Well Defined Repeated Loads. International Association for Bridge and Structural Engineering. Zurich, Switzerland, 1973.

Moharrami, Mohammadreza, and Ioannis Koutromanos. "Finite Element Analysis of Damage and Failure of Reinforced Concrete Members under Earthquake Loading." *Earthquake Engineering and Structural Dynamics* 46, no. 15 (2017): 2811–2829.

Moshref, A., M. Tehranizadeh, and M. Khanmohammadi. "Investigation of the Reliability of Nonlinear Modeling Approaches to Capture the Residual Displacements of RC Columns under Seismic Loading." *Bulletin of Earthquake Engineering* 13, no. 8 (2015): 2327–2345.

Padgett, Jamie E., and Reginald DesRoches. "Bridge Functionality Relationships for Improved Seismic Risk Assessment of Transportation Networks." *Earthquake Spectra* 23, no. 1 (2007): 115–130. Earthquake Engineering Research Institute, Oakland, CA.

Qu, Zhe. 2012. "Predicting Nonlinear Response of an RC Bridge Pier Subject to Shake Table Motions." In *Proceedings to the 9th International Conference on Urban Earthquake Engineering (9CUEE)*. Tokyo, Japan.

Saini, Amarjeet, and M. Saiid Saiidi. "Post-Earthquake Bridge Damage Mitigation - Post-Earthquake Damage Repair of Various Reinforced Concrete Bridge Components." *Report CA 13-2180*. California Department of Transportation, Sacramento, CA, 2013.

Sakai, Junichi, and Stephen A. Mahin. "Analytical Investigations of New Methods for Reducing Residual Displacements of Reinforced Concrete Bridge Columns." *Report PEER 2004/02*. Berkeley, CA: Pacific Earthquake Engineering Research Center, University of California, 2004.

Schoettler, Matthew J., Jose Ignacio Restrepo, Gabriele Guerrini, David Duck, and Francesco Carrea. "A Full-Scale, Single-Column Bridge Bent Tested by Shake-Table Excitation." *Report PEER 2015/02*. Berkeley, CA: Pacific Earthquake Engineering Research Center, University of California, 2015.

Scott, Michael H., and Gregory L. Fenves. "Plastic Hinge Integration Methods for Force-Based Beam-Column Elements." *Journal of Structural Engineering* (2006).

Shamsabadi, Anoosh, Payman Khalili-Tehrani, Jonathan P. Stewart, Ertugrul Taciroglu. "Validated Simulation Models for Lateral Response of Bridge Abutments with Typical Backfills." *Journal of Bridge Engineering* 15, no. 3 (2010): 302–311.

Taucer, Fabio F., Enrico Spacone, and Filip C. Filippou. "A Fiber Beam-Column Element for Seismic Response Analysis of Reinforced Concrete Structures." *Ucb/Eerc-91/17*. 1991.

Tazarv, Mostafa, and M. Saiid Saiidi. "Analytical Studies of the Seismic Performance of a Full-scale SMA-Reinforced Bridge Column." *International Journal of Bridge Engineering* 1, no. 1 (2013): 37–50.

Terzic, Vesna, Matthew J. Schoettler, Jose I. Restrepo, and Stephen A. Mahin. "Concrete Column Blind Prediction Contest 2010: Outcomes and Observations." *Report PEER 2015/01*. Berkeley, CA: Pacific Earthquake Engineering Research Center, University of California, 2015.

Terzic, Vesna, and Bozidar Stojadinovic. (2010a.) "Post-Earthquake Traffic Capacity of Modern Bridges in California." *Report PEER 2010/103*. Berkeley, CA: Pacific Earthquake Engineering Research Center, University of California, 2010.

Terzic, Vesna, and Bozidar Stojadinovic. (2010b.) "Traffic Load Capacity of a Bridge Damaged in an Earthquake." In *9th US National & 10th Canadian Conference on Earthquake Engineering*. Toronto, ON, Canada, 2010.

Terzic, Vesna. "Force-Based Element vs. Displacement-Based Element." UC Berkeley, OpenSees, NEES, & NEEScomm. 2011.

Terzic, Vesna, and Bozidar Stojadinovic. "Hybrid Simulation of Bridge Response to Three-Dimensional Earthquake Excitation Followed by Truck Load." *Journal of Structural Engineering* 140, no. 8 (2014). SPECIAL ISSUE: Computational Simulation in Structural Engineering.

Terzic, Vesna, and Bozidar Stojadinovic. (2015a.) "Evaluation of Post-Earthquake Axial Load Capacity of Circular Bridge Columns." *ACI Structural Journal* 112, no. 1 (2015): 23–24.

Terzic, Vesna, and Bozidar Stojadinovic. (2015b.) "Calibration and Validation of Analytical Models for Predicting the Seismic and Axial-Load Response of Circular Bridge Columns." *Journal of Bridge Engineering* 20, no. 9 (2015).

Vosooghi, Ashkan, and M. Saiid Saiidi. "Post-Earthquake Evaluation and Emergency Repair of Damaged RC Bridge Columns Using CFRP Materials." University of Nevada, Reno, 2010.

Xie, Yazhou, Qiu Zheng, Chuang-Sheng Walter Yang, Wenyang Zhang, Reginald DesRoches, Jamie E. Padgett, and Ertugrul Taciroglu. "Probabilistic Models of Abutment Backfills for Regional Seismic Assessment of Highway Bridges in California." *Engineering Structures* 180 (2019): 452–467.

About the Authors

Vesna Terzic, Ph.D.

Vesna Terzic is an Associate Professor at the Department of Civil Engineering and Construction Engineering Management, California State University, Long Beach (CSULB). She received her B.S. from the University of Belgrade, Belgrade, Serbia; her M.S. from Saints Cyril and Methodius University, Skopje, Macedonia; and her Ph.D. from the University of California, Berkeley. Dr. Terzic's expertise includes the development of advanced models and tools for seismic performance assessment and resilience evaluation of civil infrastructure, evaluation of the nonlinear dynamic behavior of structures and their protective systems, and probabilistic performance-based seismic design and evaluation of bridges and buildings. She is a recipient of the prestigious ACI Chester Paul Siess Award for Excellence in Structural Research.

William Pasco

William Pasco is a licensed Engineer-in-Training (EIT) who is a graduate student at California State University, Long Beach (CSULB) working towards his Master of Science in Civil Engineering with a focus in Structural Engineering. He obtained his degree of Bachelor of Science in Civil Engineering in the Spring of 2017 from CSULB, graduating magna cum laude. He obtained the Award for Department Outstanding Baccalaureate Graduate in the Spring of 2017 from the CSULB College of Engineering for his exemplary academic record and his engagement in various extracurricular activities. He also achieved an Award of Excellence for Upperclassman of the Year in the Spring of 2017 from the CSULB chapter of the American Society of Civil Engineers (ASCE) for his continued involvement with the organization and his many contributions.

MINETA TRANSPORTATION INSTITUTE